Proteomic Profiling Reveals the Transglutaminase-2 Externalization Pathway in Kidneys after Unilateral Ureteric Obstruction

Proteomic Profiling Reveals the Transglutaminase-2 Externalization Pathway in Kidneys after Unilateral Ureteric Obstruction

Giulia Furini,[1] Nina Schroeder,[1] Linghong Huang,[2] David Boocock,[3] Alessandra Scarpellini,[1] Clare Coveney,[3] Elisa Tonoli,[1] Raghavendran Ramaswamy,[1] Graham Ball,[3] Claudia Verderio,[4] Timothy S. Johnson,[2] and Elisabetta A.M. Verderio[1]

[1]School of Science and Technology, Nottingham Trent University, Nottingham, United Kingdom; [2]Academic Nephrology Unit, Sheffield Kidney Institute, University of Sheffield, Sheffield, United Kingdom; [3]John van Geest Cancer Research Centre, Nottingham Trent University, Nottingham, United Kingdom; and [4]National Research Council, Institute of Neuroscience, Milan, Italy

ABSTRACT

Increased export of transglutaminase-2 (TG2) by tubular epithelial cells (TECs) into the surrounding interstitium modifies the extracellular homeostatic balance, leading to fibrotic membrane expansion. Although silencing of extracellular TG2 ameliorates progressive kidney scarring in animal models of CKD, the pathway through which TG2 is secreted from TECs and contributes to disease progression has not been elucidated. In this study, we developed a global proteomic approach to identify binding partners of TG2 responsible for TG2 externalization in kidneys subjected to unilateral ureteric obstruction (UUO) using TG2 knockout kidneys as negative controls. We report a robust and unbiased analysis of the membrane interactome of TG2 in fibrotic kidneys relative to the entire proteome after UUO, detected by SWATH mass spectrometry. The data have been deposited to the ProteomeXchange with identifier PXD008173. Clusters of exosomal proteins in the TG2 interactome supported the hypothesis that TG2 is secreted by extracellular membrane vesicles during fibrosis progression. In established TEC lines, we found TG2 in vesicles of both endosomal (exosomes) and plasma membrane origin (microvesicles/ectosomes), and TGF-β1 stimulated TG2 secretion. Knockout of syndecan-4 (SDC4) greatly impaired TG2 exosomal secretion. TG2 coprecipitated with SDC4 from exosome lysate but not ectosome lysate. *Ex vivo*, EGFP-tagged TG2 accumulated in globular elements (blebs) protruding/retracting from the plasma membrane of primary cortical TECs, and SDC4 knockout impaired bleb formation, affecting TG2 release. Through this combined *in vivo* and *in vitro* approach, we have dissected the pathway through which TG2 is secreted from TECs in CKD.

Fibrotic remodeling is the primary pathologic process associated with progressive CKD leading to end stage renal disease.[1,2] Increased synthesis and especially, externalization of protein crosslinking enzyme transglutaminase-2 (TG2) by cortical tubular epithelial cells

Correspondence: Dr. Elisabetta A.M. Verderio, Nottingham Trent University, College of Science and Technology, Clifton Lane, NG11 8NS Nottingham, United Kingdom. Email: elisabetta. verderio-edwards@ntu.ac.uk

Significance Statement

Secretion of the matrix crosslinking enzyme transglutaminase 2 (TG2) from tubular epithelial cells has been shown to contribute to fibrotic remodeling, a primary pathologic process in CKD. To discover the pathway for secretion of TG2, a comparative proteomic strategy was developed. Proteins that interact with TG2 were identified by TG2 immunoprecipitation from wild type and TG2 knockout fibrotic kidney membranes followed by SWATH mass spectroscopy. The TG2 interactome was enriched in extracellular vesicle proteins, suggesting that TG2 is secreted in exosomes. Studies in cultured tubular epithelial cells support this conclusion and suggest that TG2 is a binding cargo of syndecan 4. The finding of TG2 in the urine of patients with CKD raises the possibility that block of vesicular TG2 could reduce TG2 driven matrix accumulation and diminish fibrosis.
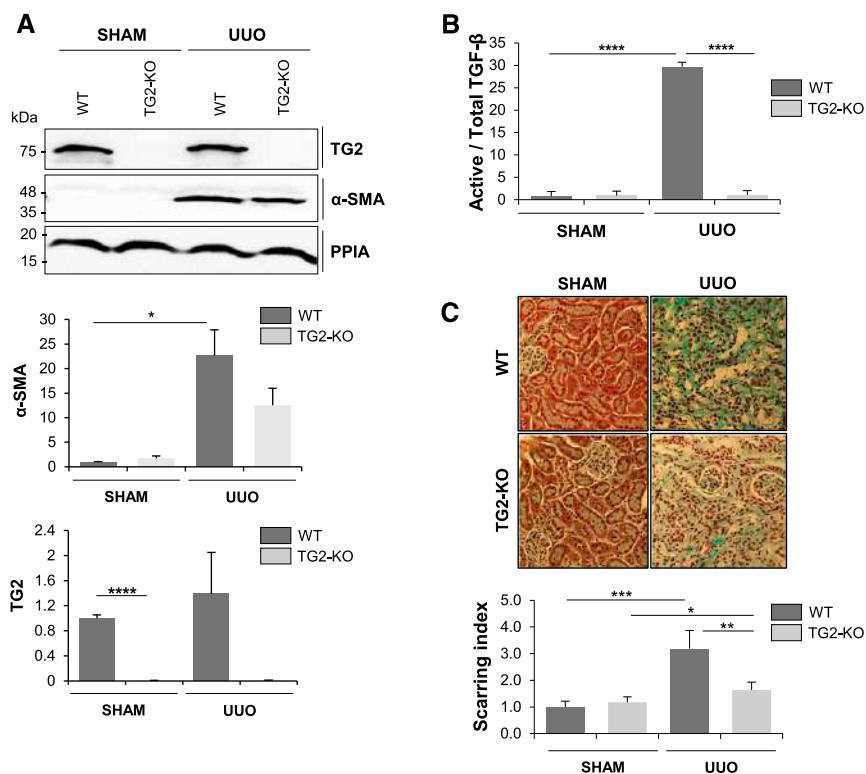
Figure 1. A UUO model in WT and TG2 KO kidneys shows that absence of TG2 reduces the development of experimental fibrosis. TG2 KO and WT mice were subjected to UUO or a sham operation. (A) Western blot analyses for the expression of TG2, α SMA, and cyclophilin A (PPIA; loading control) in the obstructed kidneys (21 days). Data represent mean band intensities normalized to PPIA relative to the WT sham operated control (equalized to one) $\pm$SEM; n 3 kidney lysates per group. (B) Active and total TGF β quantified *via* the mink lung epithelial cell bioassay. Data represent the ratio of active TGF β to total TGF β expressed relative to the WT sham operated control (equalized to one) $\pm$SEM; n 3 kidney lysates per group. (C) Repre sentative micrographs of Masson's trichrome staining; scarring index was determined as the ratio of collagen staining (light blue) over cytoplasmic staining (pink). Data represent mean values relative to the WT sham (equalized to one) $\pm$SEM; n 24 nonoverlapping fields per treatment covering tubular and glomerular areas. Mag nification, $\times$20. *$P<0.05$; **$P<0.01$; ***$P<0.01$; ****$P<0.001$.

(TECs) into the surrounding interstitium are significant features of progressive kidney scarring.[3–5] TG2 is the most widespread member of a family of Ca^{2+}-dependent enzymes, and it is able to catalyze an acyl transfer reaction between peptide-bound glutamine residues and peptide-bound lysine residues, leading to the post-translational modification of proteins through the formation of intra- or intermolecular Nε(γ-glutamyl)lysine bonds. After it is outside the cell, TG2 accelerates the deposition of available extracellular matrix (ECM) substrates and confers ECM resistance to proteases.[4] Furthermore, TG2 enhances TGF-β activation,[6–8] the prototypical profibrotic cytokine in CKD.[9] Inhibition of extracellular TG2 activity[10,11] or knockout (KO) of the heparan sulfate (HS) proteoglycan syndecan-4 (SDC4),[12] which is responsible for TG2 extracellular trafficking through an undiscovered mechanism,[13] ameliorates kidney fibrosis in experimental models of CKD.

Despite a link between externalization of TG2 and tubulointerstitial fibrosis that is well established,[10] the pathway through which TG2 is secreted from TECs, a major source of TG2 in CKD,[4] has not been fully elucidated, because TG2 lacks the leader peptide for the classic endoplasmic reticulum-Golgi secretory pathway. Preliminary work on TG2 release by TECs has suggested that an intact fibronectin (FN)-binding N-terminal β-sandwich domain is crucial for TG2 secretion but that the extracellular trafficking of TG2 is independent of FN.[14] Alternative secretory pathways have been proposed,[15] either investigated in transfected NIH3T3 fibroblasts involving TG2 loading into recycling endosomes at the perinuclear recycling compartment, small Rab11 GTPase activity, and binding to endosomal phosphoinositides[16] or in transfected HEK293 cells involving opening of a purinergic P2X7 receptor-dependent membrane pore.[17] Furthermore, we know that the association of TG2 with the HS proteoglycan SDC4 favors the enzyme secretion in mouse dermal fibroblasts[13] and *in vivo*.[12]

With the aim of unraveling the mechanism of TG2 secretion in CKD, in this study, we report a comprehensive and unbiased analysis of the membrane interactome of TG2 in kidneys subjected to unilateral ureteric obstruction (UUO). An enrichment of extracellular vesicle (EV) proteins was identified in TG2 membrane complexes. This formed the hypothesis of an EV-dependent secretion for TG2. This hypothesis was tested in established TEC lines and primary TECs. Our findings suggest, for the first time, a pathway through which TG2 is secreted from TECs and reveal the involvement of SDC4 in CKD pathogenesis.

RESULTS

Quantitative Proteomic Approach for the Analysis of TG2 Interactome in UUO Kidneys

Induction of renal fibrosis was performed in wild type (WT) and TG2-KO animals. TG2 $^{/}$ and TG2$^{+/+}$ inbred C57BL/6J mice were subjected to UUO of the left kidney or a sham operation, and kidneys were harvested at 21 days postsurgery. WT UUO kidneys were positive to α-smooth muscle actin (Figure 1A), displayed a significantly higher level of active TGF-β (mink lung epithelial cell assay) (Figure 1B), and showed increased collagen deposition in the interstitium and
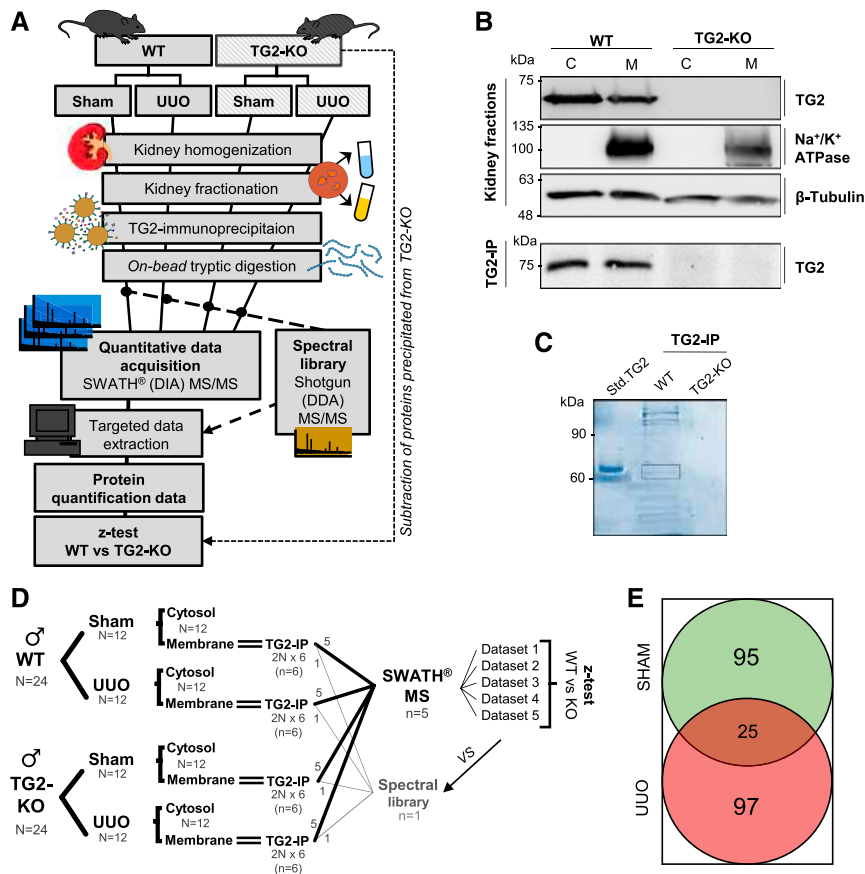
Figure 2. A comparative proteomic approach for the analysis of TG2 interactome in kidney fibrotic membranes. (A) Workflow of the strategy for the isolation of TG2 interacting proteins. TG2 was immunoprecipitated from kidney membrane fractions obtained from WT and TG2 null kidneys (used as negative controls). TG2 associated proteins were isolated by IP using a monoclonal anti TG2 antibody (IA12) crosslinked to magnetic beads. The TG2 coimmunoprecipitates (TG2 IP) were proteolytically digested directly on beads and analyzed *via* SWATH acquisition MS. Five TG2 IP samples per treatment were analyzed by data independent acquisition (DIA) using 34 static SWATH windows of *m/z* 15. A spectral library, produced by shotgun/data dependent acquisition (DDA) MS on a pool of all samples, was used for extracting the SWATH quantitative data. Differences between WT and TG2 KO precipitated proteins (representing the background) were identified by a paired sample *z* test, leading to the TG2 interactome. (B) Kidney fractions (membrane [M] and cytosolic [C]) were validated by Western blotting for enrichment of membrane marker (Na$^+$/K$^+$ ATPase) or tubulin. TG2 was detected in Western blots of the fractions before and after TG2 IP. (C) Coomassie staining of TG2 immunoprecipitates separated by SDS PAGE. The rectangular area identifies the precipitated TG2. Std. TG2, purified guinea pig liver TG2. (D) Sample size and animal numbers (*N*) used in the study; *n* indicates independent experiments. (E) Number of proteins identified as specifically associated with TG2 in UUO and sham operated kidney membranes by *z* test (*P*≤0.05; *n*≥4) after exclusion of nuclear, mitochondrial, and ribosomal proteins.

periglomerulus (Figure 1C). Notably, TG2-null UUO kidneys had a lower level of α-smooth muscle actin (Figure 1A) and active TGF-β (Figure 1B). Moreover, TG2-null kidneys displayed a reduced level of collagen deposition as confirmed by image analysis (Figure 1C). These data reveal that TG2

expression is important in fibrosis development post-UUO, because the disease develops more slowly if TG2 is absent from the extracellular environment.

To identify protein partners of TG2 in the murine UUO model of CKD (the "TG2 interactome"), we combined TG2 immunoprecipitation (IP) from whole-kidney membrane preparations of WT and TG2-null kidneys, sham and UUO, with quantitative proteomics by sequential window acquisition of all theoretical fragment ion spectra (SWATH) mass spectrometry (MS).[18] The TG2 IP proteome from the TG2 KO was subtracted from the respective TG2 IP WT proteome to reveal only the TG2-dependent interactions. An outline of this original approach is shown in Figure 2A. Cytosol and membrane fractions from WT and TG2 KO kidneys were validated by detection of Na$^+$/K$^+$ ATPase, which was solely displayed by the membrane lysate, and β-tubulin, which was present in both fractions (Figure 2B). TG2-associated complexes were isolated by IP using magnetic beads coated with anti-TG2 antibody. Western blotting confirmed the presence of TG2 in WT fractions (Figure 2B); additionally, SDS-PAGE followed by Coomassie blue staining revealed the presence of TG2-associated proteins in the membrane lysate of WT kidneys immunoprecipitated with anti-TG2 antibody and a very low level of proteins in TG2-null kidneys processed in the same way (Figure 2C). Proteins recruited by the anti-TG2 antibody beads were analyzed by quantitative proteomics. We used SWATH acquisition MS[18] to resolve proteomes at the highest possible sensitivity, reproducibility, and proteome coverage. To avoid bias from individual donors and achieve generalizable results, we performed five independent IP experiments, each on the basis of lysates generated from two animal donors, and a sixth IP to build the spectral library as outlined in Figure 2D; we used only male mice to avoid any sex/hormonal bias. Differences between WT and TG2-null precipitated proteins (representing the background) were established by a paired sample *z* test after analysis by SWATH processing (Figure 2, A and D, Supplemental Material). In this way, we could distinguish TG2-dependent protein recruitment from nonspecific background. However, not all of the TG2-associated proteins were expected to be directly bound to

Table 1. Specific TG2 partner proteins in the UUO kidney (membrane fraction)

Identification	Name	n	P Value	U/S
DESP	Desmoplakin	5	1.22E−13	U
HSP7C	Heat shock cognate 71 kD protein	5	7.67E−10	U
CALM	Calmodulin	5	1.83E−08	U/S
CAZA2	F actin capping protein subunit $\alpha 2$	5	1.97E−08	U
GPX1	Glutathione peroxidase 1	5	4.52E−07	U
ADH1	Alcohol dehydrogenase 1	5	9.40E−07	U/S
POSTN	Periostin	4	1.03E−06	U
MYO1D	Unconventional myosin Id	5	3.52E−06	U
GLRX1	Glutaredoxin 1	4	5.61E−06	U
GLRX3	Glutaredoxin 3	5	1.40E−05	U
PROF1	Profilin 1	5	1.89E−05	U
TGM2	Transglutaminase 2	5	3.31E−05	U/S
HSPB1	Heat shock protein $\beta 1$	5	3.68E−05	U
VATH	V type proton ATPase subunit H	5	5.98E−05	U
ADDG	γ Adducin	5	6.66E−05	U
AT2A2	Sarcoplasmic/endoplasmic reticulum calcium ATPase 2	5	8.58E−05	U
SVIL	Supervillin	4	1.01E−04	U
COR1C	Coronin 1C	5	1.38E−04	U
IQGA1	Ras GTPase activating like protein IQGAP1	5	1.50E−04	U/S
TCPE	T complex protein 1	5	3.17E−04	U
UBP5	Ubiquitin C terminal hydrolase 5	5	4.59E−04	U
FLOT2	Flotillin 2	4	5.38E−04	U
NAMPT	Nicotinamide phosphoribosyltransferase	5	6.56E−04	U/S
PCKGC	Phosphoenolpyruvate carboxykinase	5	8.93E−04	U/S
RAB1A	Ras related protein Rab 1A	5	9.16E−04	U
SDC4	Syndecan 4	5	9.34E−04	U
LDHA	L lactate dehydrogenase A chain	4	1.04E−03	U
MYO1G	Unconventional myosin Ig	5	1.21E−03	U
K1C20	Keratin, type I cytoskeletal 20	4	1.35E−03	U
COEA1	Collagen $\alpha 1$(XIV) chain	5	1.64E−03	U
COCA1	Collagen $\alpha 1$(XII) chain	4	1.68E−03	U
HIP1	Huntingtin interacting protein 1	4	1.86E−03	U
LIMS1	LIM and senescent cell antigen like containing domain protein 1	5	2.47E−03	U/S
SAR1B	GTP binding protein SAR1b	5	2.79E−03	U
SPTA1	Spectrin α chain, erythrocytic 1	5	2.92E−03	U/S
FLNA	Filamin A	5	2.98E−03	U
ANK3	Ankyrin 3	5	3.03E−03	U
PSD11	26S proteasome non ATPase regulatory subunit 11	5	3.09E−03	U
PGBM	Basement membrane specific heparan sulfate proteoglycan core protein (Perlecan)	5	3.16E−03	U
LSP1	Lymphocyte specific protein 1	5	3.53E−03	U
GELS	Gelsolin	5	4.61E−03	U
YKT6	Synaptobrevin homolog YKT6	5	4.72E−03	U
PTN6	Tyrosine protein phosphatase nonreceptor type 6	4	4.84E−03	U/S
FLNB	Filamin B	5	5.03E−03	U
TLN2	Talin 2	5	5.28E−03	U
PGK1	Phosphoglycerate kinase 1	4	5.39E−03	U/S
PICAL	Phosphatidylinositol binding clathrin assembly protein	4	5.65E−03	U/S
F120A	Constitutive coactivator of PPARγ like protein 1	5	6.27E−03	U/S
PRDX2	Peroxiredoxin 2	4	6.87E−03	U/S
KCC2D	Calcium/calmodulin dependent protein kinase type II subunit δ	5	7.10E−03	U
RTN4	Reticulon 4	5	7.57E−03	U
SERA	D 3 phosphoglycerate dehydrogenase	5	7.78E−03	U/S
KC1A	Casein kinase I isoform α	5	8.06E−03	U
DCTN1	Dynactin subunit 1	5	8.52E−03	U
ADDA	α Adducin	5	8.61E−03	U
PGS2	Decorin	5	1.09E−02	U

Table 1. Continued

Identification	Name	n	P Value	U/S
IF4G3	Eukaryotic translation initiation factor 4 γ3	5	1.11E−02	U/S
RHG18	Rho GTPase activating protein 18	4	1.11E−02	U
CAPZB	F actin capping protein subunit β	5	1.11E−02	U
MVP	Major vault protein	5	1.14E−02	U
TERA	Transitional endoplasmic reticulum ATPase	5	1.21E−02	U/S
ACTB	Actin, cytoplasmic 1	5	1.24E−02	U
PGS1	Biglycan	5	1.30E−02	U/S
K1C14	Keratin, type I cytoskeletal 14	5	1.33E−02	U
PLSL	Plastin 2	5	1.34E−02	U
AP2A2	AP 2 complex subunit α2	5	1.52E−02	U
FINC	Fibronectin	5	1.57E−02	U/S
CLCB	Clathrin light chain b	5	1.65E−02	U
SNX4	Sorting nexin 4	5	1.67E−02	U
SPTB1	Spectrin β chain, erythrocytic	5	1.73E−02	U
ZO1	Tight junction protein ZO 1	4	1.79E−02	U
DREB	Drebrin	5	1.83E−02	U
CAN1	Calpain1	5	1.84E−02	U
PDLI5	PDZ and LIM domain protein 5	5	1.85E−02	U
PUR6	Multifunctional protein ADE2	5	1.88E−02	U
MY18A	Unconventional myosin XVIIIa	5	1.93E−02	U
CLCA	Clathrin light chain A	5	2.07E−02	U
IRGM1	Immunity related GTPase family M protein 1	5	2.09E−02	U
NEB2	Neurabin 2	5	2.11E−02	U
K2C6B	Keratin, type II cytoskeletal 6B	5	2.14E−02	U
AP2A1	AP 2 complex subunit α1	5	2.15E−02	U
LYPA1	Acyl protein thioesterase 1	5	2.18E−02	U
PDC6I	Programmed cell death 6 interacting protein	5	2.38E−02	U/S
AP2B1	AP 2 complex subunit β	5	2.43E−02	U
K1C19	Keratin, type I cytoskeletal 19	5	2.58E−02	U
GRP78	78 kD Glucose regulated protein	5	2.59E−02	U
ARK72	Aflatoxin B1 aldehyde reductase member 2	5	2.61E−02	U
SNTB2	β2 Syntrophin	5	2.63E−02	U
MYO1B	Unconventional myosin Ib	5	2.67E−02	U
K6PP	ATP dependent 6 phosphofructokinase, platelet type	5	2.67E−02	U
C1QB	Complement C1q subcomponent subunit B	5	2.71E−02	U
F213A	Redox regulatory protein FAM213A	5	2.79E−02	U/S
HS90A	Heat shock protein HSP 90α	5	2.85E−02	U
GAK	Cyclin G associated kinase	5	2.86E−02	U
SPTN1	Spectrin α chain, nonerythrocytic 1	5	3.08E−02	U/S
UCK1	Uridine cytidine kinase 1	5	3.12E−02	U
ECHP	Peroxisomal bifunctional enzyme	5	3.15E−02	U/S
ES8L2	EGF receptor kinase substrate 8 like protein 2	4	3.29E−02	U
MOES	Moesin	5	3.33E−02	U
PNCB	Nicotinate phosphoribosyltransferase	5	3.34E−02	U
MYH10	Myosin 10	5	3.59E−02	U
RBGPR	Rab3 GTPase activating protein noncatalytic subunit	5	3.65E−02	U
VIME	Vimentin	5	3.66E−02	U
SERPH	Serpin 1H	5	3.81E−02	U
RPN1	Dolichyl diphosphooligosaccharide protein glycosyltransferase subunit 1	4	3.89E−02	U
LAMB2	Laminin subunit β2	4	3.92E−02	U/S
GSTT1	Glutathione S transferase θ1	5	3.95E−02	U
TCPQ	T complex protein 1	5	3.96E−02	U
TCPZ	T complex protein 1	5	4.23E−02	U/S
IRAK4	IL 1 receptor associated kinase 4	5	4.24E−02	U
C1TC	C 1 tetrahydrofolate synthase	5	4.28E−02	U

Table 1. Continued

Identification	Name	n	P Value	U/S
ARC1B	Actin related protein 2/3 complex subunit 1B	5	4.28E−02	U
SCFD1	Sec1 family domain containing protein 1	5	4.30E−02	U/S
COPB2	Coatomer subunit β	5	4.42E−02	U
FA49B	Protein FAM49B	5	4.62E−02	U
MYH14	Myosin 14	5	4.79E−02	U
SNX1	Sorting nexin 1	4	4.81E−02	U
PLST	Plastin 3	5	4.82E−02	U
GBP2	IFN induced guanylate binding protein 2	5	5.00E−02	U
SYEP	Bifunctional glutamate/proline tRNA ligase	5	5.17E−02	U
TCPA	T complex protein 1	5	5.25E−02	U
CLIC1	Chloride intracellular channel protein 1	5	5.33E−02	U

The association was evaluated by z analysis[58] ($P\leq0.05$; $n\geq4$) of $n=5$ independent experiments, which combined TG2 IP and SWATH MS, using the TG2-null mice as background control (as outlined in Figure 2, A and D). Nuclear and mitochondrial membrane proteins (Supplemental Figure 1) as well as ribosomal proteins (Supplemental Table 1) were manually removed. Proteins are denoted by full name and UniProtKB protein entry name (identification), and they are listed according to the specificity of the interaction with TG2 (P value). U/S, TG2-associated proteins in UUO and sham control membranes; U, TG2-associated proteins uniquely found in UUO membranes.

TG2; some molecules could be indirect partners of TG2, bound to its direct interactors. The complete list of 217 proteins di-rectly or indirectly associated with TG2 in UUO (122 proteins) or sham (120 proteins) kidney membranes, which were char-acterized by either a plasma membrane (PM) or ECM com-partmentalization or by a location in biologic fluids, is shown in Tables 1 and 2, respectively ($P\leq0.05$; identified in at least four of five experiments; $n\geq4$). Original processed data with statistical analysis are provided as Supplemental Appendix 1. There was little overlap (11.5%) between cell matrix proteins associated with TG2 in the normal (sham) and fibrotic kidneys (UUO) (Figure 2E). This is not surprising, because TG2 be-comes activated in disease both in terms of export[4,8] and in terms of enzymatic activity.[19,20] There was a considerable clus-ter of proteins uniquely part of the UUO TG2 interactome (44.7%) or exclusively associated with TG2 in the normal kidneys (43.8%) (Figure 2E). Membrane proteins previously re-ported to be exclusively located in nucleus and mitochondrial membranes were manually selected from the SWATH MS dataset according to the subcellular localization database "COMPARTMENTS" and UniProtKB (Supplemental Figure 1). Ribosomal proteins and Igs found in the membrane prep-aration are shown in Supplemental Table 1.

TG2 Interaction Networks Reveala Predominance of Vesicular Traffickingand Actin Dynamics Proteins in the UUO Kidney

Analysis of functions obtained by UniprotKB database (*Mus musculus*) revealed enrichment of TG2 interactions with proteins involved in vesicular trafficking and cytoskeletal actin dynamics in the UUO kidney (Figure 3A). Canonical TG2 partner proteins were present (*e.g.,* in cell adhesion, FN, SDC4, and collagens [COCA1 and COEA1]; in cytoskeleton, actin and filamin [FLNA and FLNB] [Figure 3B]), but there were also unexpected absences, such as the integrin family. This may be because of the transitory nature of integrin complexes, which can be only effec-tively captured by stabilizing the interaction with a chemical crosslinker.[21] Desmoplakin (involved in interepithelial cell adhe-sion), F-actin capping protein (CAZA2), and profilin-1 (PROF1; involved in actin cytoskeleton remodeling) were new highly sig-nificant partners of TG2 in UUO. Proteins that had never been associated or connected with TG2, such as a series of vesicular trafficking proteins like clathrin and adaptor proteins (CLCA, CLCB, AP2A1, AP2A2, and AP2B1), sorting nexins (SNX1 and SNX4), Alix (PDC6I), flotillin-2 (FLOT2), and heat shock cog-nate 71-kD protein (HSP7C), formed a large part of the TG2 UUO interactome (Figure 3B). Moreover, redox regulation pro-teins, such as glutathione peroxidase-1, glutaredoxin-1 (GLRX1), and GLRX3, were significant TG2 partners in the UUO (Figure 3B). There was a definite difference in the composition of the TG2 partners between the UUO and normal (sham) status, and pro-teins associated with TG2 uniquely in the UUO state were likely to influence its trafficking, activity, and regulation in fibrosis.

Network analysis of the TG2 interactomes built using the STRING v10 bioinformatics tool (on the basis of known and predicted protein-protein interactions) showed a clear cluster of proteins associated with membrane vesicles (Figure 4A, light blue), redox regulation (Figure 4A, pink), and cytoskeletal dynamics (Figure 4A, orange) in the UUO kidney. In contrast, in the TG2 interactome of the normal kidney (Figure 4B), there were changes in the topology of interconnections among the same functionally related protein groups, which were less represented, but denser clusters of metabolic proteins were evident (Figure 4B). Therefore, TG2 clearly becomes more interactive with vesicular trafficking proteins in the UUO as well as proteins linked to actin dynamics and ECM events.

Matching of the TG2 Interactome with the UUO Proteome

To exclude any concentration-dependent association with TG2, we evaluated if the proteins of the TG2 UUO interactome were also over-represented in the UUO proteome or associated with TG2 without being upregulated in the UUO. To this aim, we profiled the UUO and sham-operated kidney proteomes by

Table 2. Specific TG2 partner proteins in the sham control kidney (membrane fraction)

Identification	Name	n	P Value	U/S
PRS4	26S protease regulatory subunit 4	5	5.22E−09	S
PSME1	Proteasome activator complex subunit 1	5	8.91E−07	S
NEDD4	E3 ubiquitin protein ligase NEDD4	5	3.03E−05	S
K2C1B	Keratin, type II cytoskeletal 1b	4	8.40E−05	S
UN45A	Protein unc 45 homolog A	5	1.04E−04	S
TGM2	Transglutaminase 2	5	1.21E−04	U/S
PRUNE	Protein prune homolog	5	1.31E−04	S
NIBL1	Niban like protein 1	5	1.41E−04	S
PLEC	Plectin	5	1.80E−04	S
IF4G3	Eukaryotic translation initiation factor 4 γ3	5	1.82E−04	U/S
SERA	D 3 phosphoglycerate dehydrogenase	5	1.85E−04	U/S
TERA	Transitional endoplasmic reticulum ATPase	5	2.49E−04	U/S
PH4H	Phenylalanine 4 hydroxylase	5	2.67E−04	S
TOM1	Target of Myb protein 1	4	3.37E−04	S
PTN6	Tyrosine protein phosphatase nonreceptor type 6	4	4.04E−04	U/S
ACY3	N acyl aromatic L amino acid amidohydrolase	4	5.54E−04	S
TCPZ	T complex protein 1	5	6.52E−04	U/S
DEST	Destrin	5	8.51E−04	S
UB2D3	Ubiquitin conjugating enzyme E2 D3	5	9.25E−04	S
KAD1	Adenylate kinase isoenzyme 1	5	9.92E−04	S
G3P	Glyceraldehyde 3 phosphate dehydrogenase	5	1.05E−03	S
USP9×	Probable ubiquitin C terminal hydrolase FAF X	5	1.27E−03	S
PDIA1	Protein disulfide isomerase	4	1.40E−03	S
CASP3	Caspase 3	4	1.42E−03	S
UBP24	Ubiquitin C terminal hydrolase 24	4	1.43E−03	S
MEP1A	Meprin A subunit α	5	1.68E−03	S
ARF6	ADP ribosylation factor 6	5	1.88E−03	S
SPTA1	Spectrin α chain, erythrocytic 1	5	1.97E−03	U/S
TM55B	Type 1 phosphatidylinositol 4,5 bisphosphate 4 phosphatase	4	3.22E−03	S
KCRB	Creatine kinase B type	5	4.11E−03	S
RHEB	GTP binding protein Rheb	5	4.12E−03	S
SCFD1	Sec1 family domain containing protein 1	5	4.24E−03	U/S
ST1A1	Sulfotransferase 1A1	5	4.51E−03	S
ANXA2	Annexin A2	5	5.38E−03	S
CALM	Calmodulin	5	5.39E−03	U/S
F120A	Constitutive coactivator of PPARγ like protein 1	5	5.77E−03	U/S
OLFM4	Olfactomedin 4	5	5.80E−03	S
IST1	IST1 homolog	5	6.01E−03	S
PRDX2	Peroxiredoxin 2	4	6.07E−03	U/S
PP1A	Serine/threonine protein phosphatase PP1 α catalytic subunit	4	6.08E−03	S
NLTP	Nonspecific lipid transfer protein	5	6.29E−03	S
PPBT	Alkaline phosphatase, tissue nonspecific isozyme	5	6.39E−03	S
PDC6I	Programmed cell death 6 interacting protein	5	6.41E−03	U/S
ENOA	α Enolase	4	6.90E−03	S
FBLN1	Fibulin 1	5	7.33E−03	S
LIMS1	LIM and senescent cell antigen like containing domain protein 1	5	7.55E−03	U/S
TCPG	T complex protein 1 subunit γ	5	7.61E−03	S
GGA1	ADP ribosylation factor binding protein GGA1	5	8.30E−03	S
IRF3	IFN regulatory factor 3	4	8.39E−03	S
TBB5	Tubulin β5 chain	5	8.92E−03	S
FARP1	FERM, RhoGEF, and pleckstrin domain containing protein 1	5	9.63E−03	S
DJB11	DnaJ homolog subfamily B member 11	4	1.03E−02	S
ARF5	ADP ribosylation factor 5	5	1.03E−02	S
ARPC5	Actin related protein 2/3 complex subunit 5	4	1.06E−02	S
ARHGC	Rho guanine nucleotide exchange factor 12	5	1.10E−02	S
ARL2	ADP ribosylation factor like protein 2	5	1.14E−02	S

Table 2. Continued

Identification	Name	n	P Value	U/S
AT1B1	Sodium/potassium transporting ATPase subunit $\beta1$	5	1.21E−02	S
MGST3	Microsomal glutathione S transferase 3	5	1.21E−02	S
NSF	Vesicle fusing ATPase	5	1.28E−02	S
PGK1	Phosphoglycerate kinase 1	4	1.38E−02	U/S
ARL1	ADP ribosylation factor like protein 1	5	1.42E−02	S
AT1A1	Sodium/potassium transporting ATPase subunit $\alpha1$	5	1.43E−02	S
CUL5	Cullin 5	5	1.43E−02	S
VILI	Villin 1	5	1.51E−02	S
S12A3	Solute carrier family 12 member 3	5	1.55E−02	S
KS6A3	Ribosomal protein S6 kinase $\alpha3$	5	1.58E−02	S
TBA4A	Tubulin $\alpha4A$ chain	5	1.62E−02	S
VATA	V type proton ATPase catalytic subunit A	5	1.70E−02	S
SYWC	Tryptophan tRNA ligase	5	1.75E−02	S
CAH9	Carbonic anhydrase 9	4	1.76E−02	S
RAC2	Ras related C3 botulinum toxin substrate 2	5	1.85E−02	S
HBA	Hemoglobin subunit α	5	1.88E−02	S
RAB10	Ras related protein Rab 10	5	1.98E−02	S
PCKGC	Phosphoenolpyruvate carboxykinase	5	2.08E−02	U/S
NRK1	Nicotinamide riboside kinase 1	5	2.11E−02	S
VPS35	Vacuolar protein sorting associated protein 35	5	2.25E−02	S
SNX3	Sorting nexin 3	5	2.27E−02	S
ACSA	Acetyl CoA synthetase	5	2.29E−02	S
DNJA2	DnaJ homolog subfamily A member 2	5	2.29E−02	S
ST1D1	Sulfotransferase 1 family member D1	5	2.40E−02	S
ANFY1	Rabankyrin 5	5	2.42E−02	S
GLCTK	Glycerate kinase	5	2.42E−02	S
ARC1A	Actin related protein 2/3 complex subunit 1A	5	2.42E−02	S
PDIA6	Protein disulfide isomerase A6	5	2.53E−02	S
VATB2	V type proton ATPase subunit B	5	2.59E−02	S
GCYA3	Guanylate cyclase soluble subunit $\alpha3$	5	2.67E−02	S
LYPA2	Acyl protein thioesterase 2	5	2.68E−02	S
RUFY3	Protein RUFY3	4	2.72E−02	S
PICAL	Phosphatidylinositol binding clathrin assembly protein	4	2.73E−02	U/S
TBC9B	TBC1 domain family member 9B	5	2.78E−02	S
IQGA1	Ras GTPase activating like protein IQGAP1	5	2.99E−02	U/S
RCN1	Reticulocalbin 1	4	3.03E−02	S
ARP3	Actin related protein 3	5	3.04E−02	S
PGS1	Biglycan	5	3.18E−02	U/S
NAMPT	Nicotinamide phosphoribosyltransferase	5	3.20E−02	U/S
ECHP	Peroxisomal bifunctional enzyme	5	3.21E−02	U/S
HS90B	Heat shock protein HSP 90β	5	3.38E−02	S
ITM2B	Integral membrane protein 2B	5	3.60E−02	S
MP2K2	Dual specificity mitogen activated protein kinase kinase 2	5	3.62E−02	S
DHRS4	Dehydrogenase/reductase SDR family member 4	4	3.62E−02	S
TBA1A	Tubulin $\alpha1A$ chain	5	3.66E−02	S
IF4A1	Eukaryotic initiation factor 4A I	5	3.68E−02	S
OXSR1	Serine/threonine protein kinase OSR1	5	3.69E−02	S
F213A	Redox regulatory protein FAM213A	5	3.76E−02	U/S
CLIC4	Chloride intracellular channel protein 4	5	3.82E−02	S
VDAC1	Voltage dependent anion selective channel protein 1	5	3.87E−02	S
CAN2	Calpain 2 catalytic subunit	5	3.95E−02	S
NDRG3	Protein NDRG3	5	4.06E−02	S
CLH1	Clathrin heavy chain 1	5	4.11E−02	S
LAMB2	Laminin subunit $\beta2$	4	4.21E−02	U/S
FINC	Fibronectin	5	4.27E−02	U/S

Table 2. Continued

Identification	Name	n	P Value	U/S
TS101	Tumor susceptibility gene 101 protein	4	4.31E−02	S
DPYL3	Dihydropyrimidinase related protein 3	5	4.39E−02	S
ISG15	Ubiquitin like protein ISG15	5	4.53E−02	S
DRG2	Developmentally regulated GTP binding protein 2	5	4.71E−02	S
RN213	E3 ubiquitin protein ligase RNF213	4	4.73E−02	S
BAX	Apoptosis regulator BAX	5	4.73E−02	S
ADH1	Alcohol dehydrogenase 1	5	4.74E−02	U/S
SPTN1	Spectrin α chain, nonerythrocytic 1	5	5.25E−02	U/S
EF1A1	Elongation factor 1 α1	5	5.34E−02	S

The association was evaluated as described in Table 1. U/S, TG2-associated proteins in UUO and sham-operated membranes; S, TG2-associated proteins uniquely found in sham-operated membranes.

SWATH MS (Supplemental Tables 2 and 3). This was necessary, because current UUO proteomes are of limited coverage.[22] Of the 2106 proteins quantified in the UUO proteome, 195 were significantly upregulated in kidneys post-UUO (Supplemental Table 2), and 458 were downregulated (Supplemental Table 3) (confidence >80%). Original processed data are provided as Supplemental Appendix 2.

TG2 signal was increased but only less than twice the physiologic level (1.71-fold) (Supplemental Table 2, TGM2), consistent with prior observations that UUO leads to an increase
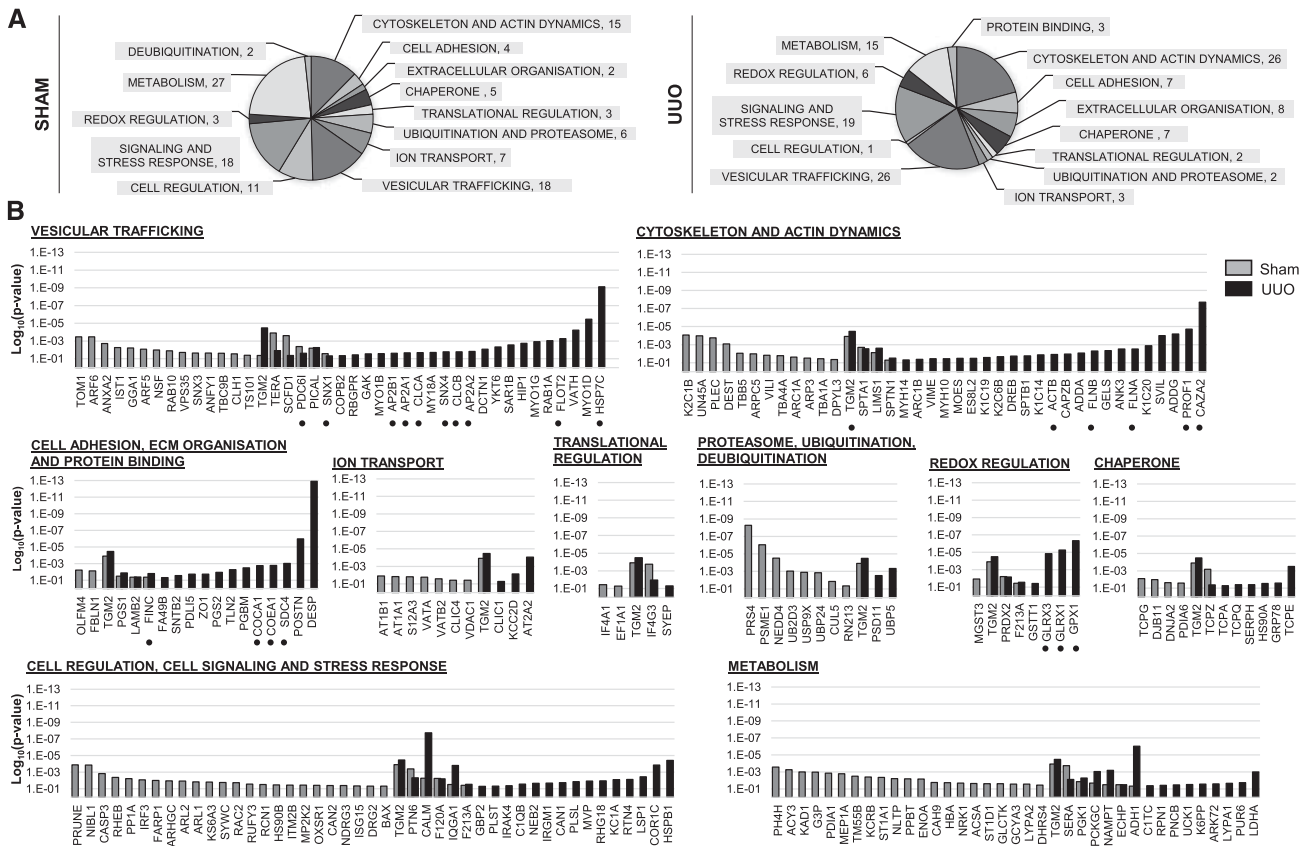

Figure 3. Functional distribution of TG2 associated proteins in kidney membranes reveals a difference in TG2 partners between the UUO and normal (sham) status. TG2 associated proteins were clustered depending on their functions in *M. musculus* investigated by protein identification search on UniProtKB database. (A) Pie charts display the distribution of the different functions of the TG2 associated proteins in UUO or sham controls, with numbers next to each function name denoting how many proteins fall in the various functional categories. (B) Column charts list proteins in the order of significance of their association with TG2 (log$_{10}$ P value) and are grouped according to their function in UUO and sham controls (histogram bars). Dots under protein names denote proteins described in Results.
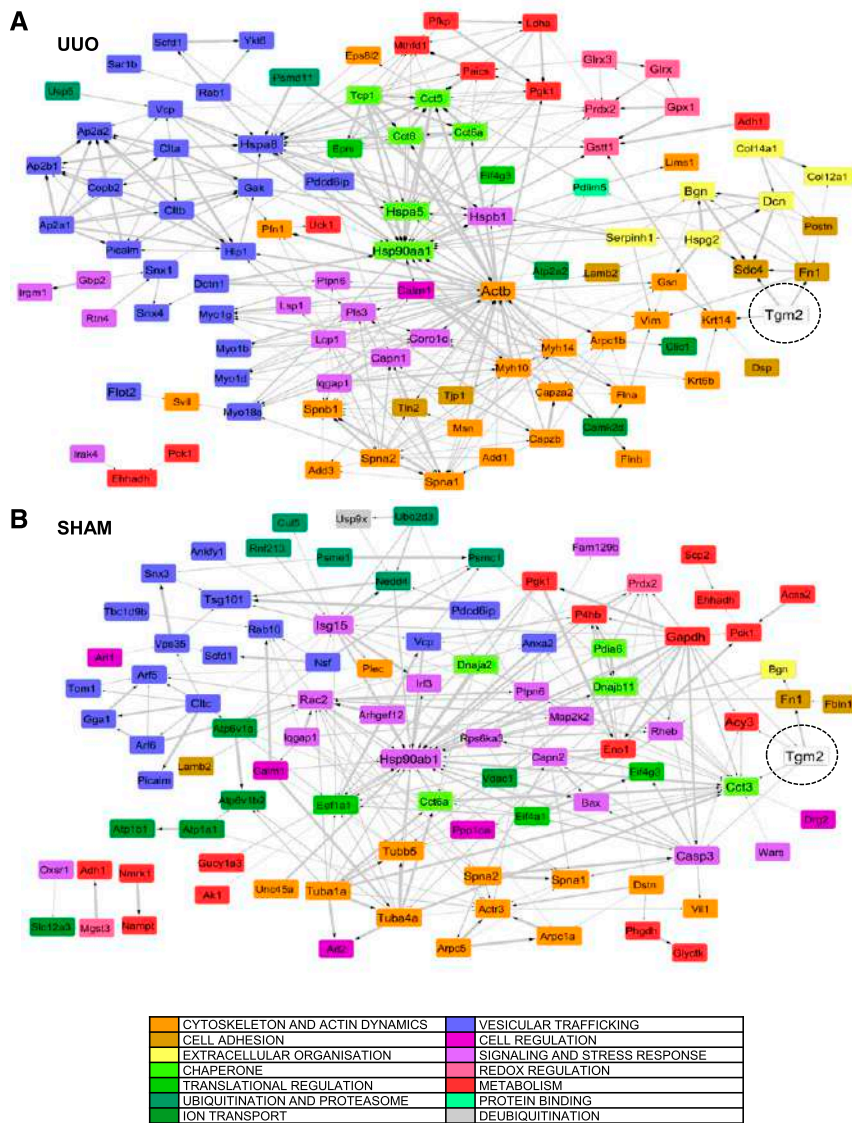
Figure 4. The interactome of TG2 in UUO and sham control kidney reveals increased interactivity of TG2 with proteins related to vesicular trafficking, cytoskeleton, and ECM dynamics in the UUO model. The protein interaction network built from TG2 associated proteins in (A) UUO and (B) sham operated kidney membranes was mapped against the *M. musculus* reference database using String V10.0 (http://string db.org). Candidates were selected using both known and predicted protein interactions and a threshold confidence level of 0.4 (default). Networks were imported in Cytoscape and color coded according to the main functional nodes. The thickness of the lines is proportional to the confidence of the interactions.

there were periostin (a marker of progressive kidney injury in animal models of CKD),[23] myosin-1D, PROF1, CAZA-2, heat shock protein β1, FN, laminin, collagen (COCA1), and actin nucleation complex ARC1B. A number of these TG2 partners sat in pathways over-represented in the UUO model ("ECM-receptor interaction" and "regulation of the actin cytoskeleton") (Supplemental Figure 2), suggesting that they act in synergy with TG2 in fibrosis progression. However, a significant level of TG2 partners, such as HSP7C, SDC4, and the antioxidant proteins glutathione peroxidase-1 and GLRX1 (Figure 5C, left panel), was either decreased or was not significantly over-represented in the UUO proteome, raising the possibility that they could be essential partners of TG2, some of which were potentially implicated in the externalization pathway of TG2 post-UUO.

TG2 Association with Exosomal Proteins Post-UUO

The TG2 interactome has revealed that TG2 primarily interacts with a number of proteins associated with vesicular trafficking and EVs, especially in the UUO condition. When the TG2 partners identified in the UUO model (Table 1) were matched with proteins collected in the EVs (exosome) database ExoCarta (and its compendium Vesiclepedia), almost all proteins associated with TG2, either directly or indirectly, were nominated in the database (Table 3). These included the prominent exosome marker Alix (PDC6I), HSP7C, PROF1, FLOT2, and heat shock protein HSP90-α, all among the top 50 proteins reported in exosomes. Other significant exosomal TG2 partners less recurrent in the exosome database were PRDX2, RAB1A, and SDC4 (Table 3). These findings support the hypothesis that TG2 may be trafficked and externalized *via* EVs, either of endosomal origin (exosomes) or shed from the PM (ectosomes).

TG2 Secretion *via* Exosomesand Ectosomesi Established Epithelial Cell Lines

Previous reports have shown that TG2 is mainly secreted by TECs, although renal fibroblasts and mesangial cells are less investigated sources.[4,5] To test the hypotheses that TG2 is externalized in the UUO in EVs and that this pathway is increased in the pathologic state, we used an established rat renal TEC line (NRK52E) stably transfected with EGFP-tagged TG2 to facilitate tracking of TG2. Exosomes and ectosomes were

in TG2 secretion rather than expression.[12] Protein class annotation terms were associated with ECM components, cytoskeletal organization, and cell adhesion, forming significant clusters of the UUO proteome ($P \leq 0.05$) (Figure 5A, Supplemental Table 4A).

Among the proteins most significantly associated with TG2 in the UUO kidney ($P \leq 0.001$ in Table 1), which were also intensified in the UUO proteome (Figure 5C, right panel),
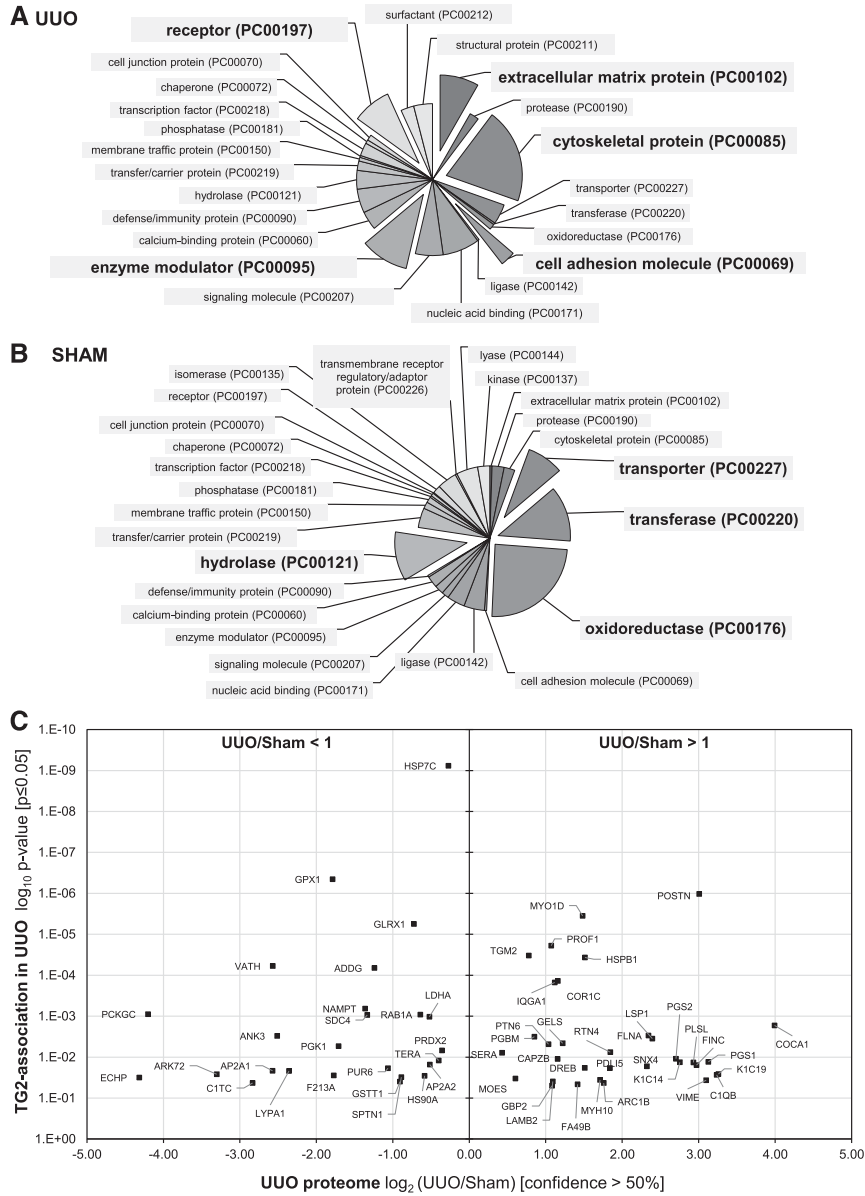
Figure 5. Interrogation of the UUO proteome with TG2 interacting proteins uncovers essential partners of TG2 in UUO kidney membranes. The proteomes of the UUO kidneys and sham operated control kidneys were resolved by quantitative SWATH acquisition proteomics. (A and B) Functional distribution of proteins with signal (A) increased (n 195) or (B) decreased (n 458) on UUO compared with sham control (confidence ≥80%) was performed in PANTHER using the relative annotation terms ontologies. Each pie chart sector represents the percentage of the proteome belonging to the specific PANTHER class over the total number of class hits. (C) Interrogation of the UUO proteome (confidence ≥50%) with the TG2 interacting proteins identified in UUO kidney membranes ($P ≤ 0.05$) and reported in Table 1. The 122 proteins specifically associated with TG2 in UUO kidney membranes were plotted on the ordinate axis according to the significance (P value) of TG2 association and the abscissa according to their expression in the UUO kidney proteome compared with sham control proteome: $\log_2$(UUO/sham). A positive value on the abscissa indicates the increased signal of a given TG2 associated protein partner on UUO compared with the sham operated condition (UUO/sham >1), and a negative value indicates its decreased signal on UUO (UUO/sham <1).

isolated from the supernatant of cells according to standard protocols[24,25] (Figure 6A). After removal of cells and cellular debris, ectosomes were recovered by differential centrifugation in the P3 fraction (2.97×10^7 particles per 1 ml medium) and smaller exosomes were recovered in the P4 fraction (5.89×10^7 particles per 1 ml medium) as revealed by tunable resistive pulse sensing analysis with a qNano instrument (Figure 6B). The EV-free medium was collected (S4), and all nonvesicular proteins were recovered by TCA precipitation. The fractions were subjected to Western blot analysis using antibodies toward the EV marker FLOT2 (Figure 6C).

To test for the presence of TG2 in the EVs fractions, equal amounts of proteins (20 μg) extracted from ectosomes (P3) and exosomes (P4) and those from the vesicles-free medium (S4; after TCA protein precipitation) were immunoprobed using antibodies against TG2 and the EGFP tag. Both endogenous (75 kD) and EGFP-tagged TG2 (100 kD) were clearly present in the exosomes (P4) and in lower amounts in the ectosome (P3) fraction (Figure 7A). Densitometric analysis of TG2 relative to FLOT2 revealed a trend of enrichment of TG2 in the exosome fraction (P4) (Figure 7A). Cells were also stimulated by recombinant TGF-β1 (10 ng/ml) to simulate conditions of fibrogenesis *in vitro*. TGF-β1 did not change the level of TG2 in the total cell lysate (TL) but caused a trend of increase in the exosome-associated TG2 (Figure 7B). The cytokine affected the expression of FLOT2 in TL and EVs but without reaching significance (Figure 7B). When the same experiment was conducted in the nontransfected NRK52E cells, TG2 was present prevalently in exosomes (Figure 7C). Treatment with TGF-β1 caused a trend of increase in TG2 in the exosomal fraction, which became enriched in TG2 relative to FLOT2 expression. As an additional analysis, we isolated exosomes and ectosomes from an established renal fibroblast cell line (NRK49F). TG2 was present in the ectosomal and exosomal fractions, and the band was increased by TGF-β1 (Supplemental Figure 3). The EV-free medium (S4) was also collected from both the EGFP-TG2 NRK52E clone and the WT NRK52E, and all proteins were recovered

Table 3. Matching of TG2 partner proteins to exosomal proteins

Identification	TG2 Associated Candidate Names in UUO	Found in Exosomes	
		Homo sapiens	*Rattus norvegicus*
DESP	Desmoplakin	Match	
HSP7C[a]	Heat shock cognate 71 kD protein	Match	Match
CALM	Calmodulin	Match	Match
CAZA2	F actin capping protein subunit α2	Match	Match
GPX1	Glutathione peroxidase 1	Match	Match
ADH1	Alcohol dehydrogenase 1	Match	Match
POSTN	Periostin	Match	Match
MYO1D	Unconventional myosin Id	Match	
GLRX1	Glutaredoxin 1	Match	
GLRX3	Glutaredoxin 3	Match	Match
PROF1[a]	Profilin 1	Match	Match
TGM2	Transglutaminase 2	Match	Match
HSPB1	Heat shock protein β1	Match	Match
VATH	V type proton ATPase subunit H	Match	Match
ADDG	γ Adducin		
AT2A2	Sarcoplasmic/endoplasmic reticulum calcium ATPase 2	Match	Match
SVIL	Supervillin		
COR1C	Coronin 1C	Match	Match
IQGA1	Ras GTPase activating like protein IQGAP1	Match	Match
TCPE	T complex protein 1		
UBP5	Ubiquitin C terminal hydrolase 5		
FLOT2[a]	Flotillin 2	Match	Match
NAMPT	Nicotinamide phosphoribosyltransferase	Match	Match
PCKGC	Phosphoenolpyruvate carboxykinase	Match	Match
RAB1A	Ras related protein Rab 1A	Match	Match
SDC4	Syndecan 4	Match	Match
LDHA[a]	L lactate dehydrogenase A chain	Match	Match
MYO1G	Unconventional myosin Ig	Match	
K1C20	Keratin, type I cytoskeletal 20	Match	
COEA1	Collagen α1(XIV) chain	Match	
COCA1	Collagen α1(XII) chain	Match	
HIP1	Huntingtin interacting protein 1	Match	
LIMS1	LIM and senescent cell antigen like containing domain protein 1	Match	Match
SAR1B	GTP binding protein SAR1b	Match	
SPTA1	Spectrin α chain, erythrocytic 1		
FLNA	Filamin A	Match	Match
ANK3	Ankyrin 3		Match
PSD11	26S proteasome non ATPase regulatory subunit 11	Match	
PGBM	Basement membrane specific heparan sulfate proteoglycan core protein (Perlecan)		
LSP1	Lymphocyte specific protein 1	Match	
GELS	Gelsolin	Match	Match
YKT6	Synaptobrevin homolog YKT6	Match	
PTN6	Tyrosine protein phosphatase nonreceptor type 6	Match	
FLNB	Filamin B	Match	Match
TLN2	Talin 2	Match	Match
PGK1[a]	Phosphoglycerate kinase 1	Match	Match
PICAL	Phosphatidylinositol binding clathrin assembly protein	Match	Match
F120A	Constitutive coactivator of PPARγ like protein 1	Match	
PRDX2	Peroxiredoxin 2	Match	Match
KCC2D	Calcium/calmodulin dependent protein kinase type II subunit δ	Match	
RTN4	Reticulon 4	Match	Match
SERA	D 3 phosphoglycerate dehydrogenase	Match	
KC1A	Casein kinase I isoform α	Match	
DCTN1	Dynactin subunit 1	Match	Match

Table 3. Continued

Identification	TG2 Associated Candidate Names in UUO	Found in Exosomes	
		Homo sapiens	*Rattus norvegicus*
ADDA	α Adducin	Match	
PGS2	Decorin	Match	
IF4G3	Eukaryotic translation initiation factor 4 γ3	Match	
RHG18	Rho GTPase activating protein 18	Match	
CAPZB	F actin capping protein subunit β	Match	Match
MVP	Major vault protein	Match	Match
TERA[a]	Transitional endoplasmic reticulum ATPase	Match	
ACTB[a]	Actin, cytoplasmic 1	Match	Match
PGS1	Biglycan	Match	
K1C14	Keratin, type I cytoskeletal 14	Match	
PLSL	Plastin 2	Match	Match
AP2A2	AP 2 complex subunit α2	Match	
FINC	Fibronectin	Match	
CLCB	Clathrin light chain b	Match	
SNX4	Sorting nexin 4	Match	
SPTB1	Spectrin β chain, erythrocytic	Match	
ZO1	Tight junction protein ZO 1	Match	
DREB	Drebrin	Match	
CAN1	Calpain1	Match	
PDLI5	PDZ and LIM domain protein 5	Match	
PUR6	Multifunctional protein ADE2	Match	Match
MY18A	Unconventional myosin XVIIIa	Match	
CLCA	Clathrin light chain A	Match	Match
IRGM1	Immunity related GTPase family M protein 1		
NEB2	Neurabin 2		
K2C6B	Keratin, type II cytoskeletal 6B	Match	
AP2A1	AP 2 complex subunit α1	Match	
LYPA1	Acyl protein thioesterase 1	Match	Match
PDC6I[a]	Programmed cell death 6 interacting protein	Match	Match
AP2B1	AP 2 complex subunit β	Match	Match
K1C19	Keratin, type I cytoskeletal 19	Match	
GRP78	78 kD Glucose regulated protein	Match	Match
ARK72	Aflatoxin B1 aldehyde reductase member 2	Match	Match
SNTB2	β2 Syntrophin	Match	
MYO1B	Unconventional myosin Ib	Match	
K6PP	ATP dependent 6 phosphofructokinase, platelet type		
C1QB	Complement C1q subcomponent subunit B	Match	Match
F213A	Redox regulatory protein FAM213A	Match	
HS90A[a]	Heat shock protein HSP 90α	Match	Match
GAK	Cyclin G associated kinase	Match	
SPTN1	Spectrin α chain, nonerythrocytic 1		Match
UCK1	Uridine cytidine kinase 1		
ECHP	Peroxisomal bifunctional enzyme	Match	Match
ES8L2	EGF receptor kinase substrate 8 like protein 2	Match	
MOES[a]	Moesin	Match	Match
PNCB	Nicotinate phosphoribosyltransferase	Match	Match
MYH10	Myosin 10	Match	Match
RBGPR	Rab3 GTPase activating protein noncatalytic subunit	Match	
VIME	Vimentin	Match	Match
SERPH	Serpin 1H	Match	Match
RPN1	Dolichyl diphosphooligosaccharide protein glycosyltransferase subunit 1		Match
LAMB2	Laminin subunit β2	Match	Match
GSTT1	Glutathione S transferase θ1		Match
TCPQ	T complex protein 1		

Table 3. Continued

Identification	TG2 Associated Candidate Names in UUO	Found in Exosomes	
		Homo sapiens	*Rattus norvegicus*
TCPZ	T complex protein 1	Match	
IRAK4	IL 1 receptor associated kinase 4		
C1TC	C 1 tetrahydrofolate synthase	Match	Match
ARC1B	Actin related protein 2/3 complex subunit 1B	Match	Match
SCFD1	Sec1 family domain containing protein 1	Match	
COPB2	Coatomer subunit β	Match	Match
FA49B	Protein FAM49B	Match	Match
MYH14	Myosin 14	Match	
SNX1	Sorting nexin 1	Match	
PLST	Plastin 3	Match	
GBP2	IFN induced guanylate binding protein 2		Match
SYEP	Bifunctional glutamate/proline tRNA ligase	Match	Match
TCPA[a]	T complex protein 1	Match	Match
CLIC1[a]	Chloride intracellular channel prot 1	Match	Match

Partners of TG2 in the UUO kidney (Table 1) listed in order of significance of their association with TG2 were matched with exosomal proteins provided by the Exocarta database[59] (*H. sapiens* and *R. norvegicus* datasets).
[a]These proteins are among the top 50 exosome markers.

by TCA precipitation. A trace of endogenous TG2 was occasionally present freely in the culture medium (S4) of NRK52E-expressing EGFP-TG2 on TCA precipitation (Figure 7, A and B), and TG2 immunoreactivity was seen in high molecular weight polymers in the S4 fraction of WT NRK52E (Figure 7C). Our data suggest that the free TG2 may be transient and unstable and that it either self-polymerizes or becomes incorporated in circulating proteins (Figure 7C, asterisk); moreover, it is not increased by TGF-β1 (Figure 7, B and C).

To gain insights into the location of TG2 within EVs, we devised an experiment aimed at measuring the catalytic activity of TG2 of whole EVs and lysed EVs (providing the total EVs homogenate) isolated from NRK52E cells. As a control, we also measured TG2 activity in lysed cell homogenates and whole cells. In the ectosomes (P3), TG2 activity was similar in the intact vesicles and vesicles lysed in a buffer dissolving cytosolic proteins; in the exosomes (P4), there was a higher proportion of TG2 detected in the intact particles compared with the EV lysate, suggesting that TG2 is enriched on the surface of exosomes but without reaching significance (P 0.14). No TG2 activity was detected in the EV-free medium, and levels of TG2 were similar on the surface of NRK52E cells and in the cell lysate (Figure 7D).

Collectively, these results show that TG2 is clearly present in EVs and suggest that TGF-β1 directs TG2 toward exosome secretion.

Inhibition of Neutral Sphingomyelinase Affects Exosome Release of TG2

In several mammalian cell types, the biogenesis of exosome secretion depends on sphingomyelinase for the production of ceramide of which exosomes are rich.[26] We, therefore, investigated whether the sphingomyelinase inhibitor GW4869, which blocks neutral sphingomyelinase (N-SMase), affected

exosome release of TG2. After treatment of NRK52E-expressing EGFP-TG2 with GW4869 (10 μM) for 16 hours,[27] FLOT2 was decreased in the exosomal fraction (P4) (Figure 8A), consistent with a reduction of total exosome release, and this was accompanied by a marked reduction of TG2 in the same fraction (Figure 8A). The ectosome fraction (P3) did not seem to be sensitive to inhibition of N-SMase as previously described in glial cells,[24] and GW4869 produced no difference in the ectosome release of TG2 (Figure 8A). Vesicular export of TG2 was visualized by immunofluorescence staining using high-resolution confocal microscopy in EGFP-TG2–expressing NRK52E cells. Extracellular TG2 was detected by an anti-EGFP antibody in nonpermeabilized cells (denoted by the red fluorescence), whereas the green fluorescence represents the total EGFP-TG2. Minimum washing of the monolayer before fixation to prevent exosome loss revealed an intense punctate pattern of extracellular EGFP-TG2 staining, which was increased in TGF-β1–stimulated cells. GW4869 visibly inhibited extracellular EGFP-TG2 staining, suggesting that it inhibits TG2 export (Figure 8B). EGFP fluorescence visualization of exosomes isolated from NRK52E-expressing EGFP-TG2 and incubated with WT NRK52E revealed a similarly punctuated staining, which was retained in the WT NRK52E monolayer after several washes, suggesting that this consists of EVs containing EGFP-TG2 (Figure 8C, Hep). Pretreatment of NRK52E with heparitinase to remove the HS chains before addition of EGFP-TG2–containing exosomes reduced the exosome uptake by 49% ($P<0.01$) (Figure 8C, +Hep), suggesting a role for cell surface HS in the capturing of EVs.

To attenuate the formation of ectosomes, we used the inhibitor of Na$^+$/H$^+$ exchanges amiloride, which interferes with the activity of the efflux pumps expressed on acidic vacuoles and the exocytosis of micropinosomes.[28–31] Ectosomes (P3) formed in a greater proportion than exosomes (P4) in a short
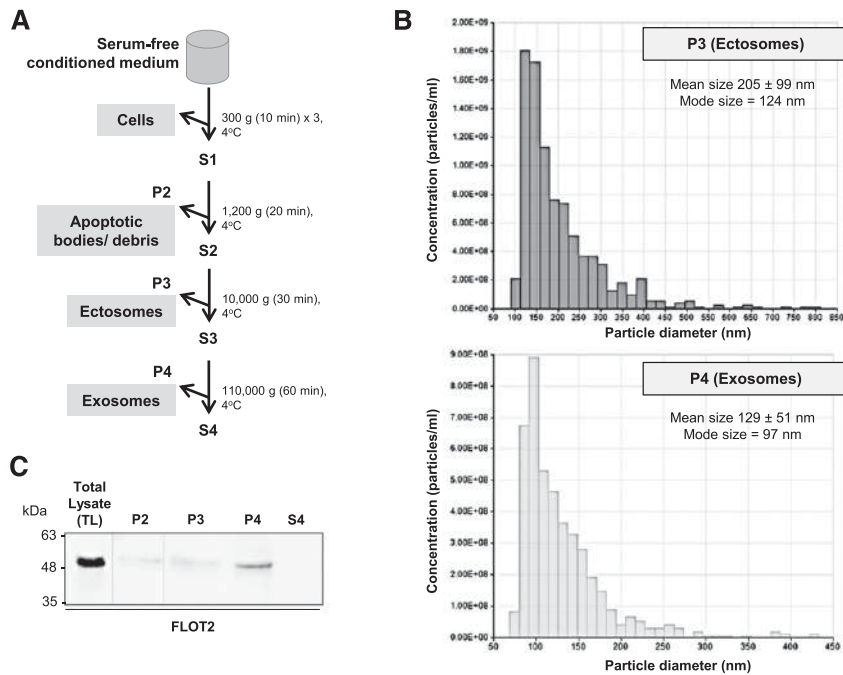
Figure 6. A differential centrifugation approach allows the isolation of EVs subpopulations from NRK52E conditioned medium. (A) Flowchart of the differential centrifugation steps for the isolation of EVs. P1 P4 indicate pellets, and S1 S4 indicate supernatants. (B) Analysis of microparticle size distribution in fractions P3 and P4 was performed by nanoparticle tracking analysis with qNano (Izon). Ectosomes were recovered from the P3 fraction, and exosomes were recovered from the P4 fraction. Representative particle size distributions of an ectosome enriched 10,000 g pellet (dark gray) and an exosome enriched 110,000 g pellet (light gray). (C) Expression of FLOT2 was measured by Western blotting in equal amounts from the differential centrifugation fractions obtained from the conditioned medium of NRK52E cells cultured in serum free conditions.

time of incubation (10 minutes) as previously shown,[32] and they were revealed by the faint FLOT2 staining in the exosome fraction (Figure 8D). Amiloride incubation lowered FLOT2 in the ectosomes (P3), being that amiloride is an inhibitor of MV formation,[33] and consistent with this, there was a reduction in TG2 in ectosomes (Figure 8D).

Collectively, these results indicate that TG2 is transported into exosomes and ectosomes and that this pathway is stimulated by profibrogenic TGF-β1 in exosomes.

Recruitment of TG2 in Exosomes Depends on SDC4

Another protein that we found specifically present in TG2 UUO interactome is the cell surface HS proteoglycan SDC4 (Table 1). Syndecans have been reported to bind cargo with HS chains, leading to their clustering and recruitment of syntenin-1 and Alix for membrane budding with exosome formation.[34] Therefore, we hypothesized that TG2 may be recruited as an HS binding cargo and targeted to exosomes by SDC4. To test the role of SDC4 in EV-associated TG2 secretion, NRK52E-expressing EGFP-TG2 was transiently transfected with either rat SDC4-targeting siRNA or scrambled control

siRNA. SDC4 reduction by SDC4-targeting siRNA (SDC4 KO) was confirmed by Western blotting of the TL (Figure 9A). As a control for the proteoglycan immunodetection (which is notoriously difficult), NRK52E transiently transfected with a hemagglutinin (HA)-tagged SDC4 construct revealed a similar band in the 30-kD range when probed with anti-HA antibody (Figure 9B). Culture medium was collected from the SDC4 KO cells and EV fractions separated by serial centrifugation. Proteins and complexes from EV-deprived medium were precipitated by TCA as described before. As shown in Figure 9C, KO of SDC4 by siRNA did not change TG2 expression in TL, but it greatly reduced TG2 in exosome (P4) fractions, affecting the vesicular secretion of TG2. SDC4 KO also reduced the low level of free TG2 found in the EV-free conditioned medium (S4) (Figure 9C). As shown by quantifications (Figure 9D), KO of SDC4 by siRNA did not change expression of FLOT in ectosome (P3) and exosome (P4) fractions. IP of SDC4 from exosomes and ectosome lysates revealed SDC4 immunoreactivity in the two fractions, but SDC4 clearly pulled down TG2 only from exosomes (Figure 9E), suggesting a direct interaction of TG2 and SDC4 within EVs only in exosomes. Given the affinity of TG2 for the HS chains of SDC4[13,35] and their coassociation within exosomes shown here, our data suggest that TG2 is recruited as an HS binding cargo and targeted to exosomes by SDC4.

Vesicular Trafficking of TG2 *Ex Vivo* Depends on SDC4

To examine TG2 release and investigate the role played by SDC4 further, primary cortical TECs, fibroblasts, and mesangial cells were isolated from WT (SDC4^{+/+}) and SDC4 KO (SDC4[/]) mice,[36] and the level of extracellular TG2 was measured in live cells by a well established enzymatic assay.[37] SDC4 deletion (SDC4[/]) resulted in lower TG2 externalization in all of the three primary renal cell types (Figure 10A), with no changes in the total level of TG2 activity between SDC4^{+/+} and SDC4[/] genotypes (Figure 10B). TECs displayed the highest level of extracellular TG2 compared with the total TG2 activity (Figure 10, A and B). The decreased TG2 externalization in SDC4[/] cells (Figure 10A) was accompanied by a lower level of membrane TG2 as measured by Western blotting of membrane fractions (Figure 10C) and an increased level of cytosolic TG2 (Figure 10D), suggesting TG2 retention. Total TG2 expression was not lowered by SDC4 KO when revealed by Western blotting of TLs (Figure 10E). The increment in total TG2
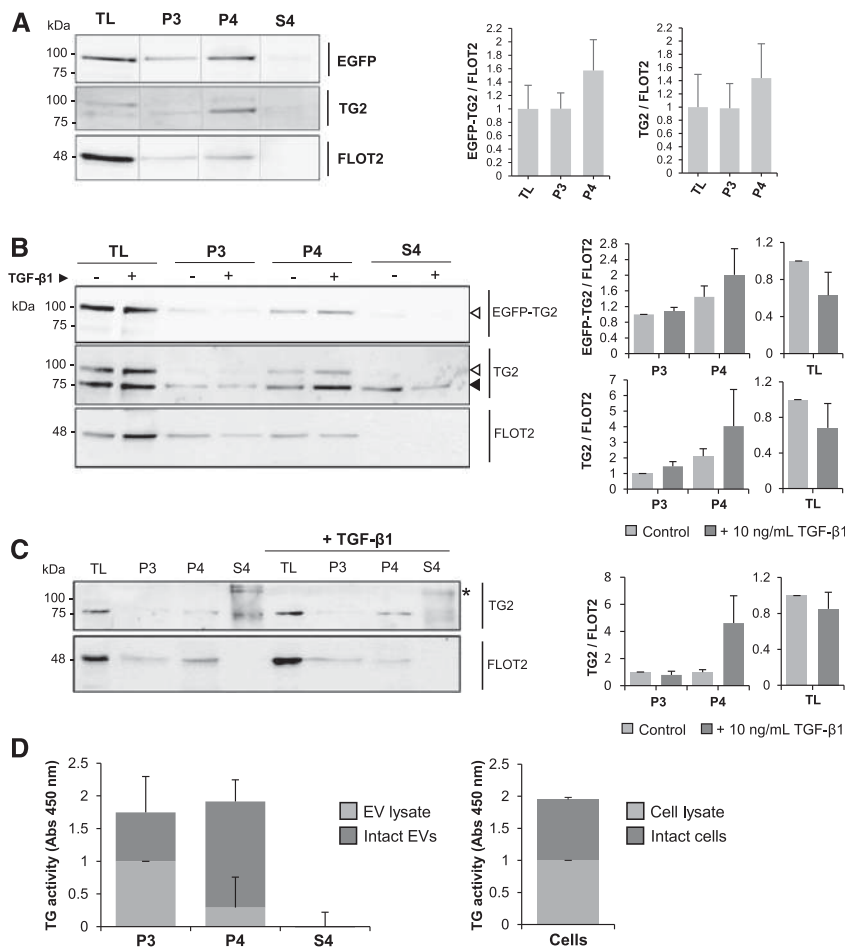
Figure 7. TG2 is present in vesicles of endosomal and plasma membrane origin in established TEC lines. (A and B) NRK52E expressing EGFP TG2 and (C) WT NRK52E cells were grown in serum free medium for 36 hours (A) without and (B and C) with supplementation of 10 ng/ml TGF β1. After incubation, culture medium was col lected, and vesicular fractions (P3 and P4) were separated by serial centrifugation as shown in Figure 6. Proteins from vesicles deprived medium were concentrated by TCA precipitation (S4). Fractions and cell lysate (TL) were immunoprobed with primary antibodies toward the EGFP tag, TG2, or FLOT2. Intensity of immunoreactive bands was quantified by densitometric analysis and normalized to FLOT2 expression. Data represent mean values of three independent experiments ±SEM. Black arrowhead, endogenous TG2; white arrowheads, EGFP TG2. *TG2 polymers. (D) EVs obtained from NRK52E EGFP TG2 conditioned medium were either lysed in a mild lysis buffer to obtain a total lysate or resuspended as intact vesicles in sample buffer (from a tissue transglutaminase picoassay kit). The transamidating activity of TG2 was measured in either the whole EVs or the EV lysate by a sensitive "picoassay." As a control, TG2 activity was also measured in TL and whole cells. Data represent mean values of three independent experiments ±SEM.

protein in SDC4 $^{/}$ mesangial cells, compared with SDC4$^{+/+}$ cells, may be a compensatory event of TG2 overproduction consequent to the defect in TG2 secretion (Figure 10E). Therefore, SDC4 KO impaired TG2 membrane distribution and externalization, with an increased retention of intracellular TG2 in the three primary renal cell types. To visualize TG2 trafficking in live cells, the primary WT and SDC4-null TECs

were transiently transfected with an EGFP-tagged TG2 cDNA and visualized by live confocal microscopy (Supplemental Movie 1). EGFP-TG2 was recruited in globular elements continuously protruding and retracting from the PM and moving along the PM at the periphery of the cell. Budding of TG2-storing vesicles from the PM was evident. However, EGFP-TG2 was less dynamic and appeared confined in the cytosol in the SDC4-null TECs, which also had less budding activity than the WT TECs. When SDC4 cDNA was transfected back to SDC4-null TECs, EGFP-TG2 vesicular blebbing was largely resumed, and budding was reconstituted to WT levels (quantifications of extracellular TG2 activity are in Figure 10F, Supplemental Movie 1). These data show for the first time a dependence of TG2 vesicular trafficking on SDC4 and also suggest that SDC4 could be implicated in general EV dynamics of TECs involving cargo proteins with affinity for HS, like TG2.

### TG2 Positive Exosomes in Urine Samples of Patients with CKD

To verify whether TG2 is released *via* exosomes in human CKD, we isolated EVs from pooled urine samples collected from a small cohort of patients with CKD (*n* 10) with stages 3 and 4 primary kidney disease and from healthy controls (*n* 5). Immunoblotting of equal amounts of samples (Supplemental Figure 4) revealed the presence of TG2 exclusively in the exosomes (P4) fractions, with an intensification of the band in the exosomes from the patients with CKD. There was no TG2 band in the ectosomes (P3) or the EV-free urine. FLOT was used as an EV marker, and it also intensified in the exosomes of patients with CKD. We previously reported the increased presence of TG2 in urines of patients with CKD by sandwich ELISA.[38] Data in this study show that TG2 is conveyed by EVs in urines, validating our finding in human CKD.
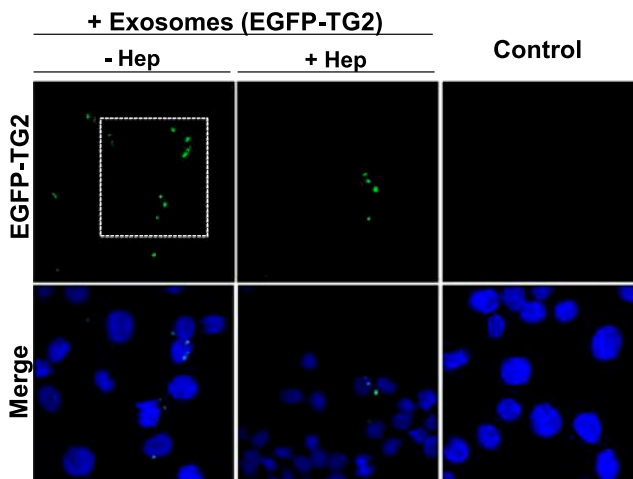
DISCUSSION

This is the first unbiased global analysis of TG2-interacting proteins in a model of CKD (the murine UUO type). TG2-associated proteins were identified using an original targeted proteomic strategy by combining TG2 IP from whole-kidney membrane preparations of WT kidneys with negative control
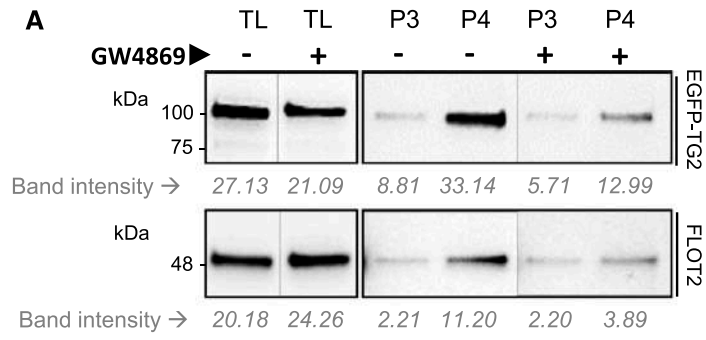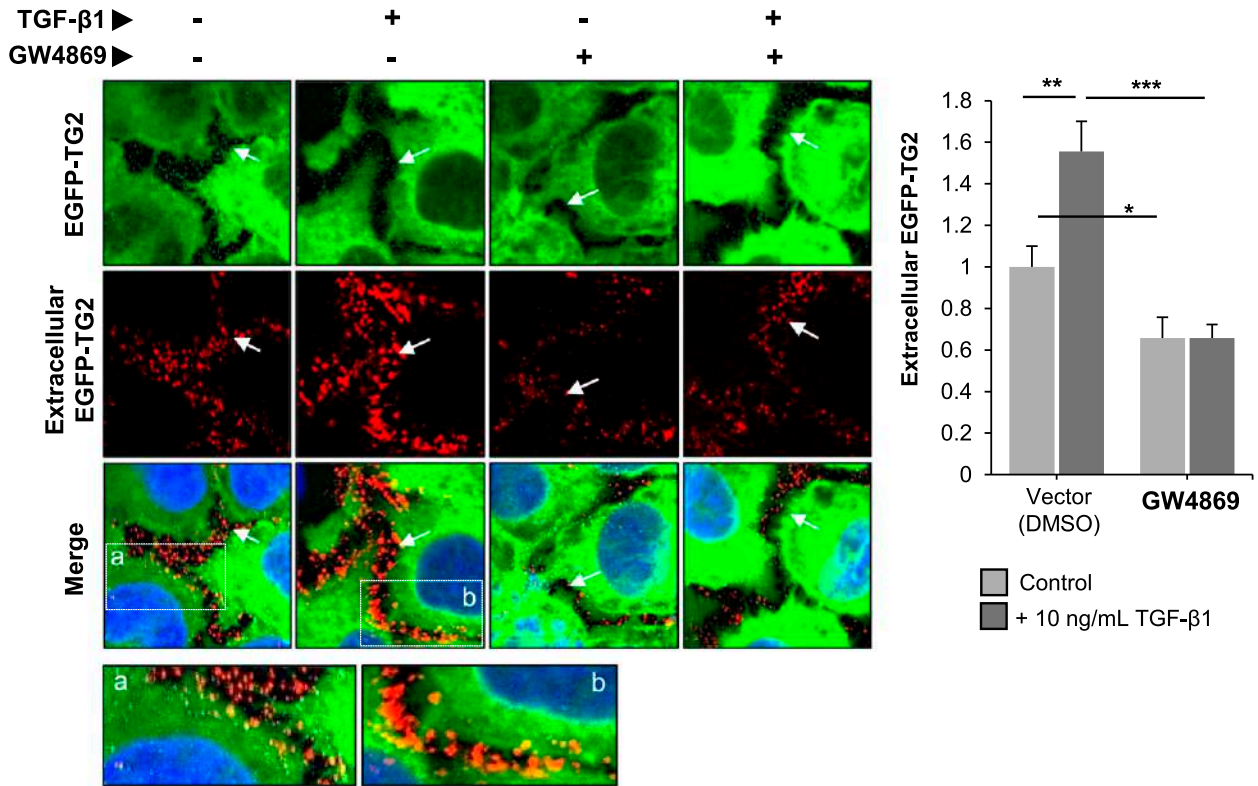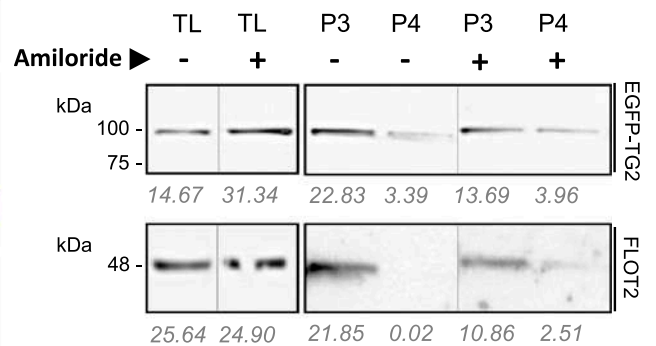
IP from TG2-null kidneys from inbred mice. Furthermore, TG2 complexes have been used to interrogate the UUO proteome. Proteomes were resolved by SWATH data-independent acquisition MS.[18] The proposed strategy could be adapted for precision-targeted proteomics in other systems.

Bioinformatic analysis of the TG2-associated proteins in the UUO model revealed enrichment of proteins involved in vesicular transport, and among them, a striking number were exosome-associated proteins. Because the TG2 partners involved in vesicular trafficking were not increased in the UUO proteome compared with the healthy proteome, we deduce that their function in TG2 trafficking is caused by their augmented interaction with TG2 on UUO, excluding the possibility of a concentration-dependent association. However, almost all proteins regulating ECM receptor organization and actin dynamics that we found significantly upregulated in the UUO proteome were also TG2-interacting proteins in the UUO. Collectively, these findings suggest the existence of a pathway of TG2 secretion during fibrosis progression driven by vesicular trafficking followed by the interaction of secreted TG2 with a protein network responsible for ECM dynamics, leading to fibrotic remodeling and expansion. The diminished scarring index and lower level of active TGF-β in the TG2 KO kidneys that we have reported here align well with the molecular connections that link TG2 to the fibrotic kidney proteome generated by this study, confirming the role of TG2 in the extracellular milieu in fibrosis progression.

By exploiting the MS data *in vitro* and *ex vivo*, we have uncovered a novel pathway for the cellular export of TG2 in TECs. We have shown that TG2 is predominantly secreted in association with exosomes and that TG2-bearing exosomes require the sphingolipid ceramide for their production. Furthermore, TG2 enrichment in exosomes is stimulated by TGF-β1, although on the basis of quantifications of exosomes *via* FLOT, a well characterized EV marker and partner of TG2 *in*

vivo post-UUO, we cannot rule out a general increase in EV production by TGF-β1. Exosomes form from endosomes by budding into late endosomes (multivesicular bodies), which then fuse with the PM, releasing intraluminal vesicles or exosomes.[39] The endosomal sorting complex required for transport (ESCRT) machinery is the main system controlling the sorting of proteins into exosomes.[39] Loading of syndecan HS proteoglycans (SDC1 and SDC4) with intracellular cargos able to bind the proteoglycan HS chains leads to syndecan clustering and recruitment of cytosolic adaptor protein syntenin-1, which by direct interaction with Alix, adapts syndecan and syndecan-bound cargoes to the ESCRT at the level multivesicular body formation.[34] In recent work, even TG2 itself has been implicated in cargo recruitment to vesicles and is present in exosomes in situations of abnormal proteostasis in an MEF model.[40]

TG2 is an HS binding protein, and HS affects TG2 trafficking as shown in previous work[12,13,35,41]; consistent with this observation, SDC4 emerged as a specific partner of TG2 in the UUO kidney in this unbiased analysis. We and others have previously identified SDC4 as a profibrotic partner of TG2[8,12,13] influencing its secretion but without a clear mechanism. Here, we have for the first time unraveled that the interaction of TG2 with HS SDC4 may play a fundamental role in the targeting of TG2 to exosomes. SDC4 and TG2 were coimmunoprecipitated from exosomal lysates, and SDC4 was required for exosomal secretion of TG2, this being greatly diminished by siRNA targeted to SDC4. *Ex vivo*, live imaging of primary cortical TECs from SDC4 KO kidney showed reduced vesicular trafficking of TG2 to the cell surface, which was compensated by SDC4 add back. TG2 was retained in the cytosolic fraction not only of SDC4 KO TECs but also, of primary fibroblasts and mesangial cells isolated from SDC4 KO kidneys, suggesting that SDC4 regulates TG2 distribution in all of the main renal cell types. *In vivo*, SDC4 was a TG2-interacting partner only in the diseased kidney, consistent with

Figure 8. EV release of TG2 is reduced by inhibition of exosome and ectosome synthesis. (A) Exponentially growing NRK52E expressing EGFP TG2 cells were cultured in serum free medium supplemented with GW4869 (10 μM; +) or DMSO (vector;) for 16 hours. TL, ectosome (P3), and exosome (P4) fractions were blotted with anti GFP (EGFP) and anti FLOT2 antibodies. Band intensities per area measured by densitometric analysis are shown underneath the blots. (B) NRK52E EGFP TG2 cells were grown in an eight well chamber with and without 10 ng/ml TGF β1 and treated with GW4869 as described in A. Extracellular EGFP TG2 was detected in cells fixed by paraformaldehyde (3% [wt/vol]) but not permeabilized using a rabbit polyclonal anti GFP antibody followed by a goat antirabbit Alexa Fluor 568 antibody (red). Nuclei were stained with 4′,6 diamidino 2 phenylindole (blue). The green fluorescence denotes total EGFP TG2. Representative confocal microscopy sections (10 μm) are presented, and they were acquired by a Leica TCS confocal microscope. White arrows identify the cell perimeter. Extracellular EGFP TG2 was quantified by ImageJ intensity analysis on at least eight nonoverlapping images per treatment and is presented as mean relative intensity of red (extracellular EGFP TG2) over green (total EGFP TG2) $\pm$SEM expressed relative to the control cells without GW4869 (equalized to one). *$P<0.05$; **$P<0.01$; ***$P<0.01$. (C) Exosomes from NRK52E EGFP TG2 cells were isolated and incubated on a monolayer of WT NRK52E cells for 3 hours. Cells were washed three times in PBS and fixed in paraformaldehyde, but they were not permeabilized. EGFP fluorescence (green) was clearly visible in particles with estimated diameter of <0.5 μm. Nuclei were stained with 4′,6 diamidino 2 phenylindole. Pretreatment of the NRK52E cell monolayer with heparitinase (+Hep) to digest cells surface HS chains led to a decrease in the uptaken EGFP TG2 bearing exosomes. (D) NRK52E expressing EGFP TG2 cells were exposed to 1 μM amiloride for 10 minutes in serum free medium. TL, ec tosome (P3), and exosome (P4) fractions were blotted with anti GFP and anti FLOT2 antibodies. Band intensities per area were measured as described in A.
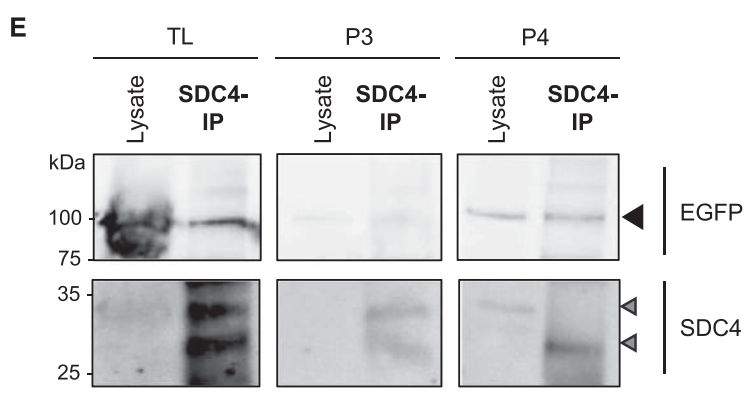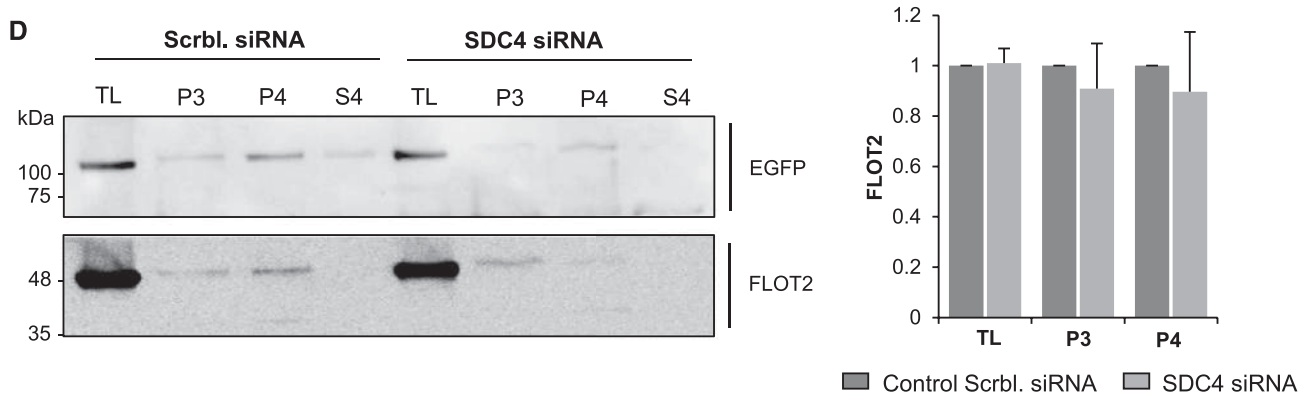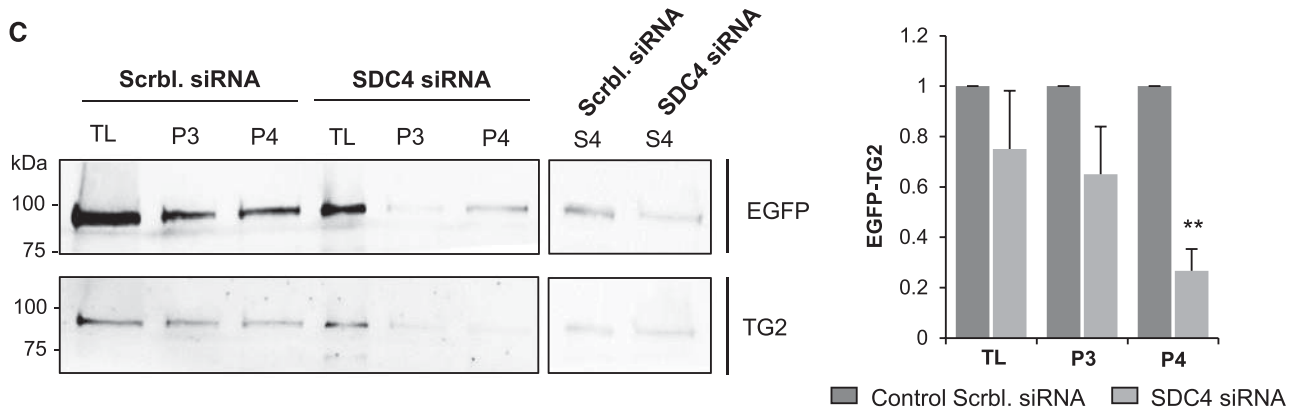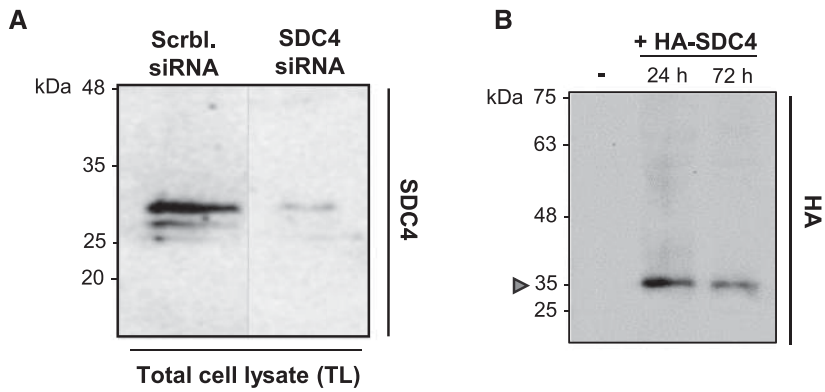
the notion that TG2 is secreted during fibrosis progression and only found in low amounts extracellularly in the normal kidney.[4,20] Therefore, our data suggest that TG2 would be recruited as an HS binding cargo and targeted to exosomes originating from late endosomes by SDC4. After secreted in the extracellular environment, TG2 meets the high calcium and low trinucleotide phosphates concentrations, which favor the opening of TG2 and the acquisition of a linear conformation on substrate binding,[42] that we and others have shown to determine loss of heparin binding.[35,41] Consistent with this idea is the finding of a small portion of free soluble TG2 in our cell experiments and the possibility that TG2 and/or EV-bound TG2 may be transferred to HS of other receptor molecules in response to local changes in calcium levels in an autocrine or paracrine fashion (Figure 11). For instance, perlecan is an ECM HS proteoglycan exclusively found in the TG2 UUO interactome, which could further recruit and distribute TG2 in the matrix *via* the long HS chains. Furthermore, we have shown that exosomal TG2 could be transferred horizontally from the extracellular environment to TECs and that HS chains of proteoglycans are required for the trafficking of TG2-rich exosomes. TG2 was also detected in ectosomes, larger vesicles that bud directly from the PM, although in much lower proportion than in exosomes. There was no clear coprecipitation of SDC4 and TG2 from ectosome lysates (only from exosome lysates), implying that SDC4 has no role or an indirect role in recruiting TG2 to ectosomes.

The role played by EVs in disease is of growing importance, although the field is novel. Exosomes function in intercellular and interorgan communication by transferring proteins, mRNAs, and microRNAs to recipient cells.[43] In seminal work, it was shown that hypoxic tubular cells but not normoxic counterparts secreted EVs that induced the expression of TGF-β1, α-SMA, and F-actin in fibroblasts, inducing their subsequent activation.[44] Therefore, it is clear that EVs cooperate in spreading and amplifying cell differentiation, leading to sustained fibrosis.[43,44] Transfer of exosomal cargo to neighboring cells allows tuning of cell behavior and rapid phenotypic adjustment, including activation of fibroblasts into myofibroblasts.[44] Given the location of TG2 outside exosomes and specific interaction of TG2 with cell surface SDC4, it is plausible that, after released, TG2 could assist in the cell-cell trafficking of exosomes, therefore influencing the transfer of pathologic molecules conducive of fibrosis. Furthermore, the topology of TG2 on the outside of EVs would suggest that it may also serve an adhesive function, which is an additional important factor in the chronic healing process underlying fibrosis development. This suggestion is in line with the adhesive role played by TG2[45] and recent evidence that exosomes influence cell migration by serving as adhesive sites in the matrix.[46]

TG2 is associated with wound healing and organ fibrosis, but what makes it an attractive target is that the enzyme is only activated in disease on externalization. Therefore, inhibition of TG2 is anticipated not to have an adverse effect in normal cells. We have begun our investigation from an *in vivo* model of CKD providing a global analysis of the TG2 interactome present at the interface between cells and the ECM niche–surrounding cells and compared this with the CKD model proteome in an unbiased manner. Our approach, which does not rely on chemical crosslinking, has not detected integrin[16] or purinergic receptor[17] as TG2 secretion partners in fibrotic kidney or attributed TG2 release to PM vesicular shedding as is observed in cancer,[47] but it has identified exosome secretion as a key novel mechanism for the cell surface trafficking of fibrogenic TG2 in an SDC4-dependent manner. The presence of TG2 in urinary exosomes from a pool of patients with CKD has confirmed the importance of the finding in human pathology. Our study changes the way that TG2 cell surface trafficking is seen and suggests that therapeutic block of vesicular TG2 could potentially impede TG2-driven matrix accumulation and exosome-mediated transfer of TG2 from cell to cell during fibrosis progression.

CONCISE METHODS

Experimental details are provided in Supplemental Material.

Experimental Models
Experimental UUO[48] was performed on fully backcrossed TG2 $^{/}$ (TG2 KO) mice originally obtained from Gerry Melino[49] and WT inbred C57BL/6J mice as described before[12] and in Supplemental Material. A total of 32 WT and 32 TG2 KO mice were used, of which 16 per genotype were subjected to either UUO or sham operation. Therefore, four groups of 16 mice were obtained: WT UUO, WT

Figure 9. Recruitment of TG2 in exosomes depends on SDC4. (A) EGFP TG2 expressing NRK52E cells were treated with RNAi targeting SDC4 (SDC4 KO) or nontargeting RNAi (Scrbl. siRNA; used as a control). TLs were analyzed by Western blotting testing for SDC4. (B) As a blotting control for SDC4, NRK52E cells were transiently transfected with HA tagged SDC4 cDNA, and cell lysates were blotted for HA. A mock transfection ( ) was performed as a control. The arrow points at HA tagged SDC4 with a molecular mass between 25 and 35 kD. (C and D) Lysates of ectosome (P3) and exosome (P4) fractions isolated from the conditioned medium of SDC4 KO cells obtained as described in A and TLs were tested for (C and D) EGFP, (C) TG2, and (D) FLOT2. Intensity of immunoreactive bands was quantified by densitometric analysis; graphs represent mean values ±SEM of (C) four (EGFP) or (D) three (FLOT2) independent experiments expressed relative to the scrambled nontargeting siRNA control (equalized to one). **$P<0.01$. (E) SDC4 was immunoprecipitated from vesicular fractions and TLs with a rabbit polyclonal anti SDC4 antibody. SDC4 immunoprecipitates were analyzed by Western blotting for the presence of EGFP TG2 (black arrowhead) and SDC4 (gray arrowheads).
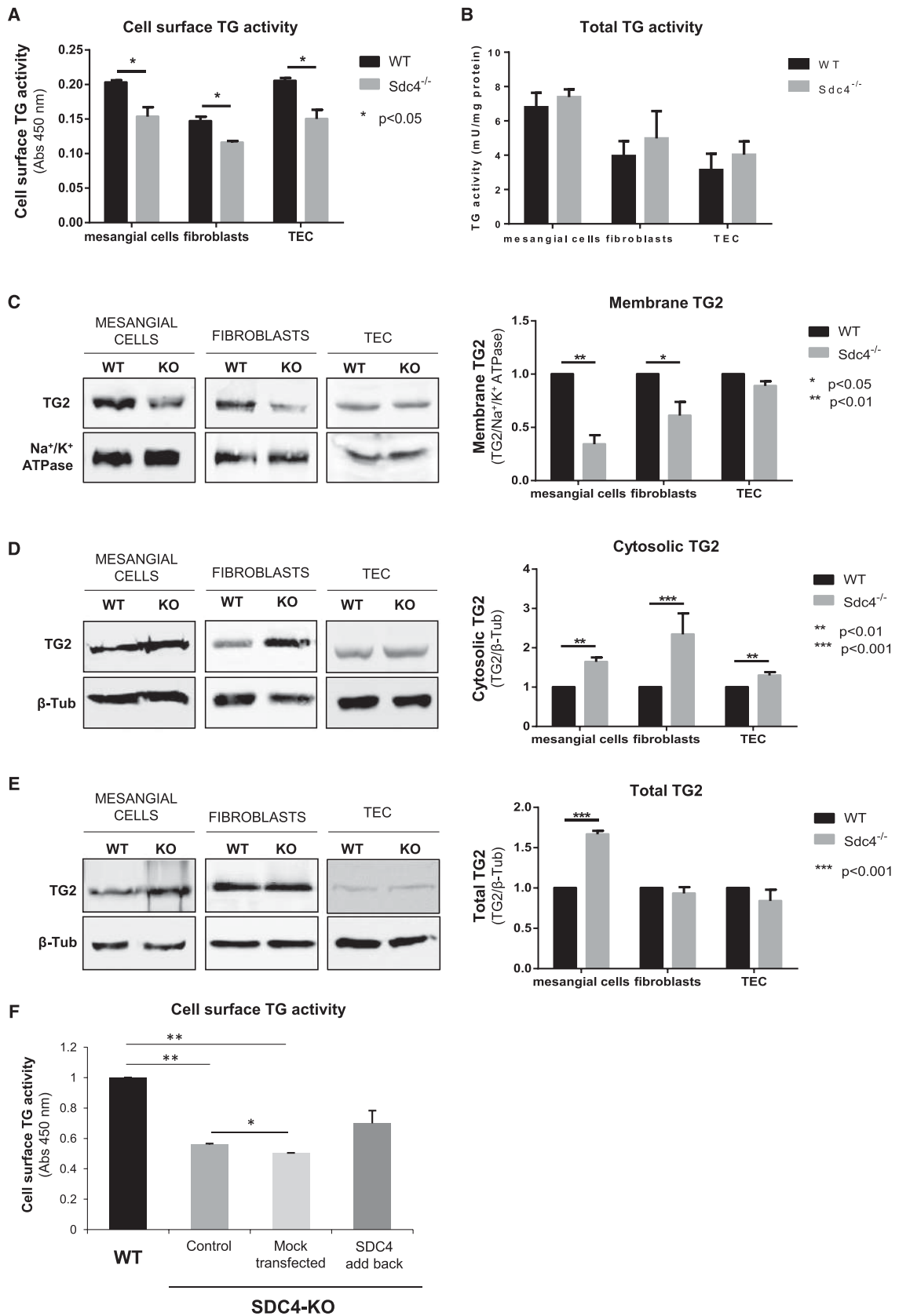
Figure 10. SDC4 KO leads to decreased TG2 membrane distribution and externalization *ex vivo*. Kidney glomeruli and tubules were isolated from WT and SDC KO (SDC4 ⁻/⁻) mice. Primary mesangial cells, fibroblasts, and TECs were grown from glomeruli or tubules

sham, TG2 KO UUO, and TG2 KO sham. The UUO and sham pro teome required lysate from one half of a kidney per animal and was carried out in kidneys from four mice per group. Kidneys were halved longitudinally pole to pole through the papilla. Each one half was then cut transversally to provide four identical quarters, with equal cortex and medullary mass in each. The TG2 interactome required two full organs per IP and was carried out in kidneys from 12 male mice per group. Western blotting analysis required one quarter of kidney per animal and was performed using kidneys from three male mice per group as described before.[8] Optimal size of biologic repli cates for the UUO and sham proteome analysis was determined by a power calculation within Statistica software (Dell), and $n=4$ individ uals per treatment were sufficient to power the experiment above 80%. In keeping with the principle of animal reduction, male and female mice kidneys were used for general proteomics (one male and three female). Linear regression analysis was performed on protein peak areas after SWATH acquisition MS and confirmed that the var iability in protein intensities produced by the male mice was not higher than the intrinsic biologic variability detected among the fe male ($P\leq0.05$; mean standard residuals ≥5). All experimental pro cedures were carried out under license in accordance with regulations laid down by Her Majesty's Government, United Kingdom (Animals Scientific Procedures Act ASPA, 1986), and they were approved by the University of Sheffield Animal Ethical Review Committee (ASPA Eth ical Review Process) and the Nottingham Trent University Ethical Review Committee (ASPA Ethical Review Process).

Fibrosis Measurement
The level of fibrosis was assessed by Masson trichrome staining as previously described.[50]

TGF-β Activity
The mink lung epithelial cell bioassay[51] was performed as described before.[12,52]

Isolation of TG2 Membrane Complexes and Data Acquisition by MS
To isolate TG2 associated proteins from kidney fractions, 10% (wt/vol) kidney homogenates were prepared from WT and TG2 KO kid neys, UUO and sham operated, by mechanical homogenization per formed on ice using an Ultra Turrax T25 homogenizer (Merck) in homogenization buffer (0.25 M sucrose, 10 mM Tris HCl, 1 mM

MgCl$_2$, and 2 mM EDTA, pH 7.4) containing protease inhibitor cocktail (Sigma Aldrich). The whole homogenate was centrifuged at 1000×g for 5 minutes at 4°C to remove larger particulates; then, membranes were separated from the cytosolic fraction by centrifu gation at 20,000×g at 4°C for 30 minutes as previously described.[12] The pellet (crude membrane fraction) was resuspended in IP buffer (25 mM Tris HCl, 150 mM NaCl, 1 mM EDTA, 1% [vol/vol] NP40 detergent solution, and 5% [vol/vol] glycerol, pH 7.4) containing protease inhibitor cocktail and membrane enrichment validated by Western blotting. TG2 with associated proteins was immunoprecipi tated from the membrane fraction using the Pierce crosslink mag netic IP kit (Thermo Scientific) by protein A/G magnetic beads to which anti TG2 antibody (IA12; University of Sheffield) was cross linked using disuccinimidyl suberate. Incubations of membrane ly sates with the antibody coated beads were performed for 15 hours at 4°C in constant rotation. TG2 associated proteins were subjected to trypsin digestion directly on the beads after washing the beads three times with 50 mM ammonium acetate and incubating for 15 hours with 200 ng/μl of proteomics grade trypsin (Sigma Aldrich) in 50 mM ammonium acetate. Peptides were analyzed by MS on re moval of the beads using a magnetic stand, by RP HPLC ESI MS/MS using a TripleTOF 5600+ mass spectrometer (SCIEX) in data dependent acquisition mode for spectral library construction, and in SWATH 2.0 data independent acquisition mode using static SWATH acquisition windows for quantification as described in Supplemental Material. The MS proteomics data have been deposited in the Proteo meXchange Consortium (http://proteomecentral.proteomexchange. org) *via* the PRIDE partner repository[53] with the dataset identifier PXD008173. To define proteins significantly associated with TG2, a *z* test statistical analysis was performed using TG2 IP from TG2 KO kidney membranes as negative controls. Five independent TG2 IP experiments were carried out, each on the basis of a lysate of two kidneys. The obtained interactome has been submitted to the database for CKD related expression data CKDdb[54] (http://www.padb.org/ckddb/) with the dataset identifier ExpGFEVabf79st4na.

The UUO Kidney Proteome
UUO and sham kidney halves were ground in liquid nitrogen, and a 10% (wt/vol) tissue homogenate was prepared in lysis buffer containing 9.5 M urea, 2% (wt/vol) dithiothreitol, 1% (wt/vol) *N* octyl β glucopyranoside, and protease inhibitors (Sigma Aldrich) with sonication. Equal amounts of total protein extracts (50 μg)

---

using selective growth medium. (A) Extracellular TG activity was measured by a well established assay in live cells (4×10^4 cells per well of a 96 well plate) cultured on FN in the presence of the TG substrate biotin cadaverine for 1 hour. Data represent mean Abs (450 nM) ±SD of three independent experiments undertaken in triplicates. (B) Total TG activity was similarly assayed but using whole cell lysate (60 μg per well) and specific activities obtained from a standard curve of purified TG2. Data represent mean TG activity ±SEM of three independent experiments undertaken in triplicates. (C E) TG2 was probed by Western blot using a mouse monoclonal anti TG2 antibody (IA12) and quantified by densitometric analysis on (C) cell membrane extracts, (D) cytosolic proteins, and (E) TLs. In each experiment, either Na$^+$/K$^+$ ATPase or β tubulin was used as the loading control. Data represent mean intensities normalized for the loading control ±SEM; n 3 per group. (F) Extracellular TG activity was measured as described in A in WT and SDC4 KO (SDC4 $^{/}$) primary TECs. Where indicated, SDC4 KO cells (SDC4 $^{/}$) were transfected back with pcDNA3 hSdc4 plasmid or subjected to mock transfection (with transfection efficiency of approximately 30%). Data represent mean Abs (450 nM) ±SEM; n 3 independent experiments undertaken in triplicates. *$P<0.05$; **$P<0.01$; ***$P<0.01$.
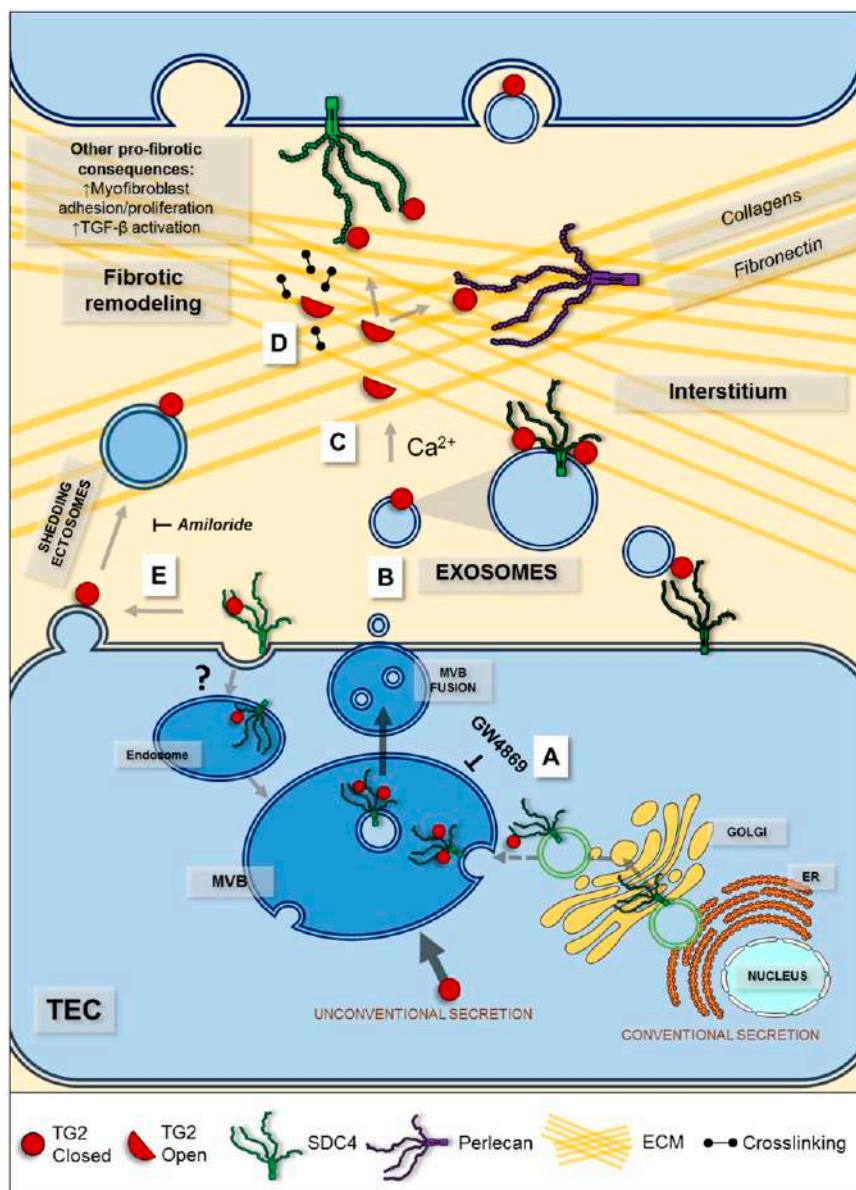
Figure 11. The proposed pathway of TG2 cell surface trafficking in TEC during fibrosis progression involves TG2 targeting to exosomes from late endosomes by SDC4. TG2 is secreted unconventionally by exosomes originating from late endosomes as multi-vesicular bodies (MVBs), which then fuse with the PM, releasing the intraluminal vesicles outside cells. (A) The biogenesis of TG2 bearing exosomes is mediated by ceramide, because the inhibitor of N SMase GW4869 significantly reduces the presence of TG2 in the exosome fraction. TG2, which has high affinity for HS, is loaded on the surface of the intraluminal vesicle as an HS/SDC4 cargo, and it is exposed on the surface of the formed exosome. (B) After fusion of the outer membrane of MVB with PM, the TG2 bearing exosomes likely accumulate in the ECM by TG2 binding to ECM/cell surface protein partners in an "autocrine" or "paracrine" fashion. (C) After released with exosomes, TG2 could also undergo a conformational change and linearize because of the high Ca^{2+} to GTP ratio of the extracellular space, with a lowering or even loss of HS affinity; the free TG2 could bind the HS of other proteoglycans or other ECM partners. (D) In the matrix, TG2 acts as an adhesive protein and matrix crosslinker, promoting fibers accumulation and latent TGF β1 recruitment. (E) TG2 is also present in ectosomes. It is possible that TG2, after it is secreted *via* exosomes, is captured by the PM and retained on ectosomes shed by the PM. ER, endoplasmic reticulum.

were diluted in 50 mM triethyl ammonium bicarbonate containing a final concentration of 0.02% (wt/vol) ProteaseMAX surfactant (Promega). Proteins were subjected to reduction (5 mM dithiothreitol at 56°C for 20 minutes) and alkylation (15 mM iodoacetamide at room temperature for 15 minutes), and then, they were trypsin digested overnight at 37°C with 0.02 mg/ml MS grade trypsin (Promega) and 0.01% (wt/vol) ProteaseMAX surfactant in a thermomixer. Samples were vacuum concentrated to dryness and resuspended in 20 μl of 5% (vol/vol) acetonitrile/0.1% (vol/vol) formic acid for MS analysis. SWATH data independent acquisition MS was performed on the obtained peptides using variable SWATH windows. The MS proteomics data have been deposited in the ProteomeXchange Consortium (http://proteomecentral.proteomexchange.org) *via* the PRIDE partner repository[53] with the dataset identifier PXD008173. Analysis of differentially expressed proteins was performed using the OneOmics cloud processing online platform (SCIEX) as described in Supplemental Material. Proteome data have been submitted to CKDdb[54] (http://www.padb.org/ckddb/) with the dataset identifier ExpGFEVyz6gt389dy.

Primary and Immortal Cell Lines
Tubules and glomeruli were isolated from WT and SDC4 $^/$ (SDC4 KO)[36] C57BL/6J mice by perfusion of kidneys *in situ* with BSA inactivated Dynabeads and subsequent magnetic separation, and they were cultured as previously described and detailed in Supplemental Methods.[55] Primary cortical TECs grew out from tubules in selective medium with insulin, transferrin, selenium, and EGF in 0.5% (vol/vol) FBS to cause proliferation of just epithelial cells and not fibroblasts (grown out in medium with 10% FBS); primary mesangial cells were derived from glomeruli in RPMI 1640 containing 20% (vol/vol) FBS. Media composition is detailed in Supplemental Material.

NRK52E rat renal proximal like TECs and NRK49F renal fibroblasts were obtained from the European Cell Culture Collection and maintained in DMEM supplemented with 5% (vol/vol) or 10% (vol/vol) heat inactivated FBS, respectively.

Plasmid Constructs and Transfections
The following constructs were prepared: pEGFP N1 TG2, where TG2 cDNA was fused in frame to the N terminus of EGFP in pEGFP N1 plasmid

(Clontech), and pcDNA3.1(+) hSdc4, where HA Sdc4 cDNA (HA downstream of the leader peptide provided by Mark Bass, Sheffield University) was subcloned from pBluescript in pcDNA3.1(+). All constructs were verified by Sanger sequencing. Cell transfection was per formed by TransIT (Mirus Bio). NRK52E was stably transfected with pEGFP N1 TG2 in medium supplemented with 700mg/ml G418, as previously described,[56] by using electroporation (Amaxa Nucleofec tor). SDC4 was knocked down by transient transfection with 100 nM rat SDC4 targeting siRNA or scrambled control siRNA (Dharmacon; Thermo Scientific) for 48 hours using DharmaFECT as transfection reagent.

EV Isolation and Characterization

EVs were isolated from conditioned medium of cells by differential centrifugation as described.[24,25] Nanoparticle tracking analysis by tunable resistive pulse sensing was performed using qNano (Izon) to ex amine microparticle size and distribution. In some cases, cells were stimulated by recombinant TGF β1 (10 ng/ml) to simulate conditions of fibrogenesis in vitro. The EV inhibitor N,N' Bis[4 (4,5 di hydro ^{1}H imidazol 2 yl)phenyl] 3,3' p phenylene bis acrylamide-dihydrochloride, GW4869 (D1692; Sigma Aldrich) was used as an inhibitor of N SMase[57] and exosome biogenesis[26] at a concentration of 10 μM in serum free medium for 16 hours. Amiloride hydrochloride (N Amidino 3,5 diamino 6 chloropyrazinecarboxamide hydrochloride hydrate; A7410; Sigma Aldrich) was used at a concentration of 1 mM for 10 minutes. For IPs from EV lysates, the Pierce crosslink magnetic IP kit was used followed by Western blotting.

Detection of TG2 in Cell Fractions by Western Blotting

Cells were fractionated into membrane and cytosolic fractions, and TG2 was detected as described before.[12,13]

Measurements of TG2 Activity at the Cell Surface of Live Cells, in Cell Fractions, and in EVs

TG2 activity associated with the extracellular surface in cells in culture and total TG2 activity in cell homogenates and fractions were assayed by measuring the incorporation of biotin cadaverine into FN by calcium dependent transamidation as previously described.[13] EVs TG2 activity was measured in both EVs lysed in a sucrose based buffer (0.32 M sucrose, 5 mM Tris HCl, and 2 mM EDTA, pH 7.4) with protease inhibitor cocktail and intact EVs kept in suspension in sample buffer (Zedira) using the commercially available tissue glutaminase picoassay kit (Zedira).

REFERENCES

1. Boor P, Ostendorf T, Floege J: Renal fibrosis: Novel insights into mechanisms and therapeutic targets. Nat Rev Nephrol 6: 643 656, 2010

2. Webster AC, Nagler EV, Morton RL, Masson P: Chronic kidney disease. Lancet 389: 1238 1252, 2017

3. Johnson TS, El Koraie AF, Skill NJ, Baddour NM, El Nahas AM, Njloma M, Adam AG, Griffin M: Tissue transglutaminase and the progression of human renal scarring. J Am Soc Nephrol 14: 2052 2062, 2003

4. Johnson TS, Skill NJ, El Nahas AM, Oldroyd SD, Thomas GL, Douthwaite JA, Haylor JL, Griffin M: Transglutaminase transcription and antigen translocation in experimental renal scarring. J Am Soc Nephrol 10: 2146 2157, 1999

5. Verderio EAM, Furini G, Burhan IW, Johnson TS: Transglutaminases: Expression in kidney and relation to kidney fibrosis. In: Transgluta minases, edited by Hitomi K, Kojima S, Fesus L, Tokyo, Japan, Springer, 2015, pp 229 262

6. Annes JP, Munger JS, Rifkin DB: Making sense of latent TGFbeta ac tivation. J Cell Sci 116: 217 224, 2003

7. Shweke N, Boulos N, Jouanneau C, Vandermeersch S, Melino G, Dussaule JC, Chatziantoniou C, Ronco P, Boffa JJ: Tissue transgluta minase contributes to interstitial renal fibrosis by favoring accumulation of fibrillar collagen through TGF beta activation and cell infiltration. Am J Pathol 173: 631 642, 2008

8. Burhan I, Furini G, Lortat Jacob H, Atobatele AG, Scarpellini A, Schroeder N, Atkinson J, Maamra M, Nutter FH, Watson P, Vinciguerra M, Johnson TS, Verderio EA: Interplay between transglutaminases and heparan sulphate in progressive renal scarring. Sci Rep 6: 31343, 2016

9. Meng XM, Nikolic Paterson DJ, Lan HY: TGF β: The master regulator of fibrosis. Nat Rev Nephrol 12: 325 338, 2016

10. Johnson TS, Fisher M, Haylor JL, Hau Z, Skill NJ, Jones R, Saint R, Coutts I, Vickers ME, El Nahas AM, Griffin M: Transglutaminase inhibition re duces fibrosis and preserves function in experimental chronic kidney disease. J Am Soc Nephrol 18: 3078 3088, 2007

11. Huang L, Haylor JL, Hau Z, Jones RA, Vickers ME, Wagner B, Griffin M, Saint RE, Coutts IG, El Nahas AM, Johnson TS: Transglutaminase in hibition ameliorates experimental diabetic nephropathy. Kidney Int 76: 383 394, 2009

12. Scarpellini A, Huang L, Burhan I, Schroeder N, Funck M, Johnson TS, Verderio EA: Syndecan 4 knockout leads to reduced extracellular transglutaminase 2 and protects against tubulointerstitial fibrosis. J Am Soc Nephrol 25: 1013 1027, 2014

13. Scarpellini A, Germack R, Lortat Jacob H, Muramatsu T, Billett E, Johnson T, Verderio EA: Heparan sulfate proteoglycans are receptors for the cell surface trafficking and biological activity of transglutamin ase 2. J Biol Chem 284: 18411 18423, 2009

14. Chou CY, Streets AJ, Watson PF, Huang L, Verderio EA, Johnson TS: A crucial sequence for transglutaminase type 2 extracellular trafficking in

renal tubular epithelial cells lies in its N terminal beta sandwich do main. *J Biol Chem* 286: 27825 27835, 2011

15. Eckert RL, Kaartinen MT, Nurminskaya M, Belkin AM, Colak G, Johnson GV, Mehta K: Transglutaminase regulation of cell function. *Physiol Rev* 94: 383 417, 2014

16. Zemskov EA, Mikhailenko I, Hsia RC, Zaritskaya L, Belkin AM: Un conventional secretion of tissue transglutaminase involves phospho lipid dependent delivery into recycling endosomes. *PLoS One* 6: e19414, 2011

17. Adamczyk M, Griffiths R, Dewitt S, Knäuper V, Aeschlimann D: P2X7 receptor activation regulates rapid unconventional export of transglu taminase 2. *J Cell Sci* 128: 4615 4628, 2015

18. Gillet LC, Navarro P, Tate S, Röst H, Selevsek N, Reiter L, Bonner R, Aebersold R: Targeted data extraction of the MS/MS spectra generated by data independent acquisition: A new concept for consistent and accurate proteome analysis. *Mol Cell Proteomics* 11: O111.016717, 2012

19. Siegel M, Strnad P, Watts RE, Choi K, Jabri B, Omary MB, Khosla C: Extracellular transglutaminase 2 is catalytically inactive, but is tran siently activated upon tissue injury. *PLoS One* 3: e1861, 2008

20. Skill NJ, Griffin M, El Nahas AM, Sanai T, Haylor JL, Fisher M, Jamie MF, Mould NN, Johnson TS: Increases in renal epsilon (gamma glutamyl) lysine crosslinks result from compartment specific changes in tissue transglutaminase in early experimental diabetic nephropathy: Patho logic implications. *Lab Invest* 81: 705 716, 2001

21. Humphries JD, Byron A, Bass MD, Craig SE, Pinney JW, Knight D, Humphries MJ: Proteomic analysis of integrin associated complexes identifies RCC2 as a dual regulator of Rac1 and Arf6. *Sci Signal* 2: ra51, 2009

22. Zhao Q, Yang Y, Wang CL, Hou Y, Chen H: Screening and identification of the differential proteins in kidney with complete unilateral ureteral obstruction. *Int J Clin Exp Pathol* 8: 2615 2626, 2015

23. Satirapoj B, Tassanasorn S, Charoenpitakchai M, Supasyndh O: Peri ostin as a tissue and urinary biomarker of renal injury in type 2 diabetes mellitus. *PLoS One* 10: e0124055, 2015

24. Bianco F, Perrotta C, Novellino L, Francolini M, Riganti L, Menna E, Saglietti L, Schuchman EH, Furlan R, Clementi E, Matteoli M, Verderio C: Acid sphingomyelinase activity triggers microparticle release from glial cells. *EMBO J* 28: 1043 1054, 2009

25. Benussi L, Ciani M, Tonoli E, Morbin M, Palamara L, Albani D, Fusco F, Forloni G, Glionna M, Baco M, Paterlini A, Fostinelli S, Santini B, Galbiati E, Gagni P, Cretich M, Binetti G, Tagliavini F, Prosperi D, Chiari M, Ghidoni R: Loss of exosomes in progranulin associated fronto temporal dementia. *Neurobiol Aging* 40: 41 49, 2016

26. Trajkovic K, Hsu C, Chiantia S, Rajendran L, Wenzel D, Wieland F, Schwille P, Brügger B, Simons M: Ceramide triggers budding of exo some vesicles into multivesicular endosomes. *Science* 319: 1244 1247, 2008

27. Chairoungdua A, Smith DL, Pochard P, Hull M, Caplan MJ: Exosome release of *β* catenin: A novel mechanism that antagonizes Wnt signal ing. *J Cell Biol* 190: 1079 1091, 2010

28. Falcone S, Cocucci E, Podini P, Kirchhausen T, Clementi E, Meldolesi J: Macropinocytosis: Regulated coordination of endocytic and exocytic membrane traffic events. *J Cell Sci* 119: 4758 4769, 2006

29. Chalmin F, Ladoire S, Mignot G, Vincent J, Bruchard M, Remy Martin JP, Boireau W, Rouleau A, Simon B, Lanneau D, De Thonel A, Multhoff G, Hamman A, Martin F, Chauffert B, Solary E, Zitvogel L, Garrido C, Ryffel B, Borg C, Apetoh L, Rébé C, Ghiringhelli F: Membrane as sociated Hsp72 from tumor derived exosomes mediates STAT3 dependent immunosuppressive function of mouse and human myeloid derived sup pressor cells. *J Clin Invest* 120: 457 471, 2010

30. Miller ME, Adhikary S, Kolokoltsov AA, Davey RA: Ebolavirus requires acid sphingomyelinase activity and plasma membrane sphingomyelin for infection. *J Virol* 86: 7473 7483, 2012

31. Savina A, Furlán M, Vidal M, Colombo MI: Exosome release is regulated by a calcium dependent mechanism in K562 cells. *J Biol Chem* 278: 20083 20090, 2003

32. Cocucci E, Meldolesi J: Ectosomes and exosomes: Shedding the confu sion between extracellular vesicles. *Trends Cell Biol* 25: 364 372, 2015

33. Stelmach H, Rusak T, Tomasiak M: The involvement of the Na(+)/H(+) exchanger in the formation of microvesicles by porcine platelets. *Haematologia (Budap)* 32: 239 252, 2002

34. Baietti MF, Zhang Z, Mortier E, Melchior A, Degeest G, Geeraerts A, Ivarsson Y, Depoortere F, Coomans C, Vermeiren E, Zimmermann P, David G: Syndecan syntenin ALIX regulates the biogenesis of exo somes. *Nat Cell Biol* 14: 677 685, 2012

35. Lortat Jacob H, Burhan I, Scarpellini A, Thomas A, Imberty A, Vivès RR, Johnson T, Gutierrez A, Verderio EA: Transglutaminase 2 interaction with heparin: Identification of a heparin binding site that regulates cell adhesion to fibronectin transglutaminase 2 matrix. *J Biol Chem* 287: 18005 18017, 2012

36. Ishiguro K, Kadomatsu K, Kojima T, Muramatsu H, Tsuzuki S, Nakamura E, Kusugami K, Saito H, Muramatsu T: Syndecan 4 deficiency impairs focal adhesion formation only under restricted conditions. *J Biol Chem* 275: 5249 5252, 2000

37. Jones RA, Kotsakis P, Johnson TS, Chau DY, Ali S, Melino G, Griffin M: Matrix changes induced by transglutaminase 2 lead to inhibition of an giogenesis and tumor growth. *Cell Death Differ* 13: 1442 1453, 2006

38. da Silva Lodge M, El Nahas M, Johnson TS: Urinary transglutaminase 2 as a potential biomarker of chronic kidney disease detection and pro gression [Abstract]. *Lancet* 381: S33, 2013

39. Villarroya Beltri C, Baixauli F, Gutiérrez Vázquez C, Sánchez Madrid F, Mittelbrunn M: Sorting it out: Regulation of exosome loading. *Semin Cancer Biol* 28: 3 13, 2014

40. Diaz Hidalgo L, Altuntas S, Rossin F, D'Eletto M, Marsella C, Farrace MG, Falasca L, Antonioli M, Fimia GM, Piacentini M: Transglutaminase type 2 dependent selective recruitment of proteins into exosomes under stressful cellular conditions. *Biochim Biophys Acta* 1863: 2084 2092, 2016

41. Wang Z, Collighan RJ, Pytel K, Rathbone DL, Li X, Griffin M: Charac terization of heparin binding site of tissue transglutaminase: Its im portance in cell surface targeting, matrix deposition, and cell signaling. *J Biol Chem* 287: 13063 13083, 2012

42. Pinkas DM, Strop P, Brunger AT, Khosla C: Transglutaminase 2 undergoes a large conformational change upon activation. *PLoS Biol* 5: e327, 2007

43. Camussi G, Deregibus MC, Bruno S, Cantaluppi V, Biancone L: Exo somes/microvesicles as a mechanism of cell to cell communication. *Kidney Int* 78: 838 848, 2010

44. Borges FT, Melo SA, Özdemir BC, Kato N, Revuelta I, Miller CA, Gattone VH 2nd, LeBleu VS, Kalluri R: TGF *β*1 containing exosomes from injured epithelial cells activate fibroblasts to initiate tissue regenerative responses and fibrosis. *J Am Soc Nephrol* 24: 385 392, 2013

45. Lorand L, Graham RM: Transglutaminases: Crosslinking enzymes with pleiotropic functions. *Nat Rev Mol Cell Biol* 4: 140 156, 2003

46. Sung BH, Ketova T, Hoshino D, Zijlstra A, Weaver AM: Directional cell movement through tissues is controlled by exosome secretion. *Nat Commun* 6: 7164, 2015

47. Antonyak MA, Li B, Boroughs LK, Johnson JL, Druso JE, Bryant KL, Holowka DA, Cerione RA: Cancer cell derived microvesicles induce transformation by transferring tissue transglutaminase and fibronectin to recipient cells. *Proc Natl Acad Sci U S A* 108: 4852 4857, 2011

48. Vielhauer V, Anders HJ, Mack M, Cihak J, Strutz F, Stangassinger M, Luckow B, Gröne HJ, Schlöndorff D: Obstructive nephropathy in the mouse: Progressive fibrosis correlates with tubulointerstitial chemokine expression and accumulation of CC chemokine receptor 2 and 5 positive leukocytes. *J Am Soc Nephrol* 12: 1173 1187, 2001

49. De Laurenzi V, Melino G: Gene disruption of tissue transglutaminase. *Mol Cell Biol* 21: 148 155, 2001

50. Huang L, Scarpellini A, Funck M, Verderio EA, Johnson TS: Development of a chronic kidney disease model in C57BL/6 mice with relevance to human pathology. *Nephron Extra* 3: 12 29, 2013

51. Abe M, Harpel JG, Metz CN, Nunes I, Loskutoff DJ, Rifkin DB: An assay for transforming growth factor beta using cells transfected with a plasminogen activator inhibitor 1 promoter luciferase construct. *Anal Biochem* 216: 276 284, 1994

52. Huang L, Haylor JL, Fisher M, Hau Z, El Nahas AM, Griffin M, Johnson TS: Do changes in transglutaminase activity alter latent transforming growth factor beta activation in experimental diabetic nephropathy? *Nephrol Dial Transplant* 25: 3897 3910, 2010

53. Vizcaíno JA, Côté RG, Csordas A, Dianes JA, Fabregat A, Foster JM, Griss J, Alpi E, Birim M, Contell J, O'Kelly G, Schoenegger A, Ovelleiro D, Pérez Riverol Y, Reisinger F, Ríos D, Wang R, Hermjakob H: The PRoteomics IDEntifications (PRIDE) database and associated tools: Status in 2013. *Nucleic Acids Res* 41: D1063 D1069, 2013

54. Fernandes M, Husi H: Establishment of a integrative multi omics expression database CKDdb in the context of chronic kidney disease (CKD). *Sci Rep* 7: 40367, 2017

55. Fisher M, Jones RA, Huang L, Haylor JL, El Nahas M, Griffin M, Johnson TS: Modulation of tissue transglutaminase in tubular epithelial cells alters extracellular matrix levels: A potential mechanism of tissue scarring. *Matrix Biol* 28: 20 31, 2009

56. Verderio E, Nicholas B, Gross S, Griffin M: Regulated expression of tissue transglutaminase in Swiss 3T3 fibroblasts: Effects on the processing of fibronectin, cell attachment, and cell death. *Exp Cell Res* 239: 119 138, 1998

57. Luberto C, Hassler DF, Signorelli P, Okamoto Y, Sawai H, Boros E, Hazen Martin DJ, Obeid LM, Hannun YA, Smith GK: Inhibition of tumor necrosis factor induced cell death in MCF7 by a novel inhibitor of neutral sphingomyelinase. *J Biol Chem* 277: 41128 41139, 2002

58. Cheadle C, Vawter MP, Freed WJ, Becker KG: Analysis of microarray data using Z score transformation. *J Mol Diagn* 5: 73 81, 2003

59. Mathivanan S, Simpson RJ: ExoCarta: A compendium of exosomal proteins and RNA. *Proteomics* 9: 4997 5000, 2009

Supplementary Movie 1

A   WT

B   SDC4^{-/-}

C   SDC4^{-/-}
     + SDC4 add back

1 **SUPPLEMENTARY METHODS**

2

3 **Antibodies**

4 Monoclonal antibodies used were against transglutaminase 2 (TG2) (IA12,

5 University of Sheffield, UK; CUB 7402, MA5-12739 Invitrogen, UK), α-smooth

6 muscle actin (α-SMA) [1A4] (ab7817, Abcam, UK) and flotillin-2 (FLOT2) (610383,

7 BD Transduction Laboratories, UK). Polyclonal antibodies used were against

8 syndecan-4 (SDC4) (ab24511, Abcam, UK), TG2 (ab421, Abcam, UK), cyclophilin-

9 A (ab41684, Abcam, UK), β-Tubulin (ab6046, Abcam, UK), hemagglutinin (HA)

10 (C29F4, Cell Signaling Technology, UK) and GFP (ab290, Abcam, UK).

11

12 **Unilateral ureteric obstruction**

13 Experimental unilateral ureteric obstruction (UUO) was performed in TG2-KO and

14 control (Wild Type, WT) C57BL/6J mice as described by Vielhauer *et al*. (2001).[1]

15 To perform UUO, mice were anaesthetized with 5% isoflurane and anesthesia

16 maintained with 2% isoflurane during the surgical process. The left ureter of the

17 mice was obstructed using a legating clip (Hemoclip Plus, Weck Closure Systems).

18 ADEPT® [4% (w/v) icodextrin solution] was dispensed in the peritoneum to

19 prevent post-surgical adhesions prior to closing. The muscle wall was sealed with

20 continuous stitching and skin wound closed with interrupted stitching using

21 absorbable sutures. After the procedure, buprenorphine (0.1 mg/kg) was

22 administered to the mice for pain-relieving. Animal were allowed free access to

23 standard rodent chow and tap water. Mice were sacrificed and the left kidneys

24 harvested 21 days post-operation. All experimental procedures were carried out

25 under license in accordance with regulations laid down by Her Majesty's

26 Government, UK (Animals Scientific Procedures Act ASPA, 1986), and were

27 approved by the University of Sheffield Animal Ethical Review Committee (ASPA

28 Ethical Review Process) and Nottingham Trent University Ethical Review

29 Committee (ASPA Ethical Review Process).

30

31 **Fibrosis measurement**

32 Kidneys were fixed in 10% formalin for 15 h at room temperature and washed

33 with phosphate buffer saline (PBS) pH 7.4 prior to paraffin embedding. Kidney

34 was then sectioned and stained with Masson's trichrome, which marks collagenous

35 material blue and nuclei, fibers, erythrocytes and elastin red/pink. Images of

36 Masson's trichrome stained kidney section were randomly acquired using Olympus

37 BX61 microscope. Quantification of kidney fibrosis was undertaken using

38 multiphase image analysis as previously described using Cell F software [2](Olympus,

39 Germany).

40

41 **Detection of TGF-β activity in kidney homogenates by mink lung epithelial**

42 **cell (MLEC) bioassay**

43 A 10% (w/v) kidney homogenate was prepared in homogenization buffer [0.25 M

44 sucrose, 10 mM Tris-HCl, 1 mM $MgCl_2$, 2 mM EDTA, pH 7.4] containing 1:100 (v/v)

45 protease inhibitors cocktail (P8340, Sigma, UK). Mechanical homogenization was

46 performed on ice using an Ultra Turrax T25 homogenizer (Merck, UK). Each

47 homogenate was centrifuged at 1000 g for 5 min at 4°C to remove large

48 particulates, then the supernatant diluted 1:10 in sterile-filtered (2 μm, Sartorius

49 Stedim, UK) serum-free DMEM with 0.1% (w/v) BSA. 100 μL of this solution was

50 assayed for the presence of active soluble TGF-β by application on the mink lung

51 epithelial cell line (MLEC) of the TGF-β quantification system[3] in a 96-well plate

52 ($5x10^4$ cells/well) for 22 h. Cells were then washed twice with PBS and lysed in 1X

53   Reporter Lysis Buffer (Promega, UK). 50 µL of cell lysate were mixed to an equal

54   volume of luciferase substrate (Promega, UK) and light emission measured with

55   Polarstar Optima luminometer (BMG Labtech, UK). Total TGF-β was measured

56   following acid treatment of the kidney homogenate and incubation with the MLEC

57   system.[4,5]

58

59   **SWATH acquisition mass spectrometry and data analysis of TG2-**

60   **immunopreciptates**

61   Tryptic peptides from TG2 immunoprecipitates were subjected to reverse-phase

62   high-pressure liquid chromatography electrospray ionization tandem mass

63   spectrometry (RP-HPLC-ESI-MS/MS) using a TripleTOF 5600+ mass spectrometer

64   from SCIEX (Canada). The mass spectrometer was used in two different modalities

65   depending on the stage of the experiment: data dependent acquisition (DDA)

66   mode was employed at the beginning for spectral library construction, while

67   SWATH® 2.0 - data independent acquisition (DIA) mode for used for the

68   quantitation.[6]

69   RP-HPLC mobile phases were solvent A [2% (v/v) LC/MS grade acetonitrile,

70   5% (v/v) DMSO and 0.1% (v/v) formic acid in LC/MS grade water] and solvent B

71   [LC/MS grade acetonitrile containing 5% (v/v) DMSO and 0.1% (v/v) formic acid].

72   Samples were injected with an Eksigent nanoLC 425 system using NanocHiPLC

73   columns (Eksigent, USA) with trap and elute system (200 µm × 0.5 mm trap

74   column and 75 µm × 15 cm analytical column packed with 3 µm ChromSP C-18

75   media - 300 Å). Samples were loaded onto the trap column at 5 µL/min for 3 min

76   in 100% solvent A, then were eluted from the analytical column at a flow rate of

77   300 nL/min using an increasing linear gradient of solvent B over solvent A, going

78   from 5% to 35% in a total time of 60 min (SWATH-DIA) or 120 min (Spectral

79   library production by DDA). Regeneration and re-equilibration of the column were

80   performed by loading 90% solvent B for 10 min followed by 5% solvent B for 10

81   min. Autocalibration was performed by the MS every four samples using an

82   injection of a standard of 25 pmol β-galactosidase digest. The electrospray

83   ionization was carried out using PicoTIP nanospray emitters uncoated SilicaTips

84   (New Objective, USA) with voltage set to +2400 V.

85   A spectral library was produced by DDA on a pool of all samples, in high

86   sensitivity mode. DDA mass spectrometry files were searched using ProteinPilot 4

87   (SCIEX) and the analysis was conducted by the software with an exhaustive

88   identification strategy, searching the UniProt/Swiss-Prot database (January 2014

89   release) for murine species. The generated file was imported into PeakView 2.0

90   software (SCIEX) as an ion library and spiked in iRT retention time standards

91   (Biognosys, Switzerland), after filtering for false discovery rate (FDR) of 1% and

92   excluding shared peptides.

93   Five TG2-IP samples per treatment were subjected to cyclic DIA using static

94   SWATH windows of m/z = 15. Thirty-four static SWATH windows from 400 to 900

95   m/z were used with an accumulation time of 96 ms, giving a cycle time of 3.3 s.

96   During different cycles, the initial survey scan (TOF-MS) was performed for each

97   window, and subsequently the MS/MS experiments was carried out on the totality

98   of the precursors detected in the SWATH window using rolling collision energy.[6]

99   Spectral alignment and targeted data extraction was performed in PeakView

100   2.0 using the reference spectral library generated by DDA in a pool of TG2-IP

101   samples. SWATH data was processed using an extraction window of 12 min and

102   applying these parameters: 100 peptides, 5 transitions, peptide confidence > 99%,

103   exclusion of shared peptides, and XIC width set at 50 ppm. The output consisted

104   of three different quantification files representing the intensity of the individual

105 transitions (the area under the intensity curve), of the different peptides

106 (cumulative peak area of the transitions) and of the proteins (cumulative peak

107 area of the peptides). To identify the proteins significantly associated to TG2, a z-

108 test statistical analysis was performed on the normalized protein peak areas (as

109 outlined in the next section), using the TG2-KO data as background.

110

111 **Z-test statistical analysis**

112 The significance of protein association with TG2 was determined by z-test analysis[7]

113 of the five independent SWATH data acquisition mass spectrometry experiments

114 performed on TG2-IP, using the TG2-null mice as background control. First, the

115 protein peak area of every detected protein was normalized within the whole

116 experiment using a Z-transformation: each intensity value was transformed using

117 the natural log transformation and then normalized by subtracting the average of

118 the entire population (μ) and dividing for the standard deviation of the entire

119 population (σ), as shown in the equation (1) below. ΔZ values were then calculated

120 by subtracting TG2-KO Z-score from WT Z-score for each protein in the same

121 treatment (sham or UUO) (equation 2). Finally, the z-test (equation 3a) was

122 performed on the five experiments together, to compare WT and TG2-KO data in

123 the same treatment: the average of the ΔZ for the protein in the different

124 experiments was divided by the standard error of the ΔZ in the different

125 experiments (equation 3b). Results were then plotted on a normal distribution

126 curve to obtain probability values (p-values). Proteins with p-value lower than

127 0.05 detected in at least 4 out of 5 experiments (n ⩾ 4) were regarded as

128 significantly associated with TG2, meaning that the protein can be considered a

129 specific partner (directly or indirectly associated) for the enzyme.

130

131 $$(1)\ Z\ score = \ Z_i = \frac{X_i - \mu}{\sigma}$$

132 $$(2)\ \Delta Z_i = Z_{WT,i} - Z_{KO,i}$$

133 $$(3a)\ Z\_test_i = \frac{X_i - H_0}{SE}$$

134 *Since* $H_0 : \Delta Z = 0 \rightarrow Z_{WT} - Z_{KO} = 0$ *(no differences between WT and TG2-KO)*

135 $$(3b)\ Z\_test_i = \frac{\Delta Z_i}{SD_i \big/ \sqrt{N}}$$

136

137 **SWATH acquisition mass spectrometry and data analysis of kidney**

138 **proteomes**

139 Kidney lysates were analyzed by RP-HPLC-ESI-MS/MS using a TripleTOF 5600+

140 mass spectrometer as outlined before, with some modification in the protocol.

141 Samples were directly injected onto an YMC Triart-C18 column (25 cm, 2 µm, 300

142 µm i.d) at 5 µL/min using microflow LC system (Eksigent ekspert nano LC 425)

143 and an increasing linear gradient of solvent B over solvent A going from 2% to

144 40% in a total time of 60 min (SWATH-DIA) or 120 min (spectral library production

145 by DDA). A spectral library was produced by DDA on a pool of all samples in high

146 sensitivity mode and DDA mass spectrometry files were searched using

147 ProteinPilot 5 (SCIEX). The analysis was conducted by the software with an

148 exhaustive identification strategy, searching the UniProt/Swiss-Prot database

149 (March 2016 release) for murine species. The generated file was imported into

150 PeakView 2.0 software (SCIEX) and spiked in iRT as outlined before.

151 SWATH-DIA was executed on four kidney lysates per treatment (WT or TG2-

152 KO, UUO or sham operated). DIA was performed using 40 variable SWATH

153 windows. Spectral alignment and targeted data extraction from the SWATH data

154 was performed in OneOmics (SCIEX) using the reference spectral library produced

155 by DDA. SWATH data were processed using an extraction window of 5 min and

156 applying the following parameters: 6 peptides/protein, 6 transitions, peptide

157 confidence of >99%, exclude shared peptides, and XIC width set at 75 ppm.

158 Analysis of the differentially expressed proteins between the different treatments

159 were carried out using SCIEX OneOmics cloud processing software, as the ratio of

160 protein peak area in UUO kidney lysates over the protein peak area of the same

161 protein in sham operated condition [log_2(UUO/Sham)]. Data were regarded as

162 differentially expressed at 0.8 (80%) confidence level.

163

164 **Bioinformatic Analysis**

165 Proteins were clustered in categories depending on their known main biological

166 function. This was performed by manual search of the protein IDs into the UniProt

167 Knowledgebase (UniProtKB) (www.uniprot.org[8]; UniProt Consortium, 2015) and

168 GeneCards® database (www.genecards.org[9]). Functional classification and

169 pathway analysis was performed using two different open source bioinformatics

170 resources: DAVID (Database for Annotation, Visualization, and Integrated

171 Discovery) bioinformatics resource 6.7 (http://david.abcc.ncifcrf.gov)[10] and

172 PANTHER (Protein ANalysis THrough Evolutionary Relationships) database

173 (www.pantherdb.org).[11] In both cases, the whole *Mus musculus* genome was

174 employed as background list. Functional enrichment analysis was performed in

175 PANTHER using PANTHER protein class terms. Pathway overrepresentation

176 analysis was performed using DAVID bioinformatics resource by comparing the

177 representation of the different Kyoto Encyclopedia of Genes and Genomes (KEGG,

178 www.genome.jp/kegg) terms (KEGG_PATHWAY) to the expected pathway

179 representation in *Mus musculus*.

180   In order to identify clusters and networks of interacting proteins, known

181   and predicted protein-protein interactions were investigated using STRING

182   (Search Tool for the Retrieval of INteracting Genes/proteins) database v10

183   (http://string-db.org).[12] The network was produced by using confidence level

184   higher than the default 0.4 and by removing all the unconnected proteins and the

185   small unconnected networks. The network was exported and analyzed using the

186   open source software Cytoscape v. 3.0.2 (www.cytoscape.org), to visualize the

187   protein clusters and assign specific colors to the nodes corresponding to the

188   different functional clusters.

189

190   **Isolation and characterization of extracellular vesicles from cell medium**

191   To extract extracellular vesicles (EVs) from cell medium, cells were cultured until

192   80% confluent. At this stage, cell monolayers were washed twice with PBS to

193   remove every fetal bovine serum (FBS) trace, the medium was replaced with

194   serum-free DMEM containing L-glutamine and penicillin/streptomycin, and cells

195   were cultured for additional 36 h.

196   After incubation, medium was collected and supplemented with protease

197   inhibitors (Roche, UK). Cells were washed with PBS, scraped in PBS, and the pellet

198   collected by centrifugation at 500 g for 5 min. Medium was centrifuged three times

199   at 300 g for 10 min at 4°C to remove remaining cells, and supernatant (S1) was

200   centrifuged at 1,200 g for 20 min at 4°C to remove large cell debris and apoptotic

201   bodies (P2). Supernatant (S2) was centrifuged 10,000 g for 30 min at 4°C in order

202   to collect the microvesicular (ectosomal) portion (P3), which supernatant (S3) was

203   centrifuged at 110,000 g for 1 h at 4°C in order to collect the exosomes (P4)[13,14].

204   All pellets were collected and resuspended in 40 µL of the suitable buffer. After

205   the last centrifugation, cleared medium (S4) was collected and proteins were

206 precipitated using trichloroacetic acid (TCA), as follows: 0.1 volume of TCA was

207 added to the medium and incubated for 1 h on ice. The mixture was centrifuged

208 for 5 min at 13,000 rpm, then pellet was washed with cold 100% acetone and

209 centrifuged again for 5 min 13,000 rpm. Pellet (EV-free medium proteins and

210 complexes) was air-dried and resuspended in 40 μL of the suitable buffer.

211 　　　For EV analysis by tunable resistive pulse sensing (TRPS) (qNano, Izon),

212 Nanopore NP150 (Izon) and calibration particles (1:1, 200 nm, Izon) were used

213 to analyze exosomes while Nanopore NP300 (Izon) and calibration particles (1:1,

214 200nm) were used for ectosome analysis. Samples were measured at three

215 pressure levels. The sizes and concentrations of particles were determined using

216 the software provided by Izon (version 3.2).

217

218 **Isolation of primary cells from WT and SDC4-null mice**

219 Kidney glomeruli and tubules were isolated from wild type and SDC4$^{-/-}$ mice

220 C57BL/6J mice using the method described by Fisher et al. [15] The kidney was

221 perfused in situ with Dynabeads® which become wedged in the glomeruli. The

222 cortex was isolated, disrupted and passed through sieves with the filtrate

223 consisting of cortical tubular fragments and some glomeruli. Any glomeruli were

224 removed and set aside by use of a strontium magnet. The remaining tubular

225 fragments were plated in tissue culture dishes containing medium with low serum

226 and growth supplements to stimulate epithelial cell proliferation. The primary

227 tubular epithelial cells (TECs) grew out from tubules in the following medium:

228 DMEM/F12, containing 0.5% heat-inactivated FBS (v/v), 100 U/mL penicillin, 100

229 μg/mL streptomycin, 22 mM L-glutamine, and supplemented with 10 μg/mL

230 insulin, 5.5 μg/mL transferrin, 5 ng/mL sodium selenite (ITS supplement, Sigma,

231 UK), 10 ng/mL epidermal growth factor (R&D Systems, UK), 5 pg/mL tri-

232 iodothyramine, 5 µg/mL dexamethasone, 12.5 µg/mL each of adenosine, cytosine,

233 guanosine, uridine and 2.5 µg/mL amphotericin B. Primary fibroblasts grew out

234 from tubules in Dulbecco's modified Eagle's medium:nutrient mixture F12

235 (DMEM/F12), containing 10% (v/v) heat-inactivated FBS (Biosera, UK), 100

236 IU/mL penicillin, 100 µg/mL streptomycin and 0.25 µg/mL amphotericin-B;

237 Primary mesangial cells grew out from glomeruli in Roswell Park Memorial Institute

238 (RPMI) 1640 medium containing 20% (v/v) heat-inactivated FBS, 2.2 mM L-

239 glutamine, 1 mM sodium pyruvate, 0.075% (w/v) sodium bicarbonate, 15 mM

240 HEPES, 100 IU/mL penicillin, 100 µg/mL streptomycin and 0.25 µg/mL

241 amphotericin-B. All media were from Invitrogen, and the supplements from Sigma,

242 unless otherwise stated.

243

244 **Western blotting**

245 10% (w/v) kidney homogenates were prepared in homogenization buffer [0.25 M

246 sucrose, 10 mM Tris-HCl, 1 mM $MgCl_2$, 2 mM EDTA, pH 7.4] containing 1:100 (v/v)

247 protease inhibitors cocktail (Sigma, UK). Mechanical homogenization was

248 performed on ice, using an Ultra Turrax T25 homogenizer (Merck, UK). Cell lysates

249 and EV lysates were prepared in in radiommunoprecipitation assay (RIPA) buffer

250 [50 mM TRIS HCl pH 8, 150 mM NaCl, 1% (v/v) NP40 detergent solution, 0.5%

251 (w/v) sodium deoxycholate, 0.1% (w/v) SDS] containing EDTA-free protease

252 inhibitors (Roche, UK). Unless differently stated, equal amounts of proteins were

253 resolved by SDS-PAGE [8% to 12% (w/v) acrylamide] under reducing and

254 denaturing conditions. Immunodetection of the proteins of interest was performed

255 by Western blot. After initial optimizations, typically the blot was cut horizontally

256 and probed with different antibodies to minimize stripping and re-probing.

257 Immunoreactive bands were detected by enhanced chemiluminescence (EZ-

258 chemiluminescence detection kit for HRP, Geneflow) after incubation with

259 appropriate HRP-conjugated secondary antibody. Secondary antibodies were

260 obtained from Dako (Denmark). Image acquisition was performed with a LAS4000

261 imaging system (GE Healthcare, UK).

262

263 **Extracellular vesicle isolation form urine samples**

264 Clinical cell-free urine samples from CKD patients characterized by stage 3 and 4

265 CKD (GFR loss higher than 4 mL/min per year; n=10) and controls (n=5) were

266 obtained by informed consent for a study approved by the Research Ethics

267 Committee of Sheffield University. EVs were isolated from 12 mL pools of cell-free

268 urine following a protocol similar to that employed to isolate EVs from cell culture

269 medium, with adaptations described by Sequeiros et al., 2017.[16] P3 (ectosomes)

270 and P4 (exosome) pellets and the TCA-precipitated EV-free urine fraction (S4)

271 were homogenized in RIPA buffer, proteins quantified (BCA assay) and equal

272 amounts analyzed in reducing and denaturing conditions by Western blotting. All

273 precautions to lower interference from DTT and urea were taken in the protein

274 assay.

275

SUPPLEMENTARY FIGURES

Supplementary Figure 1. Specific TG2 partner proteins belonging to the nuclear membrane compartment (A) or with mitochondrial/peroxisomal membrane location (B). TG2 associated proteins in UUO or sham operated kidney membranes were defined by z-analysis ($p \leq 0.05$, $n \geq 4$) of $n = 5$ independent experiments which combined TG2-IP and SWATH-MS, using the TG2-null mice as background control, as described in legend to Table 1. Membrane proteins previously reported to be exclusively located in nucleus (A) and in the mitochondrial or peroxisomal compartments (B) were manually selected from the SWATH-MS dataset according to the subcellular localization database "COMPARTMENTS" and UniProtKB. The presented histograms list proteins in order of significance of their association to TG2 (Log_{10} p-value) in UUO (red color histogram bars) and sham controls (grey color histogram bars).

Supplementary Figure 2. TG2 associated proteins in UUO-Enriched KEGG pathways likely to be involved in kidney fibrosis. Example of KEGG pathways (www.genome.jp/kegg/) overrepresented in the UUO kidney compared to sham operated kidney (with reference to Suppl. Table 4B). ECM-receptor interaction (A), regulation of the actin cytoskeleton (B). Red stars denote proteins significantly increased in the UUO kidney compared to the sham operated conditions (confidence > 80%). Blue stars denote proteins found to be significantly associated with TG2 ($p \leq 0.05$) in the UUO kidney membrane fraction.

Supplementary Figure 3. TG2 in extracellular vesicle fractions of NRK49F fibroblasts. NRK49F cells were grown in serum-free medium for 36 h without and

with supplementation of 10 ng/mL TGF-β1. After incubation, culture medium was collected and vesicular fraction separated by serial centrifugation as described in the Methods. All fractions were immunoprobed for TG2 and flotillin-2 (FLOT2).

Supplementary Figure 4. TG2 in extracellular vesicle fractions from urine. Ectosomal (P3) and exosomal (P4) fractions were isolated by serial centrifugation from pools of cell-free urine from healthy and CKD patients (stages 3-4), as described in the Suppl. methods. Proteins from EV-free urine (S4) were concentrated by TCA precipitation. Equal amounts of EV fractions and EV-free urine were immunoprobed with primary antibodies towards TG2 (mouse monoclonal CUB 7402) and FLOT2.

SUPPLEMENTARY TABLES

Supplementary Table 1. Ribosomal proteins (A and B) and immunoglobulins (C) associated with TG2 in the UUO and sham kidney membranes. The association was evaluated as described in legend to Table 1. Proteins are denoted by full gene name and ID, and listed according to specificity of the interaction with TG2. U, TG2-associated proteins uniquely found in UUO membranes; S, TG2-associated proteins uniquely found in Sham operated membranes; U/S, TG2-asociated proteins in UUO and sham control membranes.

Supplementary Table 2. UUO versus sham kidney proteome – proteins increasing upon UUO (UUO/sham > 1). The UUO and sham operated kidney proteome was resolved by SWATH acquisition MS as described in the Methods. Proteins significantly increased in UUO kidneys at confidence ≥ 80% are listed

328 according to UUO/Sham ratio as calculated by SCIEX OneOmics cloud processing

329 software. The absolute protein peak area variation ($2^{Abs\ [\log_2(UUO/Sham)]}$) is here

330 shown. Red cells represent a higher signal in UUO compared to sham, and proteins

331 are sorted by descending values. Yellow represent the confidence; a confidence ≥

332 80% was regarded as significant.

333

334 **Supplementary Table 3. UUO versus sham kidney proteome – proteins**

335 **decreasing upon UUO (UUO/sham < 1).** The UUO and sham kidney proteome

336 was resolved and UUO/Sham ratio expressed as described in legend to Suppl.

337 Table 2. The absolute peak area variation ($2^{Abs\ [\log_2(UUO/Sham)]}$) is here shown. Green

338 cells represent a lower signal in UUO compared to sham operated kidneys and

339 proteins are sorted by descending values.

340

341 **Supplementary Table 4. Functional classes and pathways significantly**

342 **overrepresented in the UUO proteome.** (A) PANTHER protein class

343 overrepresentation analysis (p≤0.05) on the pool of UUO upregulated (N=195)

344 and downregulated (N=458) proteins (respectively shown in Suppl. Table 2 and

345 Suppl. Table 3). (B) KEGG pathways overrepresentation analysis (p≤0.05),

346 performed with DAVID functional annotation, on the pool of UUO-upregulated

347 proteins.

348

349 **SUPPLEMENTARY MOVIES**

350

351 **Supplementary Movie 1. Dependence of TG2 vesicular trafficking on**

352 **Syndecan-4 in primary TECs.** Wild type (WT) and SDC4-KO (SDC4$^{-/-}$) primary

353 TECs were transiently transfected with 5 µg of pEGFP-N1-TG2 plasmid by

354 employing TransIT® transfection reagent (Mirus Bio). In order add back SDC4 in

355 SDC4$^{-/-}$ TECs, cells were co-transfected with 5 µL pcDNA3.1(+)-hSdc4 plasmid.

356 Time-lapse video clips were taken for WT TEC (A), SDC4$^{-/-}$ (B) and SDC4

357 transfected SDC4$^{-/-}$(C) TEC expressing EGFP-TG2 (green). EGFP-TG2 was

358 recruited in globular elements protruding and retracting from the PM (A). Arrows

359 indicate the formation of EGFP-TG2 vesicular blebbing on the edge of the cells.

360 EGFP-TG2 was less dynamic and appeared to be retained in the cytosol in the

361 SDC4-null TECs, which also had less budding activity than the wild type TECs (B).

362 Add back of SDC4 in SDC4-null TECs restored EGFP-TG2 vesicular blebbing and

363 "budding" reconstituted to wild type levels (C).

364

365

366 **SUPPLEMENTARY DATA**

367

368 **Supplementary Data 1. Original processed data and z-test analysis for the**

369 **TG2 interactome in UUO and sham operated kidney membranes.**

370

371 **Supplementary Data 2. Original processed for the kidney proteome in**

372 **UUO and sham operated conditions.**

373   Reference List

375   1. Vielhauer, V, Anders, HJ, Mack, M, Cihak, J, Strutz, F, Stangassinger, M, Luckow, B, Grone, HJ,
376   Schlondorff, D: Obstructive nephropathy in the mouse: progressive fibrosis correlates with
377   tubulointerstitial chemokine expression and accumulation of CC chemokine receptor 2- and
378   5-positive leukocytes. *J Am Soc Nephrol,* 12**:** 1173-1187, 2001.
379   2. Huang, L, Haylor, JL, Hau, Z, Jones, RA, Vickers, ME, Wagner, B, Griffin, M, Saint, RE, Coutts, IG, El
380   Nahas, AM, Johnson, TS: Transglutaminase inhibition ameliorates experimental diabetic
381   nephropathy. *Kidney Int,* 76**:** 383-394, 2009.
382   3. Abe, M, Harpel, JG, Metz, CN, Nunes, I, Loskutoff, DJ, Rifkin, DB: An assay for transforming growth
383   factor-beta using cells transfected with a plasminogen activator inhibitor-1 promoter-
384   luciferase construct. *Anal Biochem,* 216**:** 276-284, 1994.
385   4. van Waarde, MA, van Assen, AJ, Kampinga, HH, Konings, AW, Vujaskovic, Z: Quantification of
386   transforming growth factor-beta in biological material using cells transfected with a
387   plasminogen activator inhibitor-1 promoter-luciferase construct. *Anal Biochem,* 247**:** 45-51,
388   1997.
389   5. Scarpellini, A, Huang, L, Burhan, I, Schroeder, N, Funck, M, Johnson, TS, Verderio, EA: Syndecan-4
390   knockout leads to reduced extracellular transglutaminase-2 and protects against
391   tubulointerstitial fibrosis. *J Am Soc Nephrol,* 25**:** 1013-1027, 2014.
392   6. Gillet, LC, Navarro, P, Tate, S, Rost, H, Selevsek, N, Reiter, L, Bonner, R, Aebersold, R: Targeted data
393   extraction of the MS/MS spectra generated by data-independent acquisition: a new concept
394   for consistent and accurate proteome analysis. *Molecular & cellular proteomics : MCP,* 11**:**
395   O111 016717, 2012.
396   7. Cheadle, C, Vawter, MP, Freed, WJ, Becker, KG: Analysis of microarray data using Z score
397   transformation. *The Journal of molecular diagnostics : JMD,* 5**:** 73-81, 2003.
398   8. Magrane, M, UniProt, C: UniProt Knowledgebase: a hub of integrated protein data. *Database : the
399   journal of biological databases and curation,* 2011**:** bar009, 2011.
400   9. Safran, M, Dalah, I, Alexander, J, Rosen, N, Iny Stein, T, Shmoish, M, Nativ, N, Bahir, I, Doniger, T,
401   Krug, H, Sirota-Madi, A, Olender, T, Golan, Y, Stelzer, G, Harel, A, Lancet, D: GeneCards Version
402   3: the human gene integrator. *Database : the journal of biological databases and curation,*
403   2010**:** baq020, 2010.
404   10. Dennis, G, Jr., Sherman, BT, Hosack, DA, Yang, J, Gao, W, Lane, HC, Lempicki, RA: DAVID: Database
405   for Annotation, Visualization, and Integrated Discovery. *Genome biology,* 4**:** P3, 2003.
406   11. Mi, H, Muruganujan, A, Casagrande, JT, Thomas, PD: Large-scale gene function analysis with the
407   PANTHER classification system. *Nat Protoc,* 8**:** 1551-1566, 2013.
408   12. Szklarczyk, D, Franceschini, A, Wyder, S, Forslund, K, Heller, D, Huerta-Cepas, J, Simonovic, M, Roth,
409   A, Santos, A, Tsafou, KP, Kuhn, M, Bork, P, Jensen, LJ, von Mering, C: STRING v10: protein-
410   protein interaction networks, integrated over the tree of life. *Nucleic acids research,* 43**:** D447-
411   452, 2015.
412   13. Bianco, F, Perrotta, C, Novellino, L, Francolini, M, Riganti, L, Menna, E, Saglietti, L, Schuchman, EH,
413   Furlan, R, Clementi, E, Matteoli, M, Verderio, C: Acid sphingomyelinase activity triggers
414   microparticle release from glial cells. *The EMBO journal,* 28**:** 1043-1054, 2009.
415   14. Benussi, L, Ciani, M, Tonoli, E, Morbin, M, Palamara, L, Albani, D, Fusco, F, Forloni, G, Glionna, M,
416   Baco, M, Paterlini, A, Fostinelli, S, Santini, B, Galbiati, E, Gagni, P, Cretich, M, Binetti, G,
417   Tagliavini, F, Prosperi, D, Chiari, M, Ghidoni, R: Loss of exosomes in progranulin-associated
418   frontotemporal dementia. *Neurobiology of aging,* 40**:** 41-49, 2016.
419   15. Fisher, M, Jones, RA, Huang, L, Haylor, JL, El Nahas, M, Griffin, M, Johnson, TS: Modulation of tissue
420   transglutaminase in tubular epithelial cells alters extracellular matrix levels: a potential
421   mechanism of tissue scarring. *Matrix biology : journal of the International Society for Matrix
422   Biology,* 28**:** 20-31, 2009.

423   16. Sequeiros, T, Rigau, M, Chiva, C, Montes, M, Garcia-Grau, I, Garcia, M, Diaz, S, Celma, A, Bijnsdorp,
424   I, Campos, A, Di Mauro, P, Borros, S, Reventos, J, Doll, A, Paciucci, R, Pegtel, M, de Torres, I,
425   Sabido, E, Morote, J, Olivan, M: Targeted proteomics in urinary extracellular vesicles identifies
426   biomarkers for diagnosis and prognosis of prostate cancer. *Oncotarget,* 8**:** 4960-4976, 2017.

Supplementary Figure 1

A   **Nuclear proteins specifically associated with TG2 (Membrane fraction)**

B   **Mitochondrial and peroxisomal proteins specifically associated with TG2 (Membrane fraction)**
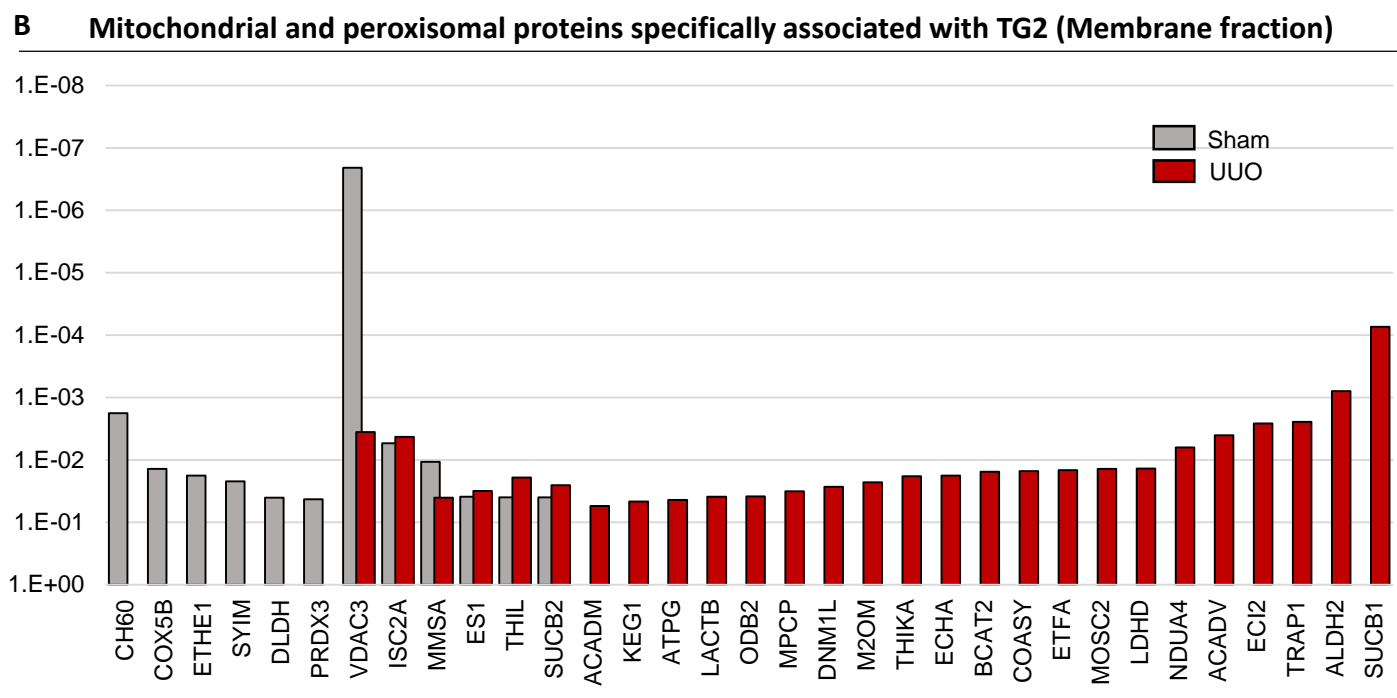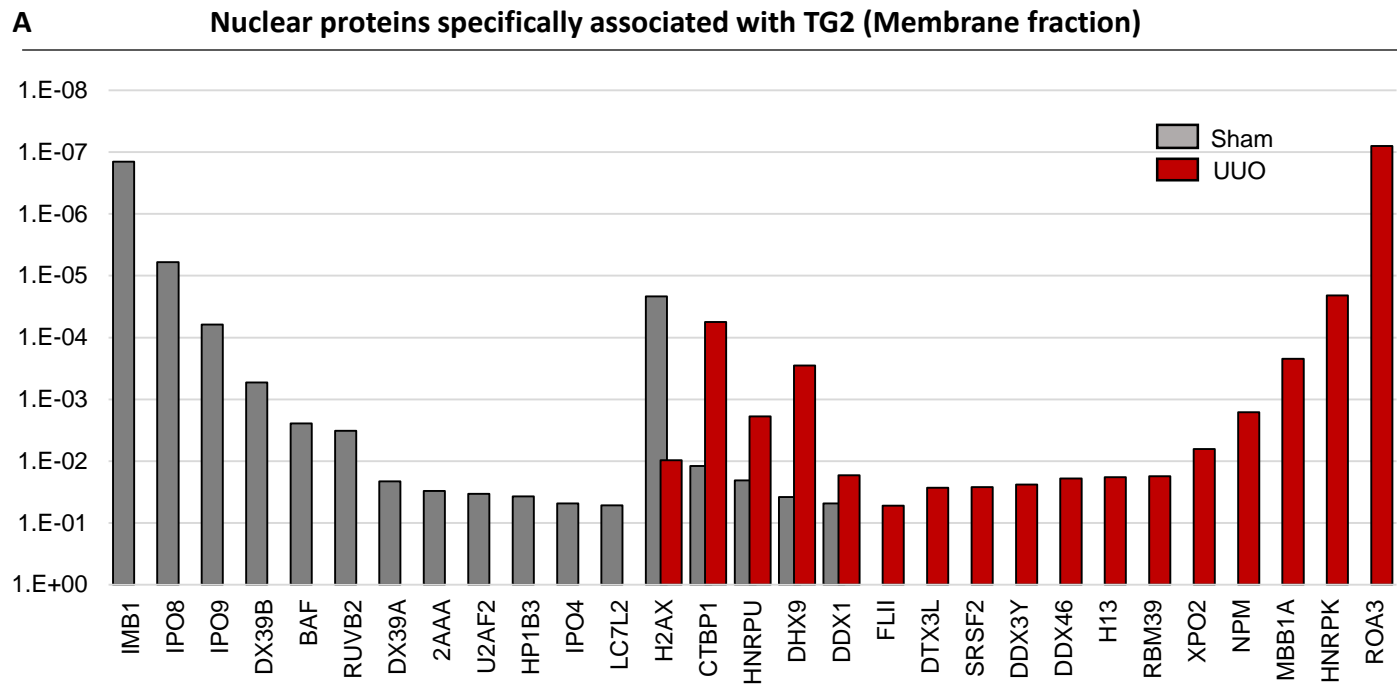
New Supplementary Figure 2

★ Interacting with TG2 in the UUO proteome
★ Increased in the UUO proteome

A ECM-RECEPTOR INTERACTION

B REGULATION OF ACTIN CYTOSKELETON
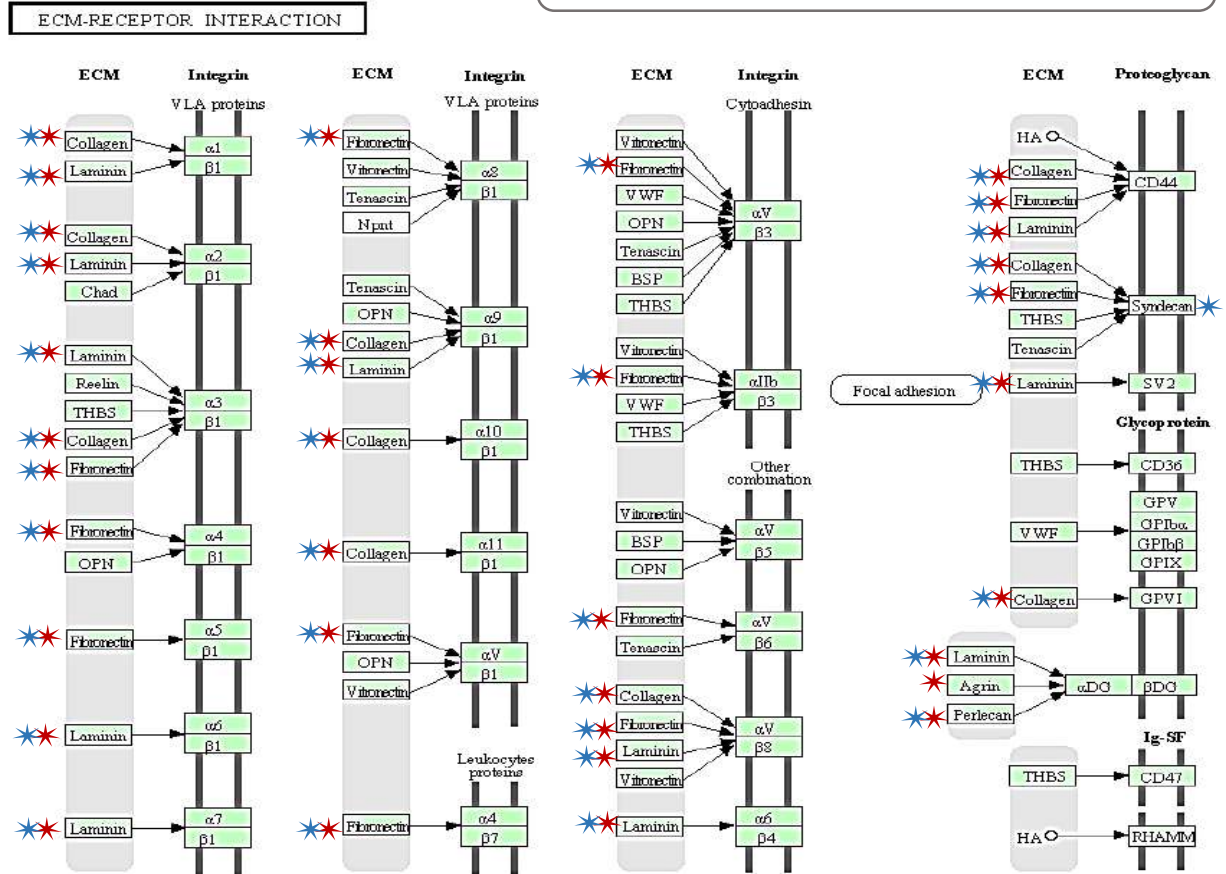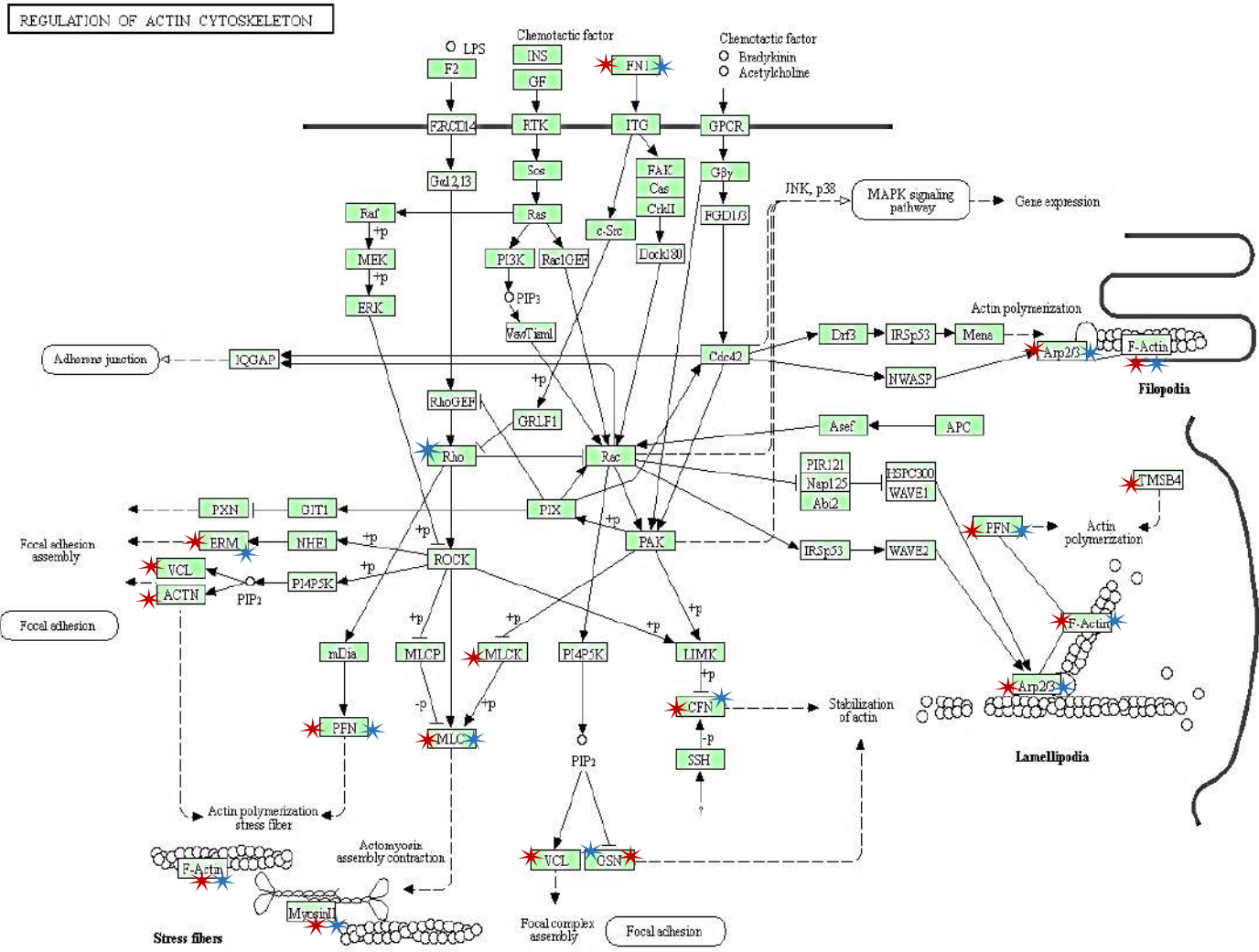
Supplementary Figure 3
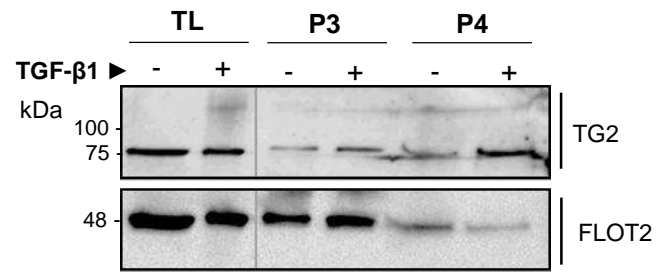
New Supplementary Figure 4
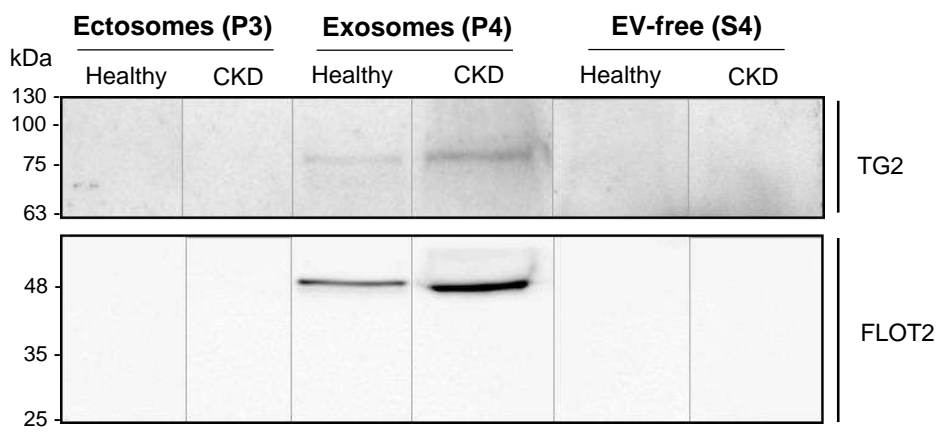
Supplementary Table 1

Ribosomal proteins specifically associated with TG2

A

UUO kidney (membrane fraction)				
Sample ID	**Name**	**N**	**P value**	**U/S**
RL3_MOUSE	60S ribosomal protein L3	5	1.26E-09	U/S
RS7_MOUSE	40S ribosomal protein S7	5	5.39E-06	U/S
RS13_MOUSE	40S ribosomal protein S13	5	3.03E-05	U/S
RS3_MOUSE	40S ribosomal protein S3	5	5.17E-05	U/S
RL6_MOUSE	60S ribosomal protein L6	5	1.36E-04	U/S
RL18A_MOUSE	60S ribosomal protein L18a	5	4.63E-04	U
RS6_MOUSE	40S ribosomal protein S6	5	2.49E-03	U/S
RLA2_MOUSE	60S acidic ribosomal protein P2	5	2.80E-03	U
RLA0_MOUSE	60S acidic ribosomal protein P0	5	2.92E-03	U/S
RL35A_MOUSE	60S ribosomal protein L35a	5	3.22E-03	U
RL18A_MOUSE	60S ribosomal protein L18a	5	3.40E-03	U
RS14_MOUSE	40S ribosomal protein S14	5	6.38E-03	U/S
RL23_MOUSE	60S ribosomal protein L23	5	7.99E-03	U
RL11_MOUSE	60S ribosomal protein L11	5	8.87E-03	U
RL10A_MOUSE	60S ribosomal protein L10a	5	9.04E-03	U
RL9_MOUSE	60S ribosomal protein L9	5	1.04E-02	U
RL17_MOUSE	60S ribosomal protein L17	5	1.05E-02	U
RS24_MOUSE	40S ribosomal protein S24	5	1.13E-02	U
RL8_MOUSE	60S ribosomal protein L8	5	1.91E-02	U
RL4_MOUSE	60S ribosomal protein L4	5	2.54E-02	U
RL23A_MOUSE	60S ribosomal protein L23a	5	2.70E-02	U
RS15_MOUSE	40S ribosomal protein S15	5	2.71E-02	U
RL40_MOUSE	Ubiquitin-60S ribosomal protein L40	5	3.64E-02	U
RL13A_MOUSE	60S ribosomal protein L13a	5	4.35E-02	U

B

Sham operated kidney (membrane fraction)				
Sample ID	**Name**	**N**	**P value**	**U/S**
RS17_MOUSE	40S ribosomal protein S17	5	4.03E-03	S
RL6_MOUSE	60S r bosomal protein L6	5	6.05E-03	U/S
RL3_MOUSE	60S r bosomal protein L3	5	6.23E-03	U/S
RS3_MOUSE	40S ribosomal protein S3	5	9.02E-03	U/S
RS13_MOUSE	40S ribosomal protein S13	5	1.21E-02	U/S
RLA0_MOUSE	60S acidic ribosomal protein P0	5	1.30E-02	U/S
RS14_MOUSE	40S ribosomal protein S14	5	2.48E-02	U/S
RS6_MOUSE	40S ribosomal protein S6	5	2.73E-02	U/S
RS7_MOUSE	40S ribosomal protein S7	5	3.52E-02	U/S

Immunoglobulin proteins specifically associated with TG2

C

UUO kidney (membrane fraction)				
Sample ID	**Name**	**N**	**P value**	**U/S**
LAC2_MOUSE	Ig lambda-1 chain C region	5	2.66E-03	U
HVM32_MOUSE	Ig heavy chain V-III region J606	5	2.30E-02	U

New Supplementary Table 2:

UUO kidney proteome – UUO / Sham > 1 (Confidence > 80%)

Protein ID	UUO/Sham	Confidence	Protein ID	UUO/Sham	Confidence	Protein ID	UUO/Sham	Confidence
UROM_MOUSE	16.34	0.85	LMNA_MOUSE	3.49	0.94	ANT3_MOUSE	2.27	0.86
COCA1_MOUSE	15.92	0.82	CO4B_MOUSE	3.44	0.86	LAMA5_MOUSE	2.26	0.83
FBN1_MOUSE	10.84	0.89	ARC1B_MOUSE	3.38	0.87	COR1C_MOUSE	2.23	0.83
FBLN2_MOUSE	9.65	0.81	TBB5_MOUSE	3.33	0.88	CAPZB_MOUSE	2.23	0.89
K1C19_MOUSE	9.57	0.86	APOE_MOUSE	3.31	0.87	FUS_MOUSE	2.22	0.80
TAGL_MOUSE	9.27	0.89	MYH11_MOUSE	3.28	0.87	AGRIN_MOUSE	2.16	0.92
PGS1_MOUSE	8.73	0.86	MYH10_MOUSE	3.27	0.85	AN32B_MOUSE	2.15	0.81
CNN1_MOUSE	8.59	0.80	FETUA_MOUSE	3.27	0.90	KHDR1_MOUSE	2.14	0.84
V ME_MOUSE	8.56	0.90	ESYT2_MOUSE	3.23	0.86	PROF1_MOUSE	2.10	0.89
HA2U_MOUSE	8.32	0.80	GCAB_MOUSE	3.21	0.91	NID1_MOUSE	2.10	0.92
ANXA1_MOUSE	8.17	0.84	ACTA_MOUSE	3.17	0.94	H2AV_MOUSE	2.07	0.86
MT2_MOUSE	8.11	0.84	VTDB_MOUSE	3.13	0.93	COR1B_MOUSE	2.06	0.86
POSTN_MOUSE	8.04	0.80	EST1C_MOUSE	3.11	0.95	A2M_MOUSE	2.05	0.85
A1AT2_MOUSE	7.86	0.82	KNG1_MOUSE	3.09	0.91	INO1_MOUSE	2.03	0.81
FINC_MOUSE	7.85	0.84	MYL9_MOUSE	3.08	0.98	LIMA1_MOUSE	2.02	0.87
COR1A_MOUSE	7.77	0.80	S10AB_MOUSE	3.08	0.88	GNAI2_MOUSE	2.02	0.83
CO3A1_MOUSE	7.72	0.92	A1AT1_MOUSE	3.07	0.86	ARPC3_MOUSE	2.01	0.87
PLSL_MOUSE	7.63	0.85	IGG2B_MOUSE	3.07	0.81	WDR1_MOUSE	2.01	0.83
CO1A1_MOUSE	7.61	0.96	SH3L1_MOUSE	3.06	0.86	UBC9_MOUSE	1.97	0.91
KCRB_MOUSE	7.56	0.83	K2C79_MOUSE	3.05	0.91	HP1B3_MOUSE	1.94	0.83
FBN2_MOUSE	7.26	0.94	TAGL2_MOUSE	3.04	0.88	ACTBL_MOUSE	1.91	0.84
MIME_MOUSE	6.67	0.83	K1C18_MOUSE	2.99	0.94	ROA3_MOUSE	1.90	0.90
CKAP4_MOUSE	6.57	0.85	ALBU_MOUSE	2.98	0.92	NONO_MOUSE	1.90	0.91
LUM_MOUSE	6.55	0.87	PTRF_MOUSE	2.96	0.84	ABCB7_MOUSE	1.89	0.89
FBLN3_MOUSE	6.33	0.80	VAT1_MOUSE	2.96	0.90	ARP3_MOUSE	1.89	0.95
SERPH_MOUSE	6.19	0.94	SEPT7_MOUSE	2.95	0.82	ARPC2_MOUSE	1.87	0.83
CNN2_MOUSE	6.15	0.80	PSME2_MOUSE	2.91	0.88	NH2L1_MOUSE	1.86	0.81
LEG1_MOUSE	6.15	0.87	B2MG_MOUSE	2.88	0.82	LAMC1_MOUSE	1.85	0.93
DESM_MOUSE	5.98	0.94	CERU_MOUSE	2.86	0.80	LAMB1_MOUSE	1.85	0.85
FBLN5_MOUSE	5.81	0.84	EPT2_MOUSE	2.83	0.82	HNRPF_MOUSE	1.82	0.83
RET1_MOUSE	5.56	0.83	COF1_MOUSE	2.74	0.87	FABP4_MOUSE	1.82	0.85
PDLI7_MOUSE	5.40	0.81	A1AT4_MOUSE	2.72	0.83	LASP1_MOUSE	1.81	0.81
CLUS_MOUSE	5.35	0.81	ANXA6_MOUSE	2.71	0.89	PGBM_MOUSE	1.80	0.81
K2C5_MOUSE	5.24	0.83	ADPRH_MOUSE	2.71	0.86	TADBP_MOUSE	1.80	0.81
FLNA_MOUSE	5.07	0.93	DPYL2_MOUSE	2.68	0.88	NUCL_MOUSE	1.79	0.83
MYOF_MOUSE	4.99	0.86	CO4A1_MOUSE	2.67	0.88	DX39B_MOUSE	1.78	0.81
K2C8_MOUSE	4.93	0.89	MAP4_MOUSE	2.66	0.82	ANXA4_MOUSE	1.78	0.85
CO6A1_MOUSE	4.78	0.88	CATD_MOUSE	2.65	0.82	TLN1_MOUSE	1.78	0.82
CO6A2_MOUSE	4.76	0.94	GBG2_MOUSE	2.65	0.81	FUBP2_MOUSE	1.78	0.80
ANXA3_MOUSE	4.73	0.83	ROA1_MOUSE	2.63	0.88	ARP2_MOUSE	1.76	0.88
FIBA_MOUSE	4.64	0.90	ISG15_MOUSE	2.62	0.84	RUXF_MOUSE	1.75	0.87
COEA1_MOUSE	4.62	0.81	FETUB_MOUSE	2.61	0.89	HNRPM_MOUSE	1.74	0.86
HEMO_MOUSE	4.60	0.86	MYH9_MOUSE	2.61	0.99	CSRP2_MOUSE	1.72	0.82
CSRP1_MOUSE	4.52	0.89	CO3_MOUSE	2.59	0.87	TGM2_MOUSE	1.71	0.90
CO4A2_MOUSE	4.50	0.80	MYLK_MOUSE	2.59	0.80	LAP2B_MOUSE	1.71	0.80
FIBG_MOUSE	4.45	0.85	S10AA_MOUSE	2.59	0.86	SRSF2_MOUSE	1.70	0.86
EMIL1_MOUSE	4.42	0.82	VMA5A_MOUSE	2.58	0.86	PDIA6_MOUSE	1.68	0.90
TBA1A_MOUSE	4.41	0.96	COIA1_MOUSE	2.57	0.96	1433G_MOUSE	1.65	0.81
TYB4_MOUSE	4.35	0.88	MYL6_MOUSE	2.53	0.92	SMAP_MOUSE	1.64	0.88
TPM1_MOUSE	4.28	0.84	CATZ_MOUSE	2.53	0.86	LSM3_MOUSE	1.62	0.91
K2C7_MOUSE	4.27	0.88	SF3B3_MOUSE	2.51	0.83	RSU1_MOUSE	1.59	0.84
PEDF_MOUSE	4.24	0.81	APOA4_MOUSE	2.50	0.82	SC11A_MOUSE	1.59	0.80
ACTN1_MOUSE	4.22	0.96	CAP1_MOUSE	2.50	0.92	ABRAL_MOUSE	1.56	0.80
TPM4_MOUSE	4.19	0.91	APOH_MOUSE	2.50	0.80	ACTB_MOUSE	1.56	0.93
IGKC_MOUSE	4.15	0.87	APOA1_MOUSE	2.46	0.92	HNRPU_MOUSE	1.53	0.85
FIBB_MOUSE	4.00	0.86	SET_MOUSE	2.46	0.83	MOES_MOUSE	1.52	0.81
MYADM_MOUSE	4.00	0.87	SFPQ_MOUSE	2.44	0.81	GDIR1_MOUSE	1.51	0.84
SH3L3_MOUSE	3.85	0.90	RBM3_MOUSE	2.36	0.84	HNRH1_MOUSE	1.48	0.87
TRFE_MOUSE	3.78	0.91	T22D1_MOUSE	2.35	0.90	SMD2_MOUSE	1.47	0.81
ANXA2_MOUSE	3.76	0.90	TIF1B_MOUSE	2.33	0.83	KAPCA_MOUSE	1.44	0.89
G6PE_MOUSE	3.71	0.90	GELS_MOUSE	2.33	0.84	PDIA4_MOUSE	1.40	0.80
CALU_MOUSE	3.69	0.84	VINC_MOUSE	2.33	0.94	HNRPK_MOUSE	1.40	0.82
SPB6_MOUSE	3.56	0.89	ML12B_MOUSE	2.33	0.83	LAMP1_MOUSE	1.38	0.81
CRIP1_MOUSE	3.55	0.90	LMNB1_MOUSE	2.30	0.86			
EFHD2_MOUSE	3.52	0.87	ANXA5_MOUSE	2.29	0.84			
ESYT1_MOUSE	3.52	0.82	PSME1_MOUSE	2.28	0.84			

New Supplementary Table 3

UUO kidney proteome – UUO / Sham < 1 (Confidence > 80%)

Protein ID	Sham/UUO	Confidence	Protein ID	Sham/UUO	Confidence	Protein ID	Sham/UUO	Confidence
G6PC_MOUSE	72.24	0.86	GSTA3_MOUSE	10.63	0.81	AUHM_MOUSE	7.85	0.85
AADAT_MOUSE	48.00	0.84	CK054_MOUSE	10.61	0.82	COASY_MOUSE	7.83	0.85
PDZ1I_MOUSE	45.76	0.84	AK1A1_MOUSE	10.56	0.91	NLTP_MOUSE	7.82	0.88
HAOX2_MOUSE	44.28	0.85	3HIDH_MOUSE	10.55	0.94	NDUB7_MOUSE	7.79	0.84
CALB1_MOUSE	32.07	0.91	SUCB2_MOUSE	10.42	0.94	TAU_MOUSE	7.76	0.83
ASSY_MOUSE	21.28	0.88	LACB2_MOUSE	10.39	0.82	THTR_MOUSE	7.75	0.89
ACSM1_MOUSE	20.87	0.83	FAHD1_MOUSE	10.39	0.84	PPA6_MOUSE	7.74	0.85
F16P1_MOUSE	20.84	0.81	FMO1_MOUSE	10.33	0.82	QOR_MOUSE	7.71	0.84
ACSM2_MOUSE	20.17	0.86	IVD_MOUSE	10.14	0.88	ACSL1_MOUSE	7.69	0.90
ECHP_MOUSE	19.92	0.84	THIL_MOUSE	10.10	0.95	CRYL1_MOUSE	7.62	0.90
KAD4_MOUSE	19.83	0.89	PROD_MOUSE	10.05	0.81	LRP2_MOUSE	7.60	0.84
AT1B1_MOUSE	19.55	0.87	SARDH_MOUSE	10.05	0.85	CX7A1_MOUSE	7.60	0.93
CAD16_MOUSE	19.54	0.92	INMT_MOUSE	10.03	0.83	HGD_MOUSE	7.58	0.84
PYC_MOUSE	18.04	0.87	AL1L1_MOUSE	9.95	0.91	CH60_MOUSE	7.56	0.96
GSTA2_MOUSE	17.14	0.85	KHK_MOUSE	9.90	0.83	C560_MOUSE	7.55	0.83
AL8A1_MOUSE	17.11	0.88	ARK72_MOUSE	9.87	0.87	NDUS1_MOUSE	7.55	0.94
ATNG_MOUSE	16.80	0.90	S22AI_MOUSE	9.86	0.90	CP013_MOUSE	7.48	0.87
UD3A2_MOUSE	16.72	0.83	HCDH_MOUSE	9.82	0.90	COX41_MOUSE	7.46	0.94
S100G_MOUSE	16.59	0.90	NDUB6_MOUSE	9.77	0.81	ACD11_MOUSE	7.41	0.80
ACS2L_MOUSE	16.56	0.89	CISD1_MOUSE	9.75	0.95	CX7A2_MOUSE	7.37	0.92
KEG1_MOUSE	16.36	0.88	NDRG1_MOUSE	9.52	0.99	NAKD2_MOUSE	7.33	0.95
SC5A2_MOUSE	16.23	0.80	S13A3_MOUSE	9.52	0.88	VATG1_MOUSE	7.31	0.83
ECHD2_MOUSE	16.09	0.87	CYC_MOUSE	9.49	0.92	NDUA4_MOUSE	7.30	0.89
CGL_MOUSE	16.04	0.86	SSDH_MOUSE	9.47	0.88	AIFM1_MOUSE	7.30	0.92
3HAO_MOUSE	15.56	0.85	SCOT1_MOUSE	9.34	0.92	CDD_MOUSE	7.28	0.81
S27A2_MOUSE	14.88	0.81	HMGCL_MOUSE	9.26	0.92	MUTA_MOUSE	7.27	0.81
MEP1B_MOUSE	14.72	0.82	ACPM_MOUSE	9.19	0.92	MCCA_MOUSE	7.25	0.82
ACADM_MOUSE	14.48	0.86	ATPK_MOUSE	9.17	0.80	NDUB4_MOUSE	7.21	0.83
TMM27_MOUSE	14.41	0.85	MSRA_MOUSE	9.12	0.83	ECHM_MOUSE	7.21	0.90
ISC2A_MOUSE	14.27	0.90	CBR1_MOUSE	9.11	0.92	ATP5H_MOUSE	7.21	0.93
BDH_MOUSE	14.24	0.89	LDHD_MOUSE	9.10	0.88	OCTC_MOUSE	7.20	0.80
ALDOB_MOUSE	14.21	0.93	COX5A_MOUSE	9.08	0.94	CMC2_MOUSE	7.20	0.80
HOT_MOUSE	14.07	0.84	ETFA_MOUSE	9.07	0.93	NDUS4_MOUSE	7.19	0.83
GATM_MOUSE	13.91	0.87	NDUB5_MOUSE	9.01	0.85	CBR4_MOUSE	7.19	0.85
GABT_MOUSE	13.84	0.93	PLSI_MOUSE	9.01	0.86	DLDH_MOUSE	7.18	0.94
KBL_MOUSE	13.82	0.85	GPDA_MOUSE	8.85	0.91	AL7A1_MOUSE	7.16	0.82
MMSA_MOUSE	13.79	0.88	NIPS1_MOUSE	8.81	0.91	MEP1A_MOUSE	7.15	0.88
PXMP2_MOUSE	13.77	0.81	NU4M_MOUSE	8.79	0.89	QCR2_MOUSE	7.14	0.94
ST1D1_MOUSE	13.74	0.85	FAHD2_MOUSE	8.76	0.80	C1TC_MOUSE	7.12	0.87
GGT1_MOUSE	13.58	0.89	CLYBL_MOUSE	8.75	0.80	QCR8_MOUSE	7.12	0.91
MAAI_MOUSE	13.49	0.82	FBX50_MOUSE	8.73	0.80	MGST3_MOUSE	7.12	0.84
PGAM2_MOUSE	13.44	0.88	NDUS6_MOUSE	8.72	0.81	ADT2_MOUSE	7.06	0.81
GLYAT_MOUSE	13.43	0.88	THNS2_MOUSE	8.70	0.83	ATP8_MOUSE	6.97	0.90
S4A4_MOUSE	13.29	0.83	NDUB8_MOUSE	8.67	0.86	ATPG_MOUSE	6.96	0.90
FAAA_MOUSE	13.16	0.92	NU5M_MOUSE	8.67	0.88	NDUAA_MOUSE	6.92	0.93
AT1A1_MOUSE	13.14	0.93	PECR_MOUSE	8.65	0.87	S12A1_MOUSE	6.91	0.96
DHSO_MOUSE	13.11	0.82	SDHA_MOUSE	8.64	0.98	AQP1_MOUSE	6.91	0.80
MPC1_MOUSE	12.91	0.93	NDUBA_MOUSE	8.63	0.86	ODO2_MOUSE	6.89	0.89
UK114_MOUSE	12.69	0.94	SUCA_MOUSE	8.55	0.94	TBA4A_MOUSE	6.89	0.88
ACE_MOUSE	12.66	0.91	NDUV2_MOUSE	8.50	0.84	ATPO_MOUSE	6.84	0.96
DECR2_MOUSE	12.62	0.90	IPYR2_MOUSE	8.50	0.83	PCCA_MOUSE	6.83	0.84
CATA_MOUSE	12.62	0.94	NDUV1_MOUSE	8.43	0.90	BPNT1_MOUSE	6.81	0.87
ACY3_MOUSE	12.43	0.80	NDUA9_MOUSE	8.38	0.89	PTER_MOUSE	6.73	0.91
S22A2_MOUSE	12.29	0.81	ABCD3_MOUSE	8.36	0.88	FGGY_MOUSE	6.73	0.85
GSTK1_MOUSE	12.27	0.82	ATPD_MOUSE	8.32	0.98	ECI2_MOUSE	6.73	0.85
PCCB_MOUSE	12.22	0.96	QCR6_MOUSE	8.31	0.93	NDUS2_MOUSE	6.72	0.91
AL4A1_MOUSE	12.17	0.93	NDUA1_MOUSE	8.25	0.86	ES1_MOUSE	6.71	0.92
CES1D_MOUSE	11.96	0.83	COX5B_MOUSE	8.24	0.91	ACON_MOUSE	6.66	0.90
GLPK_MOUSE	11.89	0.86	IDHP_MOUSE	8.21	0.93	NDUS3_MOUSE	6.64	0.96
QORL2_MOUSE	11.85	0.82	SBP1_MOUSE	8.19	0.92	MDHM_MOUSE	6.63	0.96
AAAD_MOUSE	11.84	0.85	NDUS7_MOUSE	8.16	0.94	ATP5I_MOUSE	6.62	0.90
VILI_MOUSE	11.78	0.91	BDH2_MOUSE	8.13	0.82	USMG5_MOUSE	6.60	0.97
DHAK_MOUSE	11.77	0.80	ETFB_MOUSE	8.13	0.91	FUMH_MOUSE	6.56	0.89
COX1_MOUSE	11.70	0.90	NHRF1_MOUSE	8.07	0.94	ATPB_MOUSE	6.55	0.94
SODM_MOUSE	11.66	0.93	NEP_MOUSE	8.05	0.90	FABPH_MOUSE	6.53	0.88
S2542_MOUSE	11.63	0.86	NDUAD_MOUSE	8.00	0.89	AQP3_MOUSE	6.51	0.90
MPC2_MOUSE	11.60	0.82	CSAD_MOUSE	8.00	0.90	CX6B1_MOUSE	6.48	0.92
ATP5L_MOUSE	11.54	0.80	COX2_MOUSE	7.99	0.87	NDUA5_MOUSE	6.48	0.90
OXDA_MOUSE	11.38	0.81	SDHB_MOUSE	7.99	0.89	VWA8_MOUSE	6.46	0.82
NUD19_MOUSE	11.28	0.90	TPMT_MOUSE	7.98	0.93	ATPA_MOUSE	6.46	0.96
HINT2_MOUSE	11.27	0.98	CY1_MOUSE	7.96	0.94	DHRS4_MOUSE	6.42	0.91
BPHL_MOUSE	11.09	0.87	TOM5_MOUSE	7.94	1.00	SUSD2_MOUSE	6.38	0.92
MCCB_MOUSE	10.95	0.90	COQ9_MOUSE	7.91	0.90	QCR1_MOUSE	6.37	0.94
PBLD1_MOUSE	10.91	0.87	IDHG1_MOUSE	7.91	0.91	NDUA7_MOUSE	6.36	0.91
DIC_MOUSE	10.83	0.83	THIM_MOUSE	7.90	0.91	SFXN1_MOUSE	6.35	0.83
ACD10_MOUSE	10.77	0.86	UCRI_MOUSE	7.89	0.91	QCR7_MOUSE	6.34	0.89
NHRF3_MOUSE	10.71	0.86	NDUA3_MOUSE	7.86	0.89	COX6C_MOUSE	6.33	0.91

Protein ID	Sham/UUO	Confidence	Protein ID	Sham/UUO	Confidence	Protein ID	Sham/UUO	Confidence
ODB2_MOUSE	6 31	0 81	PH4H_MOUSE	4.83	0.84	NAPSA_MOUSE	3.32	0.84
ARLY_MOUSE	6 31	0 91	ECI1_MOUSE	4.80	0.91	ESTD_MOUSE	3.28	0.86
PRDX5_MOUSE	6 30	0 91	HCD2_MOUSE	4.76	0.91	APMAP_MOUSE	3.28	0.84
PGES2_MOUSE	6 29	0 89	IDHC_MOUSE	4.75	0.90	GSTM5_MOUSE	3.27	0.87
ATP5J_MOUSE	6 29	0 97	ISCA2_MOUSE	4.73	0.82	PGK1_MOUSE	3.27	0.97
KAT3_MOUSE	6 29	0 81	MIC27_MOUSE	4.70	0.81	ISCU_MOUSE	3.25	0.81
ACOX2_MOUSE	6 24	0 84	SAM50_MOUSE	4.69	0.89	VA0D1_MOUSE	3.24	0.87
AT5F1_MOUSE	6.17	0 92	LONM_MOUSE	4.66	0.90	GVIN1_MOUSE	3.22	0.83
NU3M_MOUSE	6.15	0 95	MIC60_MOUSE	4.65	0.92	PRPS2_MOUSE	3.20	0.85
CH10_MOUSE	6.15	0 90	ATIF1_MOUSE	4.61	0.83	PGM1_MOUSE	3.13	0.90
NDUB9_MOUSE	6.10	0 83	LYZ2_MOUSE	4.60	0.93	PHB_MOUSE	3.13	0.92
AATM_MOUSE	6.10	0 97	OAT_MOUSE	4.59	0.86	EZRI_MOUSE	3.13	0.96
DHB8_MOUSE	6 07	0 87	DDAH1_MOUSE	4.57	0.83	EHD1_MOUSE	3.05	0.83
NDUA8_MOUSE	6 07	0 91	EFTU_MOUSE	4.54	0.95	HINT1_MOUSE	3.04	0.88
CHDH_MOUSE	6 06	0 88	CMC1_MOUSE	4.51	0.84	SAHH_MOUSE	2.99	0.91
ODPB_MOUSE	6 05	0 96	ECHA_MOUSE	4.46	0.97	GNPI1_MOUSE	2.96	0.89
VATA_MOUSE	6 04	0 92	RT35_MOUSE	4.43	0.81	CAH2_MOUSE	2.95	0.95
MRP2_MOUSE	6 03	0 82	THTM_MOUSE	4.41	0.83	THIKA_MOUSE	2.95	0.91
ETHE1_MOUSE	5 99	0 92	XPP1_MOUSE	4.40	0.87	HDHD2_MOUSE	2.90	0.82
VATH_MOUSE	5 94	0 90	VATD_MOUSE	4.40	0.89	TTC38_MOUSE	2.87	0.87
NDUC2_MOUSE	5 93	0 88	BCAT2_MOUSE	4.38	0.89	41_MOUSE	2.84	0.85
DCXR_MOUSE	5 92	0 88	DHE3_MOUSE	4.37	0.92	VDAC2_MOUSE	2.84	0.94
GSTT2_MOUSE	5 84	0 87	4F2_MOUSE	4.34	0.91	HEM2_MOUSE	2.82	0.91
ALDH2_MOUSE	5 82	0 95	ATAD3_MOUSE	4.30	0.80	RADI_MOUSE	2.79	0.83
TRAP1_MOUSE	5 82	0 88	TRXR2_MOUSE	4.29	0.83	CCS_MOUSE	2.75	0.99
AL9A1_MOUSE	5.76	0 94	ACADL_MOUSE	4.28	0.87	AKCL2_MOUSE	2.73	0.93
ETFD_MOUSE	5.74	0 89	CPT1A_MOUSE	4.27	0.84	GPD1L_MOUSE	2.72	0.87
CPT2_MOUSE	5.70	0 88	KCRU_MOUSE	4.24	0.88	TPIS_MOUSE	2.71	0.95
ANK3_MOUSE	5.70	0 85	AMPE_MOUSE	4.21	0.87	UGPA_MOUSE	2.66	0.87
ACOT4_MOUSE	5.68	0 81	GLRX5_MOUSE	4.20	0.93	HXK1_MOUSE	2.66	0.91
MARC2_MOUSE	5.65	0 89	MAOX_MOUSE	4.20	0.83	FIS1_MOUSE	2.65	0.89
ACOT1_MOUSE	5.63	0 85	M2OM_MOUSE	4.19	0.83	GLGB_MOUSE	2.59	0.98
DOPD_MOUSE	5.63	0 91	CLIC5_MOUSE	4.18	0.85	GTR1_MOUSE	2.58	0.80
T M13_MOUSE	5 58	0 96	ACDSB_MOUSE	4.10	0.93	NAMPT_MOUSE	2.57	0.82
ODPA_MOUSE	5 58	0 92	BASI_MOUSE	4.09	0.87	FUCM_MOUSE	2.52	0.88
MPCP_MOUSE	5 57	0 90	SCRN2_MOUSE	4.05	0.82	ENOA_MOUSE	2.51	0.98
ABHEB_MOUSE	5 57	0 93	TMM65_MOUSE	4.03	0.88	SYPL1_MOUSE	2.50	0.91
GRP75_MOUSE	5 56	0 82	T M10_MOUSE	4.01	0.86	S10A1_MOUSE	2.44	0.85
HIBCH_MOUSE	5 55	0 89	MTCH2_MOUSE	4.01	0.89	PDXK_MOUSE	2.42	0.85
NDUBB_MOUSE	5 53	0 90	PROSC_MOUSE	4.01	0.90	PARK7_MOUSE	2.42	0.93
MIC19_MOUSE	5 53	0 90	LDHB_MOUSE	3.99	0.86	PGAM1_MOUSE	2.41	0.97
VATB2_MOUSE	5 52	0 85	MOT1_MOUSE	3.98	0.91	GMPR1_MOUSE	2.41	0.81
GSH1_MOUSE	5.49	0 86	MAVS_MOUSE	3.95	0.84	GSTM1_MOUSE	2.37	0.89
NCEH1_MOUSE	5.47	0 92	T126A_MOUSE	3.93	0.85	EHD3_MOUSE	2.37	0.86
ECH1_MOUSE	5.46	0 97	GLNA_MOUSE	3.91	0.83	GSHR_MOUSE	2.33	0.80
VATF_MOUSE	5.45	0 90	CYB5_MOUSE	3.87	0.86	G3P_MOUSE	2.29	0.92
VATG3_MOUSE	5.43	0 94	AT11A_MOUSE	3.85	0.81	TMM33_MOUSE	2.28	0.86
CN159_MOUSE	5.41	0 83	CISY_MOUSE	3.83	0.88	TIM44_MOUSE	2.25	0.83
DECR_MOUSE	5 39	0 89	AMPN_MOUSE	3.83	0.95	ARL1_MOUSE	2.24	0.90
CMBL_MOUSE	5 38	0 85	ADT1_MOUSE	3.82	0.83	PRDX6_MOUSE	2.23	0.94
ACADS_MOUSE	5 36	0 89	EM55_MOUSE	3.82	0.91	NDKB_MOUSE	2.11	0.95
SUCB1_MOUSE	5 33	0 97	PTGR2_MOUSE	3.79	0.89	ADK_MOUSE	2.03	0.87
VATE1_MOUSE	5 32	0 91	NPL_MOUSE	3.76	0.88	PRDX1_MOUSE	2.03	0.91
LPPRC_MOUSE	5 26	0 88	PHB2_MOUSE	3.73	0.94	G6PI_MOUSE	2.03	0.93
ODP2_MOUSE	5 25	0 98	MIF_MOUSE	3.71	0.92	RS24_MOUSE	1.99	0.88
PRDX3_MOUSE	5 23	0 90	EBP_MOUSE	3.70	0.91	NDKA_MOUSE	1.98	0.88
KAD2_MOUSE	5 21	0 86	AATC_MOUSE	3.68	0.88	AP1B1_MOUSE	1.97	0.82
SQRD_MOUSE	5 20	0 92	DHI2_MOUSE	3.67	0.83	PACN2_MOUSE	1.96	0.85
GSHB_MOUSE	5.17	0 82	TSPO_MOUSE	3.66	0.98	MAT2B_MOUSE	1.94	0.89
LYPA1_MOUSE	5.13	0 90	NCPR_MOUSE	3.64	0.81	PEBP1_MOUSE	1.92	0.92
ACADV_MOUSE	5.12	0 89	CYB5B_MOUSE	3.62	0.93	SPTN1_MOUSE	1.85	0.88
KAD3_MOUSE	5.10	0 89	THIC_MOUSE	3.61	0.85	TMED4_MOUSE	1.84	0.90
DHPR_MOUSE	5 07	0 88	GSTA4_MOUSE	3.61	0.86	SPTB2_MOUSE	1.80	0.87
NIT1_MOUSE	5 03	0 90	RM04_MOUSE	3.59	0.91	UGDH_MOUSE	1.79	0.82
ODO1_MOUSE	5 00	0 91	AMPL_MOUSE	3.57	0.93	GSTP1_MOUSE	1.77	0.94
E41L3_MOUSE	4 96	0 86	VATC1_MOUSE	3.55	0.83	UAP1L_MOUSE	1.76	0.84
SAP3_MOUSE	4 96	0 85	GGCT_MOUSE	3.55	0.99	SNX3_MOUSE	1.72	0.84
MDHC_MOUSE	4 94	0 95	C1QBP_MOUSE	3.52	0.83	TBB4B_MOUSE	1.71	0.90
SPS2_MOUSE	4 93	0 90	ACBP_MOUSE	3.51	0.93	GALK1_MOUSE	1.64	0.85
THIOM_MOUSE	4 90	0 90	EFTS_MOUSE	3.50	0.85	ALDOA_MOUSE	1.57	0.84
RM12_MOUSE	4 89	0 91	TXTP_MOUSE	3.47	0.87	GPX3_MOUSE	1.54	0.83
NIT2_MOUSE	4 88	0 90	SPRE_MOUSE	3.47	0.96	HS90A_MOUSE	1.50	0.81
IDH3A_MOUSE	4 86	0 91	GPX1_MOUSE	3.45	0.92	CLH1_MOUSE	1.47	0.88
NDUA6_MOUSE	4 86	0 84	F213A_MOUSE	3.42	0.89			
VDAC1_MOUSE	4 85	0 96	DHB4_MOUSE	3.39	0.95			
HYES_MOUSE	4 85	0 81	ECHB_MOUSE	3.37	0.87			
ACOC_MOUSE	4 84	0 94	SODC_MOUSE	3.33	0.94			

New Supplementary Table 4

A

SIGNIFICANTLY ENRICHED PROTEIN CLASSES (PANTHER)	UUO/Sham > 1			UUO/Sham < 1		
		Fold change	p-value		Fold change	p-value
cytoskeletal protein (PC00085)	+	7.82	1.99E-28	-	0.82	1.00E+00
actin family cytoskeletal protein (PC00041)	+	11.33	2.49E-25	-	0.89	1.00E+00
extracellular matrix protein (PC00102)	+	6.76	1.92E-09	-	0.4	1.00E+00
non-motor actin binding protein (PC00165)	+	9.05	4.09E-08	-	1	1.00E+00
intermediate filament (PC00129)	+	14.19	7.22E-07	-	< 0.2	1.00E+00
extracellular matrix structural protein (PC00103)	+	14.87	2.99E-06	-	< 0.2	1.00E+00
serine protease inhibitor (PC00204)	+	8.79	1.52E-05	-	< 0.2	1.00E+00
mRNA splicing factor (PC00148)	+	9.89	2.06E-05	-	< 0.2	1.00E+00
mRNA processing factor (PC00147)	+	7.99	3.86E-05	-	< 0.2	1.00E+00
surfactant (PC00212)	+	15.36	1.01E-04	-	< 0.2	1.00E+00
structural protein (PC00211)	+	7.31	3.11E-04	-	< 0.2	1.00E+00
extracellular matrix linker protein (PC00101)	+	23.2	6.28E-04	-	< 0.2	1.00E+00
actin and actin related protein (PC00039)	+	20.8	1.06E-03	-	< 0.2	1.00E+00
protease inh bitor (PC00191)	+	4.7	2.51E-03	-	< 0.2	4.04E-01
enzyme modulator (PC00095)	+	2.22	2.48E-02	-	0.39	2.52E-02
actin binding motor protein (PC00040)	+	10.22	3.03E-02	-	< 0.2	1.00E+00
ant bacterial response protein (PC00051)	+	5.95	4.21E-02	-	< 0.2	1.00E+00
transferase (PC00220)	-	< 0.2	4.95E-02	+	2.67	4.96E-11
nucleotide kinase (PC00172)	-	< 0.2	1.00E+00	+	6.23	3.35E-02
transaminase (PC00216)	-	< 0.2	1.00E+00	+	10.38	2.91E-02
G-protein coupled receptor (PC00021)	-	< 0.2	1.00E+00	-	< 0.2	1.39E-02
transporter (PC00227)	+	1.15	1.00E+00	+	1.93	4.81E-03
nucleic acid binding (PC00171)	+	1.03	1.00E+00	-	0.47	3.34E-03
peroxidase (PC00180)	-	< 0.2	1.00E+00	+	11.96	2.87E-03
transfer/carrier protein (PC00219)	+	1.41	1.00E+00	+	2.79	1.92E-03
anion channel (PC00049)	-	< 0.2	1.00E+00	+	14.23	1.08E-03
carbohydrate kinase (PC00065)	-	< 0.2	1.00E+00	+	11.25	8.17E-04
hydrolase (PC00121)	-	0.77	1.00E+00	+	1.91	2.85E-04
ligase (PC00142)	-	0.31	1.00E+00	+	3.18	1.29E-04
receptor (PC00197)	+	1.43	1.00E+00	-	0.28	4.20E-05
mitochondrial carrier protein (PC00158)	-	< 0.2	1.00E+00	+	9.61	7.16E-06
cation transporter (PC00068)	-	< 0.2	1.00E+00	+	4.87	1.06E-06
acyltransferase (PC00042)	+	1.28	1.00E+00	+	7.95	3.05E-07
epimerase/racemase (PC00096)	-	< 0.2	1.00E+00	+	12.03	5.59E-09
transcription factor (PC00218)	-	0.55	1.00E+00	-	< 0.2	2.07E-09
acetyltransferase (PC00038)	-	< 0.2	1.00E+00	+	9.41	1.90E-09
ATP synthase (PC00002)	-	< 0.2	1.00E+00	+	15.06	1.86E-09
isomerase (PC00135)	-	< 0.2	1.00E+00	+	6.99	5.53E-11
hydratase (PC00120)	-	< 0.2	1.00E+00	+	35.17	6.73E-13
lyase (PC00144)	-	< 0.2	1.00E+00	+	8.25	1.26E-13
oxidase (PC00175)	-	0.83	1.00E+00	+	9.28	2.02E-15
reductase (PC00198)	-	0.6	1.00E+00	+	10.61	1.60E-27
dehydrogenase (PC00092)	-	0.91	1.00E+00	+	16.29	3.41E-73
oxidoreductase (PC00176)	-	0.56	1.00E+00	+	10.38	1.77E-91

B

KEGG PATHWAYS SIGNIFICANTLY ENRICHED IN UUO KIDNEYS	Fold Change	p-value
mmu04510:Focal adhesion	6.36	1.29E-09
mmu04810:Regulation of actin cytoskeleton	5.48	3.82E-08
mmu04512:ECM-receptor interaction	9.27	1.89E-07
mmu04610:Complement and coagulation cascades	8.40	8.72E-06
mmu03040:Spliceosome	5.64	5.41E-05
mmu05414:Dilated cardiomyopathy	5.32	1.78E-03
mmu04530:Tight junction	4.15	2.79E-03
mmu04670:Leukocyte transendothelial migration	4.12	6.42E-03
mmu05222:Small cell lung cancer	4.94	6.72E-03
mmu05416:Viral myocarditis	4.47	1.02E-02
mmu04666:Fc gamma R-mediated phagocytosis	4.28	1.21E-02
mmu05322:Systemic lupus erythematosus	4.08	1.48E-02
mmu04270:Vascular smooth muscle contraction	3.50	2.67E-02
mmu05410:Hypertrophic cardiomyopathy (HCM)	4.17	3.03E-02

SIGNIFICANCE STATEMENT

Secretion of the matrix crosslinking enzyme transglutaminase-2 (TG2) from tubular epithelial cells has been shown to contribute to fibrotic remodeling, a primary pathologic process in CKD. To discover the pathway for secretion of TG2, a comparative proteomic strategy was developed. Proteins that interact with TG2 were identified by TG2 immunoprecipitation from wild-type and TG2 knockout fibrotic kidney membranes followed by SWATH mass spectroscopy. The TG2 interactome was enriched in extracellular vesicle proteins, suggesting that TG2 is secreted in exosomes. Studies in cultured tubular epithelial cells support this conclusion and suggest that TG2 is a binding cargo of syndecan-4. The finding of TG2 in the urine of patients with CKD raises the possibility that block of vesicular TG2 could reduce TG2-driven matrix accumulation and diminish fibrosis.